[112] R. H. Stolen, C. Lee and R. K. Jain, 'Development of the stimulated Raman spectrum in single-mode silica fibers', *J. Opt. Soc. Am.* **B**, **1**, pp. 652–657, 1984.

[113] M. Vampouille and J. Marty, 'Controlled phase modulation in single-mode optical fibres', *Opt. Quantum Electron.*, **13**, pp. 393–400, 1981.

[114] L. F. Mollenauer, R. H. Stolen, J. P. Gordon and W. J. Tomlinson, 'Extreme picosecond pulse narrowing by means of soliton effect in single-mode optical fibers', *Opt. Lett.*, **8**, pp. 289–291, 1983.

[115] E. E. Bordon and W. L. Andeson, 'Dispersion-adapted monomode fiber for propagation of nonlinear pulses', *J. Lightwave Technol.*, 7(2), pp. 353–357, 1989.

4

Optical fibers and cables

4.1 Introduction

Optical fiber waveguides and their transmission characteristics have been considered in some detail in Chapters 2 and 3. However, we have yet to discuss the practical considerations and problems associated with the production, application and installation of optical fibers within a line transmission system. These factors are of paramount importance if optical fiber communication systems are to be considered as viable replacements for conventional metallic line communication systems. Optical fiber communication is of little use if the many advantages of optical fiber

transmission lines outlined in the preceding chapters may not be applied in practice in the telecommunications network without severe degradation of their performance.

It is therefore essential that:

1. Optical fibers may be produced with good stable transmission characteristics in long lengths at a minimum cost and with maximum reproducibility.
2. A range of optical fiber types with regard to size, refractive indices and index profiles, operating wavelengths, materials, etc., be available in order to fulfil many different system applications.
3. The fibers may be converted into practical cables which can be handled in a similar manner to conventional electrical transmission cables without problems associated with the degradation of their characteristics or damage.
4. The fibers and fiber cables may be terminated and connected together (jointed) without excessive practical difficulties and in ways which limit the effect of this process on the fiber transmission characteristics to keep them within acceptable operating levels. It is important that these jointing techniques may be applied with ease in the field locations where cable connection takes place.

In this chapter, we therefore consider the first three of the above practical elements associated with optical fiber communications. The final element, however, concerned with fiber termination and jointing is discussed immediately following, in Chapter 5. The various methods of preparation for silica-based optical fibers (both liquid and vapour phase) with characteristics suitable for telecommunications applications are dealt with in Sections 4.2 to 4.4. Techniques employed for the preparation of heavy metal fluoride glass fibers designed for transmission in the mid-infrared wavelength range are then outlined in Section 4.5. This is followed in Section 4.6 by consideration of the major commercially available fibers describing in general terms both the types and their characteristics. In particular, consideration is given to the recent developments in the area of plastic or polymeric fibers for lower bandwidth, very short-haul applications. The requirements for optical fiber cabling in relation to fiber protection are then described in Section 4.7 prior to discussion in Section 4.8 of the factors which cause modification to the cabled fiber transmission characteristics in a practical operating environment (i.e. microbending, hydrogen absorption, nuclear radiation exposure). Finally, cable design strategies and their influence upon typical examples of optical fiber cable constructions are dealt with in Section 4.9.

4.2 Preparation of optical fibers

From the considerations of optical waveguiding of Chapter 2 it is clear that a variation of refractive index inside the optical fiber (i.e. between the core and the cladding) is a fundamental necessity in the fabrication of fibers for light transmission. Hence at least two different materials which are transparent to light

over the current operating wavelength range (0.8 to 1.6 μm) are required. In practice these materials must exhibit relatively low optical attenuation and they must therefore have low intrinsic absorption and scattering losses. A number of organic and inorganic insulating substances meet these conditions in the visible and near-infrared regions of the spectrum.

However, in order to avoid scattering losses in excess of the fundamental intrinsic losses, scattering centres such as bubbles, strains and grain boundaries must be eradicated. This tends to limit the choice of suitable materials for the fabrication of optical fibers to either glasses (or glass-like materials) and monocrystalline structures (certain plastics).

It is also useful, and in the case of graded index fibers essential, that the refractive index of the material may be varied by suitable doping with another compatible material. Hence these two materials should have mutual solubility over a relatively wide range of concentrations. This is only achieved in glasses or glass-like materials, and therefore monocrystalline materials are unsuitable for the fabrication of graded index fibers, but may be used for step index fibers. However, it is apparent that glasses exhibit the best overall material characteristics for use in the fabrication of low loss optical fibers. They are therefore used almost exclusively in the preparation of fibers for telecommunications applications. Plastic clad [Ref. 1] and all plastic fibers find some use in short-haul, low bandwidth applications.

In this chapter the discussion will therefore be confined to the preparation of glass fibers. This is a two stage process in which initially the pure glass is produced and converted into a form (rod or preform) suitable for making the fiber. A drawing or pulling technique is then employed to acquire the end product. The methods of preparing the extremely pure optical glasses generally fall into two major categories which are:

(a) conventional glass refining techniques in which the glass is processed in the molten state (melting methods) producing a multicomponent glass structure;
(b) vapour-phase deposition methods producing silica-rich glasses which have melting temperatures that are too high to allow the conventional melt process.

These processes, with their respective drawing techniques, are described in the following sections.

4.3 Liquid-phase (melting) techniques

The first stage in this process is the preparation of ultra pure material powders which are usually oxides or carbonates of the required constituents. These include oxides such as SiO_2, GeO_2, B_2O_2 and A_2O_3, and carbonates such as Na_2CO_3, K_2CO_3, $CaCO_3$ and $BaCO_3$ which will decompose into oxides during the glass melting. Very high initial purity is essential and purification accounts for a large proportion of the material cost; nevertheless these compounds are commercially available with total transition metal contents below 20 parts in 10^9 and below 1 part in 10^9 for some specific impurities [Ref. 2]. The purification may therefore involve

combined techniques of fine filtration and coprecipitation, followed by solvent extraction before recrystallization and final drying in a vacuum to remove any residual OH ions [Ref. 3].

The next stage is to melt these high purity, powdered, low melting point glass materials to form a homogeneous, bubble-free multicomponent glass. A refractive index variation may be achieved by either a change in the composition of the various constituents or by ion exchange when the materials are in the molten phase. The melting of these multicomponent glass systems occurs at relatively low temperatures between 900 and 1300 °C and may take place in a silica crucible as shown in Figure 4.1 [Ref. 4]. However, contamination can arise during melting from several sources including the furnace environment and the crucible. Both fused silica and platinum crucibles have been used with some success, although an increase in impurity content was observed when the melt was held in a platinum crucible at high temperatures over long periods [Ref. 5].

Silica crucibles can give dissolution into the melt which may introduce inhomogeneities into the glass, especially at high melting temperatures. A technique for avoiding this involves melting the glass directly into a radiofrequency (RF

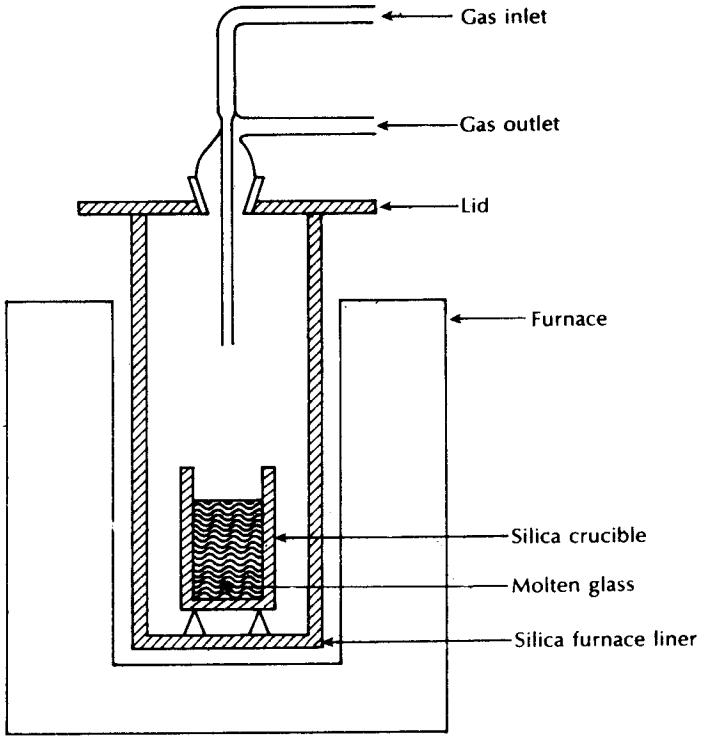

Figure 4.1 Glassmaking furnace for the production of high purity glasses [Ref. 4].

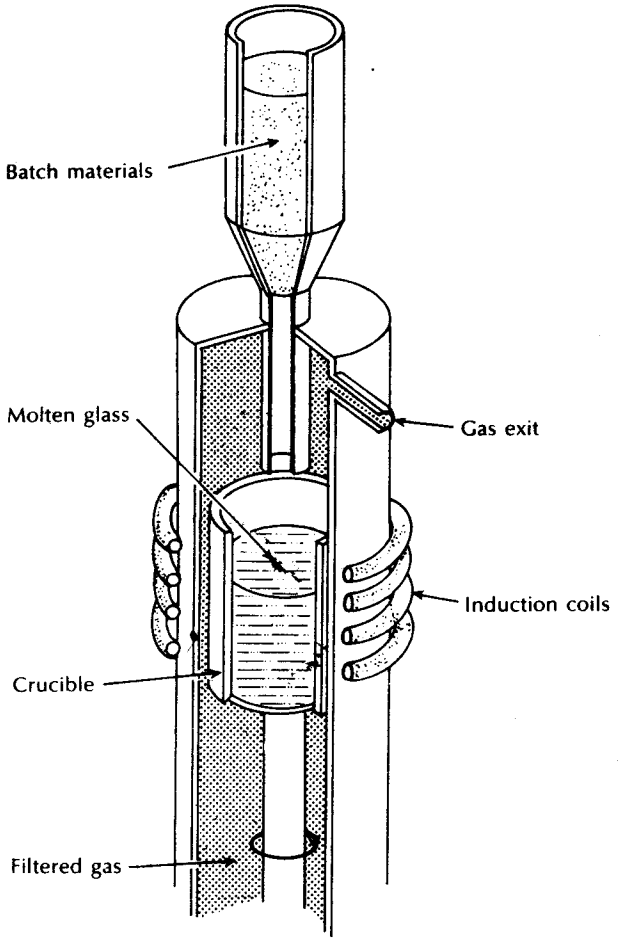

Figure 4.2 High-purity melting using a radiofrequency induction furnace [Refs. 6 to 8].

approximately 5 MHz) induction furnace while cooling the silica by gas or water flow, as shown in Figure 4.2 [Refs. 6 to 8]. The materials are preheated to around 1000 °C where they exhibit sufficient ionic conductivity to enable coupling between the melt and the RF field. The melt is also protected from any impurities in the crucible by a thin layer of solidified pure glass which forms due to the temperature difference between the melt and the cooled silica crucible.

In both techniques the glass is homogenized and dried by bubbling pure gases through the melt, whilst protecting against any airborne dust particles either originating in the melt furnace or present as atmospheric contamination. After the melt has been suitably processed, it is cooled and formed into long rods (cane) of multicomponent glass.

4.3.1 Fiber drawing

The traditional technique for producing fine optical fiber waveguides is to make a preform using the rod in tube process. A rod of core glass is inserted into a tube of cladding glass and the preform is drawn in a vertical muffle furnace, as illustrated in Figure 4.3 [Ref. 9]. This technique is useful for the production of step index fibers with large core and cladding diameters where the achievement of low attenuation is not critical as there is a danger of including bubbles and particulate matter at the core–cladding interface.

Another technique which is also suitable for the production of large core diameter step index fibers, and reduces the core–cladding interface problems, is called the stratified melt process. This process, developed by Pilkington Laboratories [Ref. 10], involves pouring a layer of cladding glass over the core glass in a platinum crucible as shown in Figure 4.4 [Ref. 11]. A bait glass rod is dipped into the molten combination and slowly withdrawn giving a composite core–clad preform which may then be drawn into a fiber.

Subsequent development in the drawing of optical fibers (especially graded index) produced by liquid-phase techniques has concentrated on the double crucible method. In this method the core and cladding glass in the form of separate rods is fed into two concentric platinum crucibles, as illustrated in Figure 4.5 [Ref. 4]. The assembly is usually located in a muffle furnace capable of heating the crucible contents to a temperature of between 800 and 1200 °C. The crucibles have nozzles in their bases from which the clad fiber is drawn directly from the melt, as shown in Figure 4.5. Index grading may be achieved through the diffusion of mobile ions across the core–cladding interface within the molten glass. It is possible to achieve

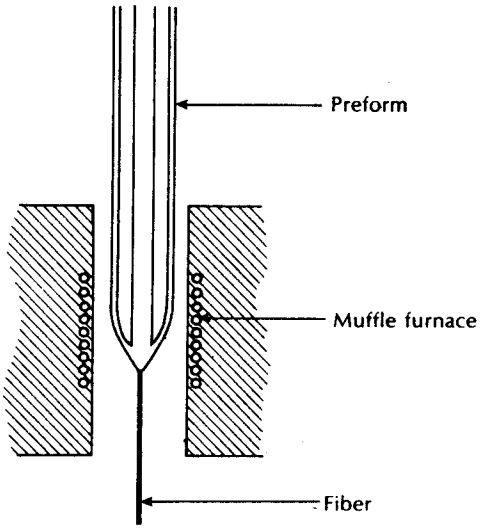

Figure 4.3 Optical fiber from a preform [Ref. 9].

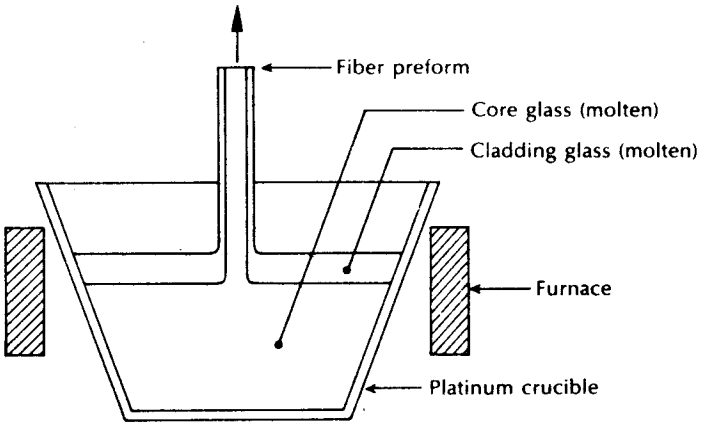

Figure 4.4 The stratified melt process (glass on glass technique) for producing glass clad rods or preforms [Ref. 11].

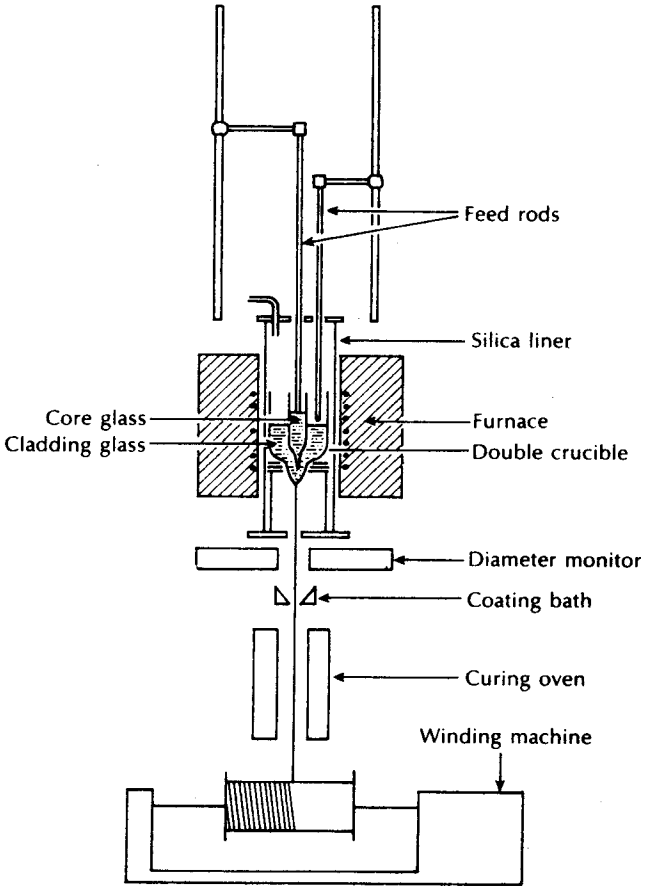

Figure 4.5 The double crucible method for fiber drawing [Ref. 4].

Table 4.1 Material systems used in the fabrication of multicomponent glass fibers by the double crucible technique

Step index	
Core glass	Cladding glass
Na_2O–B_2O_3–SiO_2	Na_2O–B_2O_3–SiO_2
Na_2O–LiO–CaO–SiO_2	Na_2O–Li_2O–CaO–SiO_2
Na_2O–CaO–GeO_2	Na_2O–CaO–SiO_2
Tl_2O–Na_2O–B_2O_3–GeO_2–BaO–CaO–SiO_2	Na_2O–B_2O_3–SiO_2
Na_2O–BaO–GeO_2–B_2O_3–SiO_2	Na_2O–B_2O_5–SiO_2
P_2O_5–Ga_2O_3–GeO_2	P_2O_5–Ga_2O_3–SiO_2
Graded index	
Base glass	Diffusion mechanism
R_2O–GeO_2–CaO–SiO_2	$Na^+ \rightleftharpoons K^+$
R_2O–B_2O_3–SiO_2	$Tl^+ \rightleftharpoons Na^+$
Na_2O–B_2O_3–SiO_2	Na_2O diffusion
Na_2O–B_2O_3–SiO_2	CaO, BaO, diffusion

a reasonable refractive index profile via this diffusion process, although due to lack of precise control it is not possible to obtain the optimum near parabolic profile which yields the minimum pulse dispersion (see Section 3.10.2). Hence graded index fibers produced by this technique are subsequently less dispersive than step index fibers, but do not have the bandwidth–length products of optimum profile fibers. Pulse dispersion of 1 to 6 ns km^{-1} [Refs. 12, 13] is quite typical, depending on the material system used.

Some of the material systems used in the fabrication of multicomponent glass step index and graded index fibers are given in Table 4.1.

Using very high purity melting techniques and the double crucible drawing method, step index and graded index fibers with attenuations as low as 3.4 dB km^{-1} [Ref. 14] and 1.1 dB km^{-1} [Ref. 2], respectively, have been produced. However, such low losses cannot be consistently obtained using liquid-phase techniques and typical losses for multicomponent glass fibers prepared continuously by these methods are between 5 and 10 dB km^{-1}. Therefore, liquid-phase techniques have the inherent disadvantage of obtaining and maintaining extremely pure glass which limits their ability to produce low loss fibers. The advantage of these techniques is in the possibility of continuous production (both melting and drawing) of optical fibers.

4.4 Vapour-phase deposition techniques

Vapour-phase deposition techniques are used to produce silica-rich glasses of the highest transparency and with the optimal optical properties The starting materials

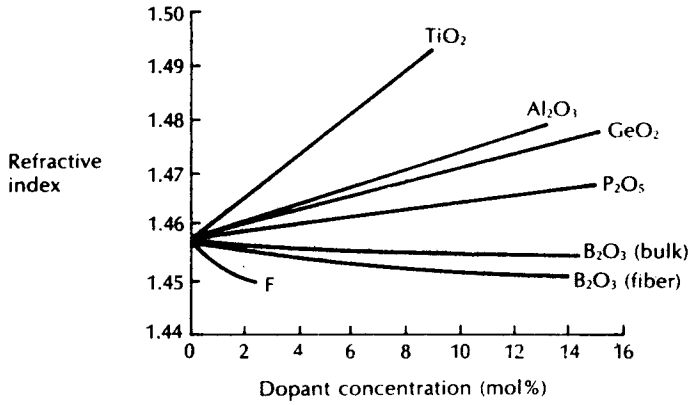

Figure 4.6 The variation in the refractive index of silica using various dopants. Reproduced with permission from the publishers, Society of Glass Technology, *Phys. Chem. Glasses*, **21**, p. 5, 1980.

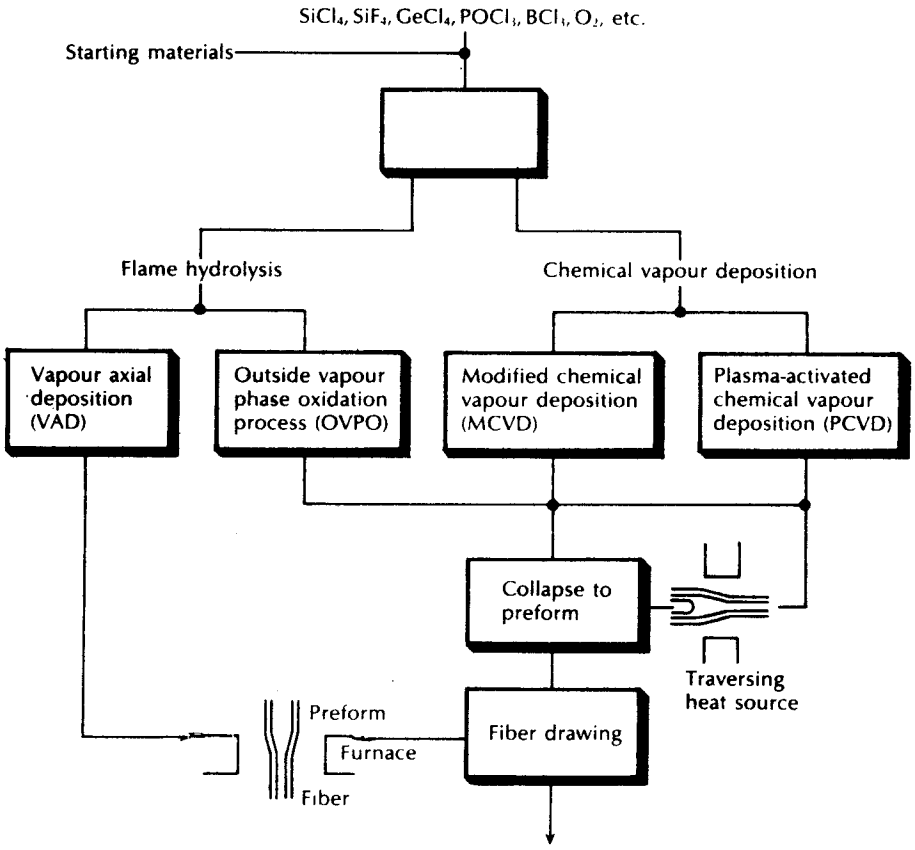

Figure 4.7 Schematic illustration of the vapour-phase deposition techniques used in the preparation of low loss optical fibers.

are volatile compounds such as $SiCl_4$, $GeCl_4$, SiF_4, BCl_3, O_2, BBr_3 and $POCl_3$ which may be distilled to reduce the concentration of most transition metal impurities to below one part in 10^9, giving negligible absorption losses from these elements. Refractive index modification is achieved through the formation of dopants from the nonsilica starting materials. These vapour-phase dopants include TiO_2, GeO_2, P_2O_5, Al_2O_3, B_2O_3 and F, the effects of which on the refractive index of silica are shown in Figure 4.6 [Ref. 2]. Gaseous mixtures of the silica-containing compound, the doping material and oxygen are combined in a vapour-phase oxidation reaction where the deposition of oxides occurs. The deposition is usually on to a substrate or within a hollow tube and is built up as a stack of successive layers. Hence the dopant concentration may be varied gradually to produce a graded index profile or maintained to give a step index profile. In the case of the substrate this directly results in a solid rod or preform whereas the hollow tube must be collapsed to give a solid preform from which the fiber may be drawn.

There are a number of variations of vapour-phase deposition which have been successfully utilized to produce low loss fibers. The major techniques are illustrated in Figure 4.7, which also indicates the plane (horizontal or vertical) in which, the deposition takes place as well as the formation of the preform. These vapour-phase deposition techniques fall into two broad categories: flame hydrolysis and chemical vapour deposition (CVD) methods. The individual techniques are considered in the following sections.

4.4.1 Outside vapour-phase oxidation (OVPO) process

This process which uses flame hydrolysis stems from work on 'soot' processes originally developed by Hyde [Ref. 16] which were used to produce the first fiber with losses of less than 20 dB km^{-1} [Ref. 17]. The best known technique of this type is often referred to as the outside vapour-phase oxidation process. In this process the required glass composition is deposited laterally from a 'soot' generated by hydrolyzing the halide vapours in an oxygen–hydrogen flame. Oxygen is passed through the appropriate silicon compound (i.e. $SiCl_4$) which is vaporized, removing any impurities. Dopants such as $GeCl_4$ or $TiCl_4$ are added and the mixture is blown through the oxygen–hydrogen flame giving the following reactions:

$$SiCl_4\ (\text{vapour}) + 2H_2O\ (\text{vapour}) \xrightarrow{\text{heat}} SiO_2\ (\text{solid}) + 4HCl\ (\text{gas}) \tag{4.1}$$

and

$$SiCl_4\ (\text{vapour}) + O_2\ (\text{gas}) \xrightarrow{\text{heat}} SiO_2\ (\text{solid}) + 2Cl_2\ (\text{gas}) \tag{4.2}$$

$$GeCl_4\ (\text{vapour}) + O_2\ (\text{gas}) \xrightarrow{\text{heat}} GeO_2\ (\text{solid}) + 2Cl_2\ (\text{gas}) \tag{4.3}$$

or

$$TiCl_4\ (\text{vapour}) + O_2\ (\text{gas}) \xrightarrow{\text{heat}} TiO_2\ (\text{solid}) + 2Cl_2\ (\text{gas}) \tag{4.4}$$

The silica is generated as a fine soot which is deposited on a cool rotating mandrel, as illustrated in Figure 4.8(a) [Ref. 18]. The flame of the burner is reversed back and forth over the length of the mandrel until a sufficient number of layers of silica (approximately 200) are deposited on it. When this process is completed the mandrel is removed and the porous mass of silica soot is sintered (to form a glass body), as illustrated in Figure 4.8(b). The preform may contain both core and cladding glasses by properly varying the dopant concentrations during the deposition process. Several kilometres (around 10 km of 120 μm core diameter fiber have been produced [Ref. 2]) can be drawn from the preform by collapsing and closing the central hole, as shown in Figure 4.8(c). Fine control of the index gradient for graded index fibers may be achieved using this process as the gas flows can be adjusted at the completion of each traverse of the burner. Hence fibers with bandwidth–length products as high as 3 GHz km have been achieved [Ref. 19] through accurate index grading with this process.

The purity of the glass fiber depends on the purity of the feeding materials and also upon the amount of OH impurity from the exposure of the silica to water vapour in the flame following the reactions given in Eqs. (4.1) to (4.4). Typically, the OH content is between 50 and 200 parts per million and this contributes to the fiber attenuation. It is possible to reduce the OH impurity content by employing gaseous chlorine as a drying agent during sintering. This has given losses as low as 1 dB km^{-1} and 1.8 dB km^{-1} at wavelengths of 1.2 and 1.55 μm respectively [Ref. 20] in fibers prepared using the OVPO process.

Other problems stem from the use of the mandrel which can create some difficulties in the formation of the fiber preform. Cracks may form due to stress

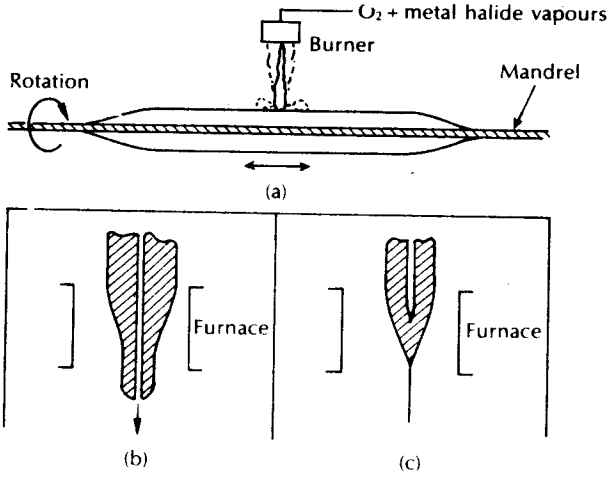

Figure 4.8 Schematic diagram of the OVPO process for the preparation of optical fibers; (a) soot deposition; (b) preform sintering; (c) fiber drawing [Ref. 19].

concentration on the surface of the inside wall when the mandrel is removed. Also the refractive index profile has a central depression due to the collapsed hole when the fiber is drawn. Therefore, although the OVPO process is a useful fiber preparation technique, it has several drawbacks. Furthermore, it is a batch process, which limits its use for the volume production of optical fibers. Nevertheless, a number of proprietary approaches to scaling-up the process have provided preforms capable of producing 250 km of fiber [Ref. 21].

4.4.2 Vapour axial deposition (VAD)

This process was developed by Izawa *et al.* [Ref. 22] in the search for a continuous (rather than batch) technique for the production of low loss optical fibers. The VAD technique uses an end-on deposition on to a rotating fused silica target, as illustrated in Figure 4.9 [Ref. 23]. The vaporized constituents are injected from burners and react to form silica soot by flame hydrolysis. This is deposited on the end of the starting target in the axial direction forming a solid porous glass preform in the shape of a boule. The preform which is growing in the axial direction is pulled upwards at a rate which corresponds to the growth rate. It is initially dehydrated by heating with $SOCl_2$ using the reaction:

$$\underset{\text{(vapour)}}{H_2O} + \underset{\text{(vapour)}}{SOCl_2} \xrightarrow{\text{heat}} \underset{\text{(gas)}}{2HCl} + \underset{\text{(gas)}}{SO_2} \tag{4.5}$$

and is then sintered into a solid preform in a graphite resistance furnace at an elevated temperature of around 1500 °C. Therefore, in principle this process may be adapted to draw fiber continuously, although at present it tends to be operated as a batch process partly because the resultant preforms can yield more than 100 km of fiber [Ref. 21].

A spatial refractive index profile may be achieved using the deposition properties of SiO_2–GeO_2 particles within the oxygen–hydrogen flame. The concentration of these constituents deposited on the porous preform is controlled by the substrate temperature distribution which can be altered by changing the gas flow conditions. Fibers produced by the VAD process still suffer from some OH impurity content due to the flame hydrolysis and hence very low loss fibers have not been achieved using this method. Nevertheless, fibers with attenuation in the range 0.7 tc 2.0 dB km^{-1} at a wavelength of 1.181 μm have been reported [Ref. 24].

4.4.3 Modified chemical vapour deposition (MCVD)

Chemical vapour deposition techniques are commonly used at very low deposition rates in the semiconductor industry to produce protective SiO_2 films on silicon semiconductor devices. Usually an easily oxidized reagent such as SiH_4 diluted by inert gases and mixed with oxygen is brought into contact with a heated silicon surface where it forms a glassy transparent silica film. This heterogeneous reaction (i.e. requires a surface to take place) was pioneered for the fabrication of optical

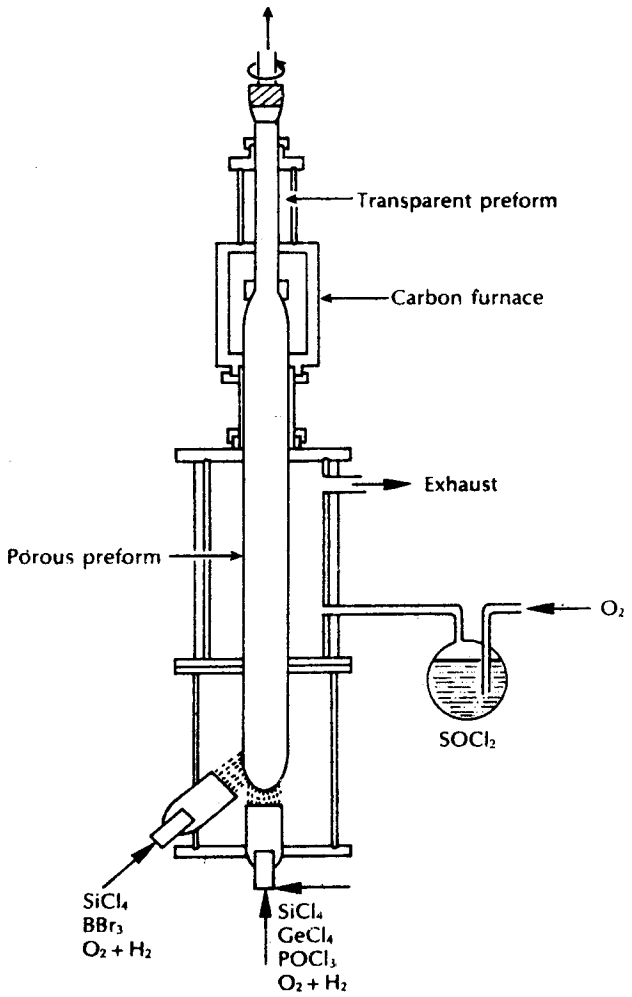

Figure 4.9 The VAD process [Ref. 23].

fibers using the inside surface of a fused quartz tube [Ref. 25]. However, these processes gave low deposition rates and were prone to OH contamination due to the use of hydride reactants. This led to the development of the modified chemical vapour deposition (MCVD) process by Bell Telephone Laboratories [Ref. 26] and Southampton University, UK [Ref. 27], which overcomes these problems and has found widespread application throughout the world.

The MCVD process is also an inside vapour-phase oxidation (IVPO) technique taking place inside a silica tube, as shown in Figure 4.10. However, the vapour-phase reactants (halide and oxygen) pass through a hot zone so that a substantial

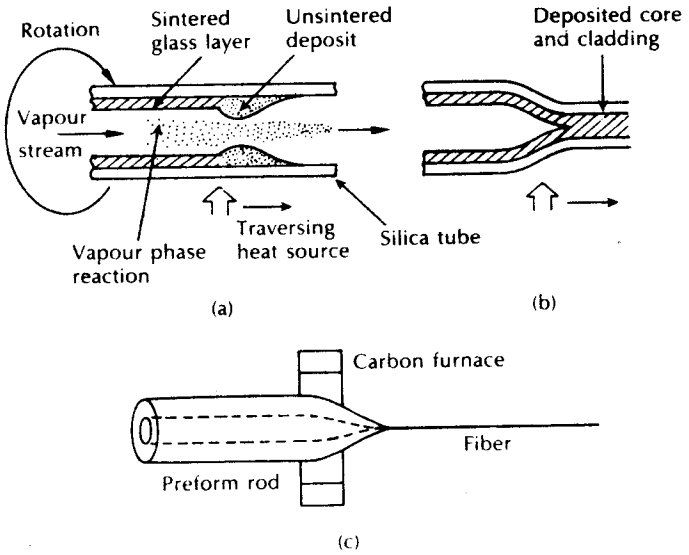

Figure 4.10 Schematic diagram showing the MCVD method for the preparation of optical fibers: (a) deposition; (b) collapse to produce a preform; (c) fiber drawing.

part of the reaction is homogeneous (i.e. involves only one phase; in this case the vapour phase). Glass particles formed during this reaction travel with the gas flow and are deposited on the walls of the silica tube. The tube may form the cladding material but usually it is merely a supporting structure which is heated on the outside by an oxygen–hydrogen flame to temperatures between 1400 °C and 1600 °C. Thus a hot zone is created which encourages high temperature oxidation reactions such as those given in Eqs. (4.2) and (4.3) or (4.4) (not Eq. (4.1)). These reactions reduce the OH impurity concentration to levels below those found in fibers prepared by hydride oxidation or flame hydrolysis.

The hot zone is moved back and forth along the tube allowing the particles to be deposited on a layer by layer basis giving a sintered transparent silica film on the walls of the tube. The film may be up to 10 μm in thickness and uniformity is maintained by rotating the tube. A graded refractive index profile can be created by changing the composition of the layers as the glass is deposited. Usually, when sufficient thickness has been formed by successive traverses of the burner for the cladding, vaporized chlorides of germanium ($GeCl_4$) or phosphorus ($POCl_3$) are added to the gas flow. The core glass is then formed by the deposition of successive layers of germanosilicate or phosphosilicate glass. The cladding layer is important as it acts as a barrier which suppresses OH absorption losses due to the diffusion of OH ions from the silica tube into the core glass as it is deposited. After the deposition is completed the temperature is increased to between 1700 and 1900 °C.

The tube is then collapsed to give a solid preform which may then be drawn into fiber at temperatures of 2000 to 2200 °C as illustrated in Figure 4.10.

This technique is the most widely used at present as it allows the fabrication of fiber with the lowest losses. Apart from the reduced OH impurity contamination the MCVD process has the advantage that deposition occurs within an enclosed reactor which ensures a very clean environment. Hence, gaseous and particulate impurities may be avoided during both the layer deposition and the preform collapse phases. The process also allows the use of a variety of materials and glass compositions. It has produced GeO_2 doped silica single-mode fiber with minimum losses of only 0.2 dB km^{-1} at a wavelength of 1.55 μm [Ref. 28]. More generally, the GeO_2–B_2O_3–SiO_2 system (B_2O_3 is added to reduce the viscosity and assist fining) has shown minimum losses of 0.34 dB km^{-1} with multimode fiber at a wavelength of 1.55 μm [Ref. 29]. Also, graded index germanium phosphosilicate fibers have exhibited losses near the intrinsic level for their composition of 2.8, 0.45 and 0.35 dB km^{-1} at wavelengths of 0.82, 1.3 and 1.5 μm respectively [Ref. 30].

The MCVD process has also demonstrated the capability of producing fibers with very high bandwidths, although still well below the theoretical values which may be achieved. Multimode graded index fibers with measured bandwidth–length products of 4.3 GHz km and 4.7 GHz km at wavelengths of 1.25 and 1.29 μm have been reported [Ref. 31]. Large-scale batch production (30 000 km) of 50 μm core graded index fiber has maintained bandwidth–length products of 825 MHz km and 735 MHz km at wavelengths of 0.825 and 1.3 μm respectively [Ref. 30]. The median attenuation obtained with this fiber was 3.4 dB km^{-1} at 0.825 μm and 1.20 dB km^{-1} at 1.3 μm. Hence, although it is not a continuous process, the MCVD technique has proved suitable for the mass production of high performance optical fiber and is the predominant technique used to prepare polarization maintaining fibers (see Section 3.13.2). Moreover it can be scaled-up to produce preforms which provide 100 to 200 km of fiber [Ref. 21].

4.4.4 Plasma-activated chemical vapour deposition (PCVD)

A variation on the MCVD technique is the use of various types of plasma to supply energy for the vapour-phase oxidation of halides. This method, first developed by Kuppers and Koenings [Ref. 32], involves plasma-induced chemical vapour deposition inside a silica tube, as shown in Figure 4.11. The essential difference between this technique and the MCVD process is the stimulation of oxide formation by means of a nonisothermal plasma maintained at low pressure in a microwave cavity (2.45 GHz) which surrounds the tube. Volatile reactants are introduced into the tube where they react heterogeneously within the microwave cavity, and no particulate matter is formed in the vapour phase.

The reaction zone is moved backwards and forwards along the tube by control of the microwave cavity and a circularly symmetric layer growth is formed. Rotation of the tube is unnecessary and the deposition is virtually 100% efficient. Film deposition can occur at temperatures as low as 500 °C but a high chlorine

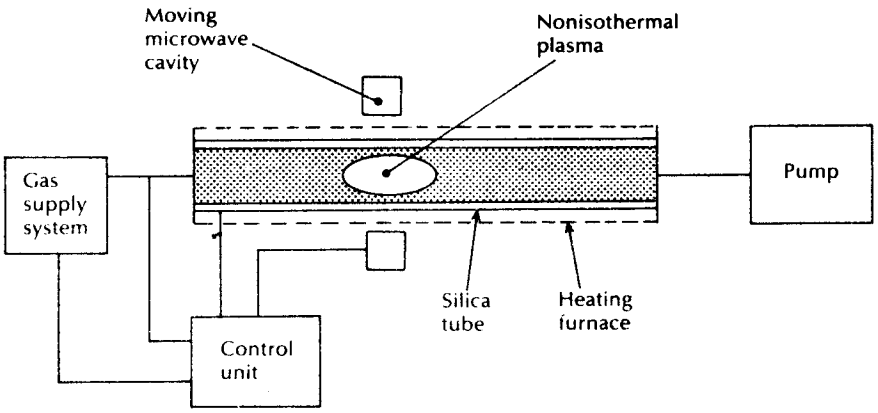

Figure 4.11 The apparatus utilized in the PCVD process.

content may cause expansivity and cracking of the film. Hence the tube is heated to around 1000 °C during deposition using a stationary furnace.

The high deposition efficiency allows the composition of the layers to be accurately varied by control of the vapour-phase reactants. Also, when the plasma zone is moved rapidly backwards and forwards along the tube, very thin layer deposition may be achieved giving the formation of up to 2000 individual layers. This enables very good graded index profiles to be realized which are a close approximation to the optimum near parabolic profile. Thus low pulse dispersion of less than 0.8 ns km^{-1}, for fibers with attenuations of between 3 and 4 dB km^{-1}, at a wavelength of 0.85 μm have been reported [Ref. 2].

A further PCVD technique uses an inductively coupled radiofrequency argon plasma which operates at a frequency of 3.4 MHz [Ref. 33]. The deposition takes place at 1 atmosphere pressure and is predominantly a homogeneous vapour-phase reaction which, via the high temperature discharge, causes the fusion of the deposited material into glass. This technique has proved to have a reaction rate five times faster than the conventional MCVD process. However, fiber attenuation was somewhat higher with losses of 6 dB km^{-1} at a wavelength of 1.06 μm. Variations on this theme operating at frequencies of 3 to 6 MHz and 27 MHz have produced GeO_2–P_2O_5–SiO_2 fibers with minimum losses of 4 to 5 dB km^{-1} at a wavelength of 0.85 μm [Ref. 34]. In addition, fiber attenuation as low as 0.3 dB km^{-1} at a wavelength of 1.55 μm has been obtained for dispersion flattened single-mode fibers (see Section 3.12.2) prepared using a low pressure PCVD process [Ref. 35]. The PCVD process also lends itself to the large scale production of optical fibers with preform sizes which would allow the preparation of over 200 km of fiber [Ref. 36].

4.4.5 Summary of vapour-phase deposition techniques

The salient features of the four major vapour-phase deposition techniques are summarized in Table 4.2 [Ref. 37]. These techniques have all demonstrated

Table 4.2 Summary of vapour-phase deposition techniques used in the preparation of low loss optical fibers

Reaction type	
Flame hydrolysis	OVPO, VAD
High temperature oxidation	MCVD
Low temperature oxidation	PCVD
Depositional direction	
Outside layer deposition	OVPO
Inside layer deposition	MCVD, PCVD
Axial layer deposition	VAD
Refractive index profile formation	
Layer approximation	OVPO, MCVD, PCVD
Simultaneous formation	VAD
Process	
Batch	OVPO, MCVD, PCVD
Continuous	VAD

relatively similar performance for the fabrication of both multimode and single-mode fiber of standard step and graded index designs [Ref. 21]. For the production of polarization maintaining fiber, however, the MCVD and VAD processes have been employed, together with a hybrid MCVD–VAD technique.

4.5 Fluoride glass fibers

Developments in heavy metal fluoride glass fibers for mid-infrared transmission (wavelength range 2 to 5 μm) were outlined in Section 3.7. It was indicated that the fluorozirconate (ZrF_4) and fluorohafnate (HfF_4) glass systems displayed the most promise and had received the greatest attention. In particular, a number of fluorozirconate glasses for fiber production have been investigated, the compositions of which are displayed in Table 4.3 [Ref. 40]. Such glasses have been synthesized from the melt by the same basic techniques as described in Section 4.3 for oxide (i.e. silica) glasses. Preforms for fiber drawing can then be cast from these melts. However, problems have occurred with contamination even using platinum or vitreous carbon crucibles. In addition, it has been found that ZrF_4 tends to be reduced to black ZrF_2 or ZrF_3 which results in melts containing dark particulate matter.

The use of inert glass glove boxes for raw material handling, glass melting and casting helps avoid major oxidation and OH pick-up which causes infrared absorption with the possibility of nucleation and growth of crystals. The latter conditions can also occur in reheating of the glass which is usually required for fiber

Table 4.3 Compositions of the major fluorozirconate glasses currently being employed for the fabrication of optical fibers

	Composition (mol %)							
Glass	ZrF_4	BaF_2	GdF_3	LaF_3	YF_3	AlF_3	LiF	NaF
ZBG	63	33	4	—	—	—	—	—
ZBGA	60	32	4	—	—	4	—	—
ZBLAL	52	20	—	5	—	3	20	—
ZBLYAL	49	22	—	3	3	3	20	—
ZBLAN	51	20	—	4.5	—	4.5	—	20
ZBLYAN	47.5	23.5	—	2.5	2	4.5	—	20

drawing. Typically, the glasses are very fluid at their liquid temperature and exhibit a very rapid decrease in viscosity above the glass transition temperature which results in sensitivity to crystallization and creates a very narrow temperature range for successful fiber drawing [Ref. 21]. Furthermore, oxidizing conditions are often found to be necessary to avoid fluoride reduction. This can be achieved by reactive atmosphere processing (RAP) where traces of CCl_4, SF_6, NF_3 or CS_2 entrained in the inert gaseous atmosphere are employed [Ref. 42].

An alternative approach to the purification of a number of the fluorides required for the preparation of heavy metal fluoride glasses is called chemical vapour purification (CVP) [Ref. 43]. This technique utilizes nonstoichiometric conditions in haloginating the metal. It is anticipated that the products will have transition metal contents close to undetectable levels, or less than 10^{-10} mole fraction of the fluoride. The process uses two sequential vapour-phase reactions to accomplish the preparation. Initially, a direct halogenation of the metal with Cl, Br or I is undertaken to form a volatile halide. Subsequently, this volatile halide is reacted with a fluorinating agent such as HF or SF to form the desired fluoride. This preparation method is considered to be appropriate for fluorides of Zr, Hf, Al, Ga and In [Ref. 44].

Using these purified raw materials and extreme care in handling the glass melting and preform casting it may be feasible to produce sufficiently pure glass to obtain fluorozirconate glass fibers with losses around 0.03 dB km^{-1} at a wavelength of 2.56 μm [Ref. 44]. This overall loss estimate takes into account extrinsic absorption losses together with the intrinsic losses associated with the infrared absorption edge and Rayleigh scattering which alone give the lower figure of 0.01 dB km^{-1} at a wavelength of 2.55 μm. Crucible drawing as well as preform techniques have been employed to prepare the fiber structures. Variations on the conventional double crucible method described in Section 4.3.1 have been proposed to overcome the crystallization and deformation problems which occur with these glasses [Ref.45].

Alternatively, preforms have been made by casting the core and cladding glasses in a mould. One such process is illustrated in Figure 4.12 where the cladding glass

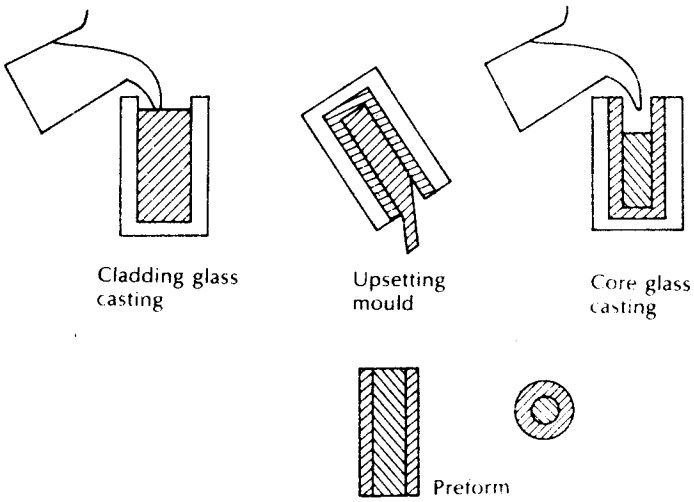

Figure 4.12 Schematic representation of the built-in casting technique for heavy metal fluoride glass preparation [Ref. 46].

is initially poured into the heated mould maintained near the glass transition temperature [Ref. 46]. The mould is then inverted allowing the unsolidified glass to flow out. Core glass is then poured into the hollow centre region and the entire structure is annealed to produce the core–cladding preform. Moreover, a rotational casting technique [Ref. 47] has provided improvements in preform uniformity and a reduction in the contamination obtained at the core–cladding interface. As indicated previously, fiber drawing from the preform requires stringent control of the hot zone and its temperature to avoid nucleation and growth of crystals. Drawing temperatures in the range 300 to 400 °C are generally used. Furthermore, since the glasses are hydroscopic and reactive with water and oxygen at these temperatures, then controlled atmospheres must be employed.

Following the achievements with low loss silica fiber preparation using chemical vapour deposition synthesis techniques (see Section 4.4), such approaches are also being investigated for the production of fluoride glass fibers [Ref. 44]. Unfortunately, whilst vapour-phase processing of silicate glasses is able to benefit from the large differential vapour pressure of the reagents used to prepare the glasses relative to the impurities contained within the raw materials, similar vapour-phase processing advantages do not exist at present for fluorozirconate glasses. Moreover, the complexity of the glass compositions creates a severe constraint to vapour-phase techniques and hence little progress has been reported [Ref. 21].

4.6 Optical fibers

In order to plan the use of optical fibers in a variety of line communication applications it is necessary to consider the various optical fibers currently available.

The following is a summary of the dominant optical fiber types with an indication of their general characteristics. The performance characteristics of the various fiber types discussed vary considerably depending upon the materials used in the fabrication process and the preparation technique involved. The values quoted are based upon both manufacturers' and suppliers' data, and practical descriptions [Refs. 48 to 52] for commercially available fibers, presented in a general form rather than for specific fibers. Hence in some cases the fibers may appear to have somewhat poorer performance characteristics than those stated for the equivalent fiber types produced by the best possible techniques and in the best possible conditions which were indicated in Chapter 3. It is interesting to note, however, that although the high performance values quoted in Chapter 3 were generally for fibers produced and tested in the laboratory, the performance characteristics of commercially available fibers in many cases are now quite close to these values. This factor is indicative of the improvements made over recent years in the fiber materials preparation and fabrication technologies.

This section therefore reflects the relative maturity of the technology associated with the production of both multicomponent and silica glass fibers. In particular, high performance silica-based fibers for operation in three major wavelength regions (0.8 to 0 9, 1.3 and 1.55 μm) are now widely commercially available. Moreover, complex refractive index profile single-mode fibers, including dispersion modified fibers (see Section 3.12) and polarization maintaining fibers (see Section 3.13.2), are also commercially available and in the former case are starting to find system application within communications. Nevertheless, in this section we concentrate on the conventional circularly symmetric step index design which remains at present the major single-mode fiber provision within telecommunications.

Another relatively new area of commercial fiber development is concerned with mid-infrared wavelength range (2 to 5 μm), often employing heavy metal fluoride glass technology. However, the fiber products that exist for this wavelength region tend to be multimode with relatively high losses* and hence at present are only appropriate for specialized applications. Such fibers are therefore considered no further in this section. Finally, it should be noted that the bandwidths quoted are specified over a 1 km length of fiber (i.e. $B_{opt} \times L$). These are generally obtained from manufacturers' data which does not always indicate whether the electrical or the optical bandwidth has been measured. It is likely that these are in fact optical bandwidths which are significantly greater than their electrical equivalents (see Section 7.4.3).

4.6.1 Multimode step index fibers

Multimode step index fibers may be fabricated from either multicomponent glass compounds or doped silica. These fibers can have reasonably large core diameters and large numerical apertures to facilitate efficient coupling to incoherent light

* For example, the loss obtained at a wavelength of 2.6 μm with a commercially available multimode step index zirconium fluoride glass fiber is 20 dB km^{-1}

sources such as light emitting diodes (LEDs). The performance characteristics of this fiber type may vary considerably depending on the materials used and the method of preparation; the doped silica fibers exhibit the best performance. Multicomponent glass and doped silica fibers are often referred to as multicomponent glass/glass (glass-clad glass) and silica/silica (silica-clad silica), respectively, although the glass-clad glass terminology is sometimes used somewhat vaguely to denote both types. A typical structure for a glass multimode step index fiber is shown in Figure 4.13.

Structure

Core diameter:	50 to 400 μm
Cladding diameter:	125 to 500 μm
Buffer jacket diameter:	250 to 1000 μm
Numerical aperture:	0.16 to 0.5.

Performance characteristics

Attenuation: 2.6 to 50 dB km^{-1} at a wavelength of 0.85 μm, limited by absorption or scattering. The wide variation in attenuation is due to the large differences both within and between the two overall preparation methods (melting and deposition). To illustrate this point Figure 4.14 shows the attenuation spectra from suppliers' data [Ref. 48] for a multicomponent glass fiber (glass-clad glass) and a doped silica fiber (silica-clad silica). It may be observed that the multicomponent glass fiber has an attenuation of around 40 dB km^{-1} at a wavelength of 0.85 μm, whereas the doped silica fiber has an attenuation of less than 5 dB km^{-1} at a similar wavelength. Furthermore, at a wavelength of 1.3 μm losses reduced to around 0.4 dB km^{-1} can be obtained [Ref. 49].

Bandwidth: 6 to 50 MHz km.

Applications: These fibers are best suited for short-haul, limited bandwidth and relatively low cost applications.

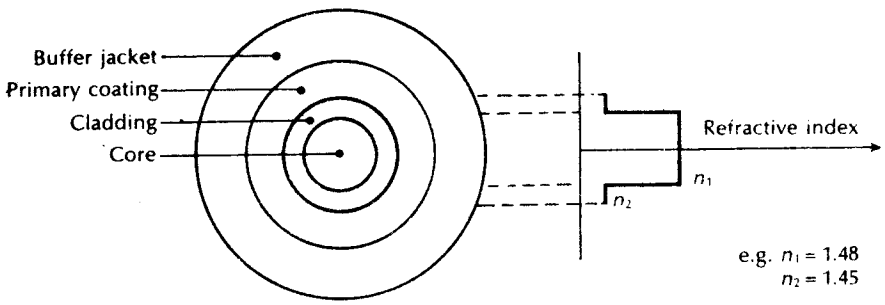

Figure 4.13 Typical structure for a glass multimode step index fiber.

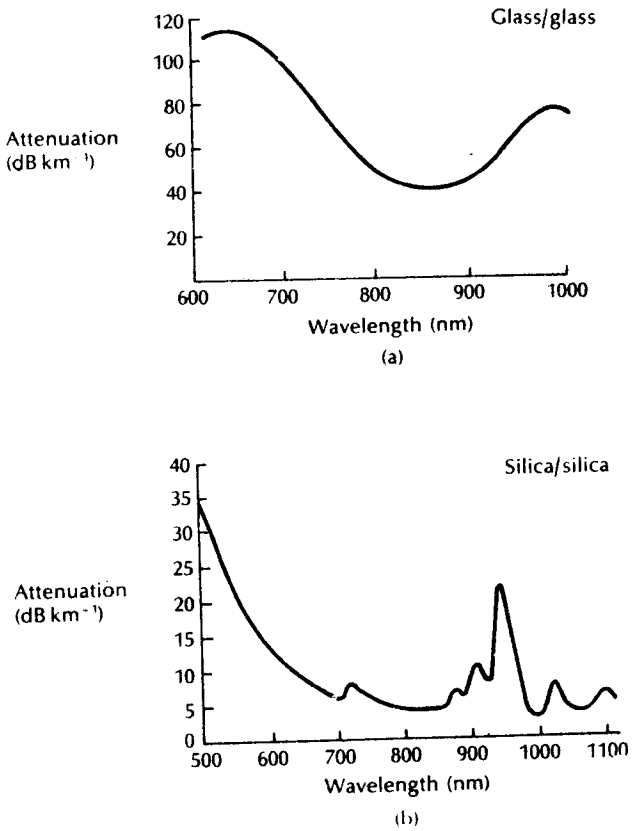

Figure 4.14 Attenuation spectra for multimode step index fibers: (a) multicomponent glass fiber; (b) doped silica fiber. Reproduced with the permission of Rayproof.

4.6.2 Multimode graded index fibers

These multimode fibers which have a graded index profile may also be fabricated using multicomponent glasses or doped silica. However, they tend to be manufactured from materials with higher purity than the majority of multimode step index fibers in order to reduce fiber losses. The performance characteristics of multimode graded index fibers are therefore generally better than those for multimode step index fibers due to the index grading and lower attenuation. Multimode graded index fibers tend to have smaller core diameters than multimode step index fibers, although the overall diameter including the buffer jacket is usually about the same. This gives the fiber greater rigidity to resist bending. A typical structure is illustrated in Figure 4.15.

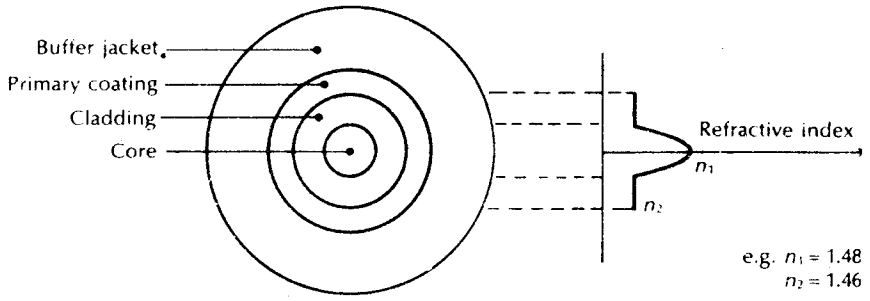

Figure 4.15 Typical structure for a glass multimode graded index fiber.

Structure

Core diameter:	30 to 100 μm.
Cladding diameter:	100 to 150 μm,
Buffer jacket diameter:	250 to 1000 μm.
Numerical aperture:	0.2 to 0.3.

Although the above general parameters encompass most of currently available multimode graded index fibers, in particular the following major groups have now emerged:

1. 50 μm/125 μm (core–cladding) diameter fibers with typical numerical apertures between 0.20 and 0.24. These fibers were originally developed and standardized by the CCITT (Recommendation G. 651) for telecommunication applications at wavelengths of 0.85 and 1.3 μm but now they are mainly utilized within data links and local area networks (LANs).
2. 62.5 μm/125 μm (core–cladding) diameter fibers with typical numerical apertures between 0.26 and 0.29. Although these fibers were developed for longer distance subscriber loop applications at operating wavelengths of 0.85 and 1.3 μm, they are now mainly used within LANs (see Section 14.7).
3. 85 μm/125 μm (core/cladding) diameter fibers with typical numerical apertures 0.26 and 0.30. These fibers were developed for operation at wavelengths of 0.85 and 1.3 μm in short-haul systems and LANs.
4. 100 μm/125 μm (core–cladding) diameter fibers with a numerical aperture of 0.29. These fibers were developed to provide high coupling efficiency to LEDs at a wavelength of 0.85 μm in low cost, short distance applications. They can, however, be utilized at the 1.3 μm operating wavelength and have therefore also found application within LANs.

Performance characteristics

Attenuation: 2 to 10 dB km^{-1} at a wavelength of 0.85 μm with generally a scattering limit. Average losses of around 0.4 and 0.25 dB km^{-1} can be obtained at wavelengths of 1.3 and 1.55 μm respectively [Ref. 49].

Bandwidth: 300 MHz km to 3 GHz km.
Applications: These fibers are best suited for medium-haul, medium to high bandwidth applications using incoherent and coherent multimode sources (i.e. LEDs and injection lasers respectively).

It is useful to note that there are a number of partially graded index fibers commercially available. These fibers generally exhibit slightly better performance characteristics than corresponding multimode step index fibers but are somewhat inferior to the fully graded index fibers described above.

4.6.3 Single-mode fibers

Single-mode fibers can have either a step index or graded index profile. The benefits of using a graded index profile are to provide dispersion modified single-mode fibers (see Section 3.12). The more sophisticated single-mode fiber structures used to produce polarization maintaining fibers (see Section 3.13.2) make these fibers quite expensive at present and thus they are not generally utilized within optical fiber communication systems. Therefore at present, commercially available single-mode fibers are still usually step index. They are high quality fibers for wideband, long-haul transmission and are generally fabricated from doped silica (silica-clad silica) in order to reduce attenuation.

Although single-mode fibers have small core diameters to allow single-mode propagation, the cladding diameter must be at least ten times the core diameter to avoid losses from the evanescent field. Hence with a buffer jacket to provide protection and strength, single-mode fibers have similar overall diameters to multimode fibers. A typical example of a single-mode step index fiber is shown in Figure 4.16.

Structure
Core diameter 5 to 10 μm, typically around 8.5 μm
Cladding diameter: generally 125 μm
Buffer jacket diameter: 250 to 1000 μm
Numerical aperture: 0.08 to 0.15, usually around 0.10.

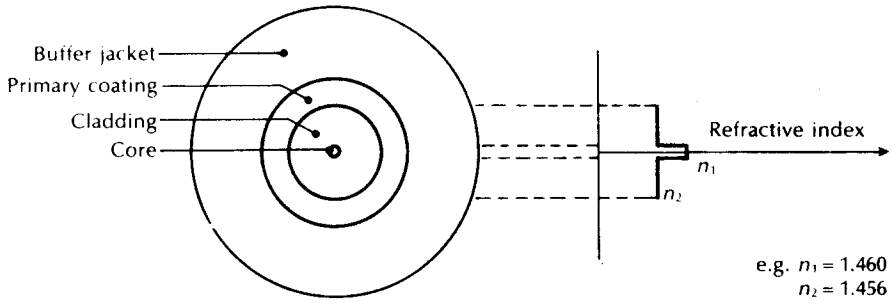

Figure 4.16 Typical structure for a silica single-mode step index fiber.

Performance characteristics

2 to 5 dB km^{-1} with a scattering limit of around 1 dB km^{-1} at a wavelength of 0.85 μm. In addition, average losses of 0.35 and 0.21 dB km^{-1} at wavelengths of 1.3 and 1.55 μm can be obtained in a manufacturing environment.

Bandwidth: Greater than 500 MHz km. In theory the bandwidth is limited by waveguide and material dispersion to approximately 40 GHz km at a wavelength of 0.85 μm. However, practical bandwidths in excess of 10 GHz km are obtained at a wavelength of 1.3 μm.

Applications: These fibers are ideally suited for high bandwidth very long-haul applications using single-mode injection laser sources.

4.6.4 Plastic-clad fibers

Plastic-clad fibers are multimode and have either a step index or a graded index profile. They have a plastic cladding (often a silicone rubber) and a glass core which is frequently silica (i.e. plastic clad silica—PCS fibers). The PCS fibers exhibit lower radiation-induced losses than silica-clad silica fibers and, therefore, have an improved performance in certain environments. Plastic-clad fibers are generally slightly cheaper than the corresponding glass fibers, but usually have more limited performance characteristics. A typical structure for a step index plastic-clad fiber (which is more common) is shown in Figure 4.17.

Structure

Core diameter:	Step index	100 to 500 μm
	Graded index	50 to 100 μm
Cladding diameter:	Step index	300 to 800 μm
	Graded index	125 to 150 μm
Buffer jacket diameter:	Step index	500 to 1000 μm
	Graded index	250 to 1000 μm
Numerical aperture:	Step index	0.2 to 0.5
	Graded index	0.2 to 0.3.

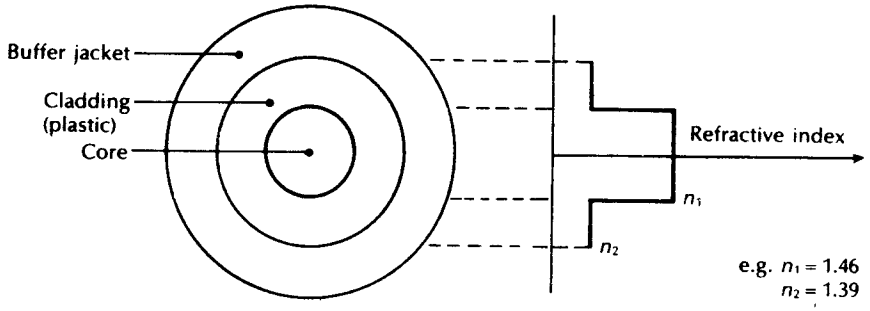

Figure 4.17 Typical structure for a plastic-clad silica multimode step index fiber.

Performance characteristics

Attenuation:	Step index	5 to 50 dB km^{-1}
	Graded index	4 to 15 dB km^{-1}.

4.6.5 All-plastic fibers

All-plastic or polymeric fibers are exclusively of the multimode step index type with large core and cladding diameters. Hence there is a reduced requirement for a buffer jacket for fiber protection and strengthening. These fibers are usually cheaper to produce and easier to handle than the corresponding silica-based glass variety. However, their performance (especially for optical transmission in the infrared) is restricted, giving them limited use in communication applications. All plastic fibers, however, generally have large numerical apertures which allow easier coupling of light into the fiber from a multimode source.

Early plastic fibers fabricated with a polymethyl methacrylate (PMMA) and a fluorinated acrylic cladding exhibited losses around 500 dB km^{-1}. Subsequently, a continuous casting process was developed for PMMA and losses as low as 110 dB km^{-1} were achieved in the visible wavelength region. The loss mechanisms in PMMA and polystyrene core fibers are similar to those in glass fibers. These fibers exhibit both intrinsic and extrinsic loss mechanisms including absorption and Rayleigh scattering which results from density fluctuations and the anisotropic structure of the polymers. Significant absorption occurs due to the long wavelength tail caused by the intrinsic effect, but this can be relatively small over the 0.5 to 0.9 μm wavelength range where these fibers tend to be utilized. Moreover, extrinsic absorption results from transition metal and organic contaminants as well as overtone bands from the OH ion.

Although substantial progress in the fabrication of higher performance plastic fibers has been made over recent years with losses as low as 20 dB km^{-1} being obtained in the laboratory for PMMA core fiber operating at a wavelength of 0.68 μm [Ref. 21], it is clearly the case that such fibers will not compete with doped silica fibers in any other than the very short distance applications. Current work, however, is focusing on improving their environmental performance, in particular at higher temperatures, as well as their chemical durability and mechanical properties to enhance their use as lower performance fibers for harsh conditions. A typical all-plastic fiber structure is illustrated in Figure 4.18.

Structure

Core diameter:	200 to 600 μm
Cladding diameter:	450 to 1000 μm
Numerical aperture:	0.5 to 0.6.

Performance characteristics

Attenuation:	50 to 1000 dB km^{-1} at a wavelength of 0.65 μm.
Bandwidth:	This is not usually specified as transmission is generally limited to tens of metres.

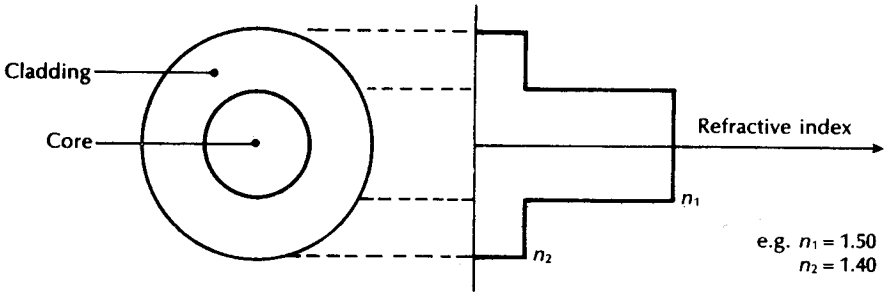

Figure 4.18 Typical structure for an all-plastic fiber.

Applications: These fibers can only be used for very short-haul (i.e. 'in-house') low cost links. However, fiber coupling and termination are relatively easy and do not require sophisticated techniques.

4.7 Optical fiber cables

It was indicated in Section 4.1 that if optical fibers are to be alternatives to electrical transmission lines it is imperative that they can be safely installed and maintained in all the environments (e.g. underground ducts) in which metallic conductors are normally placed. Therefore, when optical fibers are to be installed in a working environment their mechanical properties are of prime importance. In this respect the unprotected optical fiber has several disadvantages with regard to its strength and durability. Bare glass fibers are brittle and have small cross sectional areas which make them very susceptible to damage when employing normal transmission line handling procedures. It is therefore necessary to cover the fibers to improve their tensile strength and to protect them against external influences. This is usually achieved by surrounding the fiber with a series of protective layers, which is referred to as coating and cabling. The initial coating of plastic with high elastic modulus is applied directly to the fiber cladding, as illustrated in Section 4.6. It is then necessary to incorporate the coated and buffered fiber into an optical cable to increase its resistance to mechanical strain and stress as well as adverse environmental conditions.

The functions of the optical cable may be summarized into four main areas. These are as follows:

1. Fiber protection. The major function of the optical cable is to protect against fiber damage and breakage both during installation and throughout the life of the fiber.
2. Stability of the fiber transmission characteristics. The cabled fiber must have good stable transmission characteristics which are comparable with the uncabled

fiber. Increases in optical attenuation due to cabling are quite usual and must be minimized within the cable design.

3. Cable strength. Optical cables must have similar mechanical properties to electrical transmission cables in order that they may be handled in the same manner. These mechanical properties include tension, torsion, compression, bending, squeezing and vibration. Hence the cable strength may be improved by incorporating a suitable strength member and by giving the cable a properly designed thick outer sheath.
4. Identification and jointing of the fibers within the cable. This is especially important for cables including a large number of optical fibers. If the fibers are arranged in a suitable geometry it may be possible to use multiple jointing techniques rather than jointing each fiber individually.

In order to consider the cabling requirements for fibers with regard to (1) and (2), it is necessary to discuss the fiber strength and durability as well as any possible sources of degradation of the fiber transmission characteristics which are likely to occur due to cabling.

4.7.1 Fiber strength and durability

Optical fibers for telecommunications usage are almost exclusively fabricated from silica or a compound of glass (multicomponent glass). These materials are brittle and exhibit almost perfect elasticity until their breaking point is reached. The bulk material strength of flawless glass is quite high and may be estimated for individual materials using the relationship [Ref. 51]:

$$S_t = \left(\frac{\gamma_p E}{4l_a}\right)^{\frac{1}{2}} \tag{4.6}$$

where S_t is the theoretical cohesive strength, γ_p is the surface energy of the material, E is Young's modulus for the material (stress/strain), and l_a is the atomic spacing or bond distance. However, the bulk material strength may be drastically reduced by the presence of surface flaws within the material.

In order to treat surface flaws in glass analytically, the Griffith theory [Ref. 56] is normally used. This theory assumes that the surface flaws are narrow cracks with small radii of curvature at their tips, as illustrated in Figure 4.19. It postulates that the stress is concentrated at the tip of the crack which leads to crack growth and eventually catastrophic failure. Figure 4.19 shows the concentration of stress lines at the crack tip which indicates that deeper cracks have higher stress at their tips. The Griffith theory gives a stress intensity factor K_I as:

$$K_I = SYC^{\frac{1}{2}} \tag{4.7}$$

where S is the macroscopic stress on the fiber, Y is a constant dictated by the shape of the crack (e.g. $Y = \pi^{\frac{1}{2}}$ for an elliptical crack, as illustrated in Figure 4.19) and C is the depth of the crack (this is the semimajor axis length for an elliptical crack).

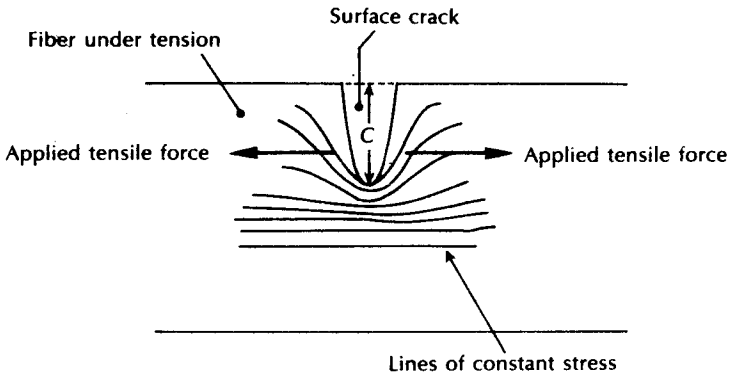

Figure 4.19 An elliptical surface crack in a tensioned optical fiber.

Further, the Griffith theory gives an expression for the critical stress intensity factor K_{IC} where fracture occurs as:

$$K_{IC} = (2E\gamma_p)^{\frac{1}{2}} \tag{4.8}$$

Combining Eqs. (4.7) and (4.8) gives the Griffith equation for fracture stress of a crack S_f as:

$$S_f = \left(\frac{2E\gamma_p}{Y^2C}\right)^{\frac{1}{2}} \tag{4.9}$$

It is interesting to note that S_f is proportional to $C^{-\frac{1}{2}}$. Therefore, S_f decreases by a factor of 2 for a fourfold increase in the crack depth C.

Example 4.1

The Si—O bond has a theoretical cohesive strength of 2.6×10^6 psi which corresponds to a bond distance of 0.16 nm. A silica optical fiber has an elliptical crack of depth 10 nm at a point along its length. Estimate

(a) the fracture stress in psi for the fiber if it is dependent upon this crack:
(b) the percentage strain at the break.

Young's modulus for silica is approximately $9 \times 10^{10}\,\mathrm{N\,m^{-2}}$ and 1 psi $\equiv 6894.76\,\mathrm{N\,m^{-2}}$.

Solution: (a) Using Eq. (4.6), the theoretical cohesive strength for the Si—O bond is:

$$S_t = \left(\frac{\gamma_p E}{4l_a}\right)^{\frac{1}{2}}$$

Hence

$$\gamma_p = \frac{4l_a S_f^2}{E} = \frac{4 \times 0.16 \times 10^{-9}(2.6 \times 10^6 \times 6894.76)^2}{9 \times 10^{10}}$$

$$= 2.29 \text{ J}$$

The fracture stress for the silica fiber may be obtained from Eq. (4.9) where:

$$S_f = \left(\frac{2E\gamma_p}{Y^2 C}\right)^{\frac{1}{2}}$$

For an elliptical crack:

$$S_f = \left(\frac{2E\gamma_p}{\pi C}\right)^{\frac{1}{2}} = \left(\frac{2 \times 9 \times 10^{10} \times 2.29}{\pi \times 10^{-8}}\right)^{\frac{1}{2}}$$

$$= 3.62 \times 10^9 \text{ N m}^{-1}$$

$$= 5.25 \times 10^5 \text{ psi}$$

It may be noted that the fracture stress is reduced from the theoretical value for flawless silica of 2.6×10^6 psi by a factor of approximately 5.

(b) Young's modulus is defined as:

$$E = \frac{stress}{strain}$$

Therefore

$$strain = \frac{stress}{E} = \frac{S_f}{E} = \frac{3.62 \times 10^9}{9 \times 10^{10}} = 0.04$$

Hence the strain at the break is 4%, which corresponds to the change in length over the original length for the fiber.

In Example 4.1 we considered only a single crack when predicting the fiber fracture. However, when a fiber surface is exposed to the environment and is handled, many flaws may develop. The fracture stress of a length of fiber is then dependent upon the dominant crack (i.e. the deepest) which will give a fiber fracture at the lowest strain. Hence, the fiber surface must be protected from abrasion in order to ensure high fiber strength. A primary protective plastic coating is usually applied to the fiber at the end of the initial production process so that mechanically induced flaws may be minimized. Flaws also occur due to chemical and structural causes. These flaws are generally smaller than the mechanically induced flaws and may be minimized within the fiber fabrication process.

There is another effect which reduces the fiber fracture stress below that predicted by the Griffith equation. It is due to the slow growth of flaws under the action of stress and water and is known as stress corrosion. Stress corrosion occurs because

the molecular bonds at the tip of the crack are attacked by water when they are under stress. This causes the flaw to grow until breakage eventually occurs. Hence stress corrosion must be taken into account when designing and testing optical fiber cables. It is usual for optical fiber cables to have some form of water-protective barrier, as is the case for most electrical cable designs.

In order to predict the life of practical optical fibers under particular stresses it is necessary to use a technique which takes into account the many flaws a fiber may possess, rather than just the single surface flaw considered in Example 4.1. This is approached using statistical methods due to the nature of the problem which involves many flaws of varying depths over different lengths of fiber.

Calculations of strengths of optical fibers are usually conducted using Weibull statistics [Ref. 57] which describe the strength behaviour of a system that is dependent on the weakest link within the system. In the case of optical fibers this reflects fiber breakage due to the dominant or deepest crack. The empirical relationship established by Weibull and applied to optical fibers indicates that the probability of failure F at a stress S is given by:

$$F = 1 - \exp\left[-\left(\frac{S}{S_0}\right)^m \left(\frac{L}{L_0}\right)\right] \tag{4.10}$$

where m is the Weibull distribution parameter, S_0 is a scale parameter, L is the fiber length and L_0 is a constant with dimensions of length.

The expression given in Eq. (4.10) may be plotted for a fiber under test by breaking a large number of 10 to 20 m fiber lengths and measuring the strain at the break. The various strains are plotted against the cumulative probability of their occurrence to give the Weibull plot as illustrated in Figure 4.20 [Ref. 58]. It may be observed from Figure 4.20 that most of the fiber tested breaks at strain due to the prevalence of many shallow surface flaws. However, some of the fiber tested contains deeper flaws (possibly due to external damage) giving the failure at lower

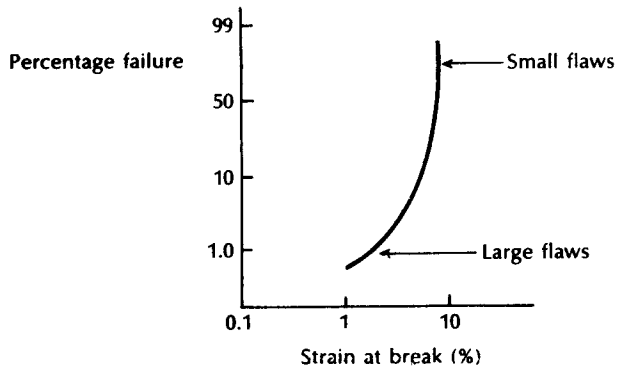

Figure 4.20 A schematic representation of a Weibull plot. Reproduced with permission from M. H. Reeve. *The Radio and Electron. Eng.*, **51**, p. 327.

strain depicted by the tail of the plot. This reduced strength region is of greatest interest when determining the fiber's lifetime under stress.

Finally, the additional problem of stress corrosion must be added to the information on the fiber under stress gained from the Weibull plot. The stress corrosion is usually predicted using an empirical relationship for the crack velocity v_c in terms of the applied stress intensity factor K_I, where [Ref. 58]:

$$v_c = AK_I^n \tag{4.11}$$

The constant n is called the stress corrosion susceptibility (typically in the range 15 to 50 for glass), and A is also a constant for the fiber material. Equation (4.11) allows estimation of the time to failure of a fiber under stress corrosion conditions. Therefore, from a combination of fiber testing (Weibull plot) and stress corrosion, information estimates of the maximum allowable fiber strain can be made available to the cable designer. These estimates may be confirmed by straining the fiber up to a specified level (proof testing) such as 1% strain. Fiber which survives this test can be accepted. However, proof testing presents further problems, as it may cause fiber damage. Also, it is necessary to derate the maximum allowable fiber strain from the proof test value to increase confidence in fiber survival under stress conditions. It is suggested [Ref. 58] that a reasonable derating for use by the cable designer for fiber which has survived a 1% strain proof test is around 0.3% in order that the fiber has a reasonable chance of surviving with a continuous strain for twenty years.

4.8 Stability of the fiber transmission characteristics

Optical fiber cables must be designed so that the transmission characteristics of the fiber are maintained after the cabling process and cable installation. Therefore, potential increases in the optical attenuation and reduction in the bandwidth of the cabled fiber should be avoided.

Certain problems can occur either within the cabling process or subsequently which can significantly affect the fiber transmission characteristics. In particular, a problem which often occurs in the cabling of optical fiber is the meandering of the fiber core axis on a microscopic scale within the cable form. This phenomenon, known as microbending, results from small lateral forces exerted on the fiber during the cabling process and it causes losses due to radiation in both multimode and single-mode fibers.

In addition to microbending losses caused by fiber stress and deformation on a micron scale, macrobending losses occur when the fiber cable is subjected to a significant amount of bending above a critical value of curvature. Such fiber bend losses are discussed in Section 3.6. However, additional optical losses can occur when fiber cables are *in situ*. These losses may result from hydrogen absorption by the fiber material or from exposure of the fiber cable to ionizing radiation. The above phenomena are discussed in this section in order to provide an insight into

the problems associated with the stability of the cabled fiber transmission characteristics.

4.8.1 Microbending

Microscopic meandering of the fiber core axis, known as microbending, can be generated at any stage during the manufacturing process, the cable installation process or during service. This is due to environmental effects, particularly temperature variations causing differential expansion or contraction [Ref. 59]. Microbending introduces slight surface imperfections which can cause mode coupling between adjacent modes, which in turn creates a radiative loss which is dependent on the amount of applied fiber deformation, the length of fiber, and the exact distribution of power among the different modes.

It has become accepted to consider, in particular, two forms of modal power distribution. The first form occurs when a fiber is excited by a diffuse Lambertian source, launching all possible modes, and is referred to as a uniform, or fully filled mode distribution. The second form occurs when, due to a significant amount of mode coupling and mode attenuation, the distribution of optical power becomes essentially invariant with the distance of propagation along the fiber. This second distribution is generally referred to as a steady state, or equilibrium mode distribution, which typically occurs after transmission over approximately one kilometre of fiber (see Section 13.1).

Since microbending losses are mode dependent and from Eq. (2.69) the number of modes is an inverse function of the wavelength of the transmitted light within a particular fiber, it is to be expected that microbending losses will be wavelength dependent. This effect is demonstrated for multimode fiber in Figure 4.21 [Ref. 60], which illustrates the theoretical microbending loss for both the uniform and the steady state mode distributions as a function of applied linear pressure (i.e. simulated microbending), for a normalized frequency $V = 39$, corresponding to a wavelength of 0.82 μm and $V = 21$, corresponding to a wavelength of 1.55 μm. It may be observed from Figure 4.21 that the microbending loss decreases at longer wavelengths, and that it is also dependent on the modal power distribution present within the fiber; microbending losses corresponding to a uniform power distribution being approximately 1.75 times greater than those obtained with a steady state distribution. In addition it has been predicted [Ref. 61] that microbending losses for single-mode fiber follow an approximately exponential form, with increasing losses at longer wavelengths. Minimal losses were predicted at operating wavelengths below 1.3 μm, with a rapid rise in attenuation at wavelengths above 1.5 μm. Experimental measurements have confirmed these predictions.

It is clear that excessive microbending can create additional fiber losses to an unacceptable level. To avoid deterioration in the optical fiber transmission characteristics resulting from mode coupling induced microbending, it is important that the fiber is free from irregular external pressure within the cable. Carefully

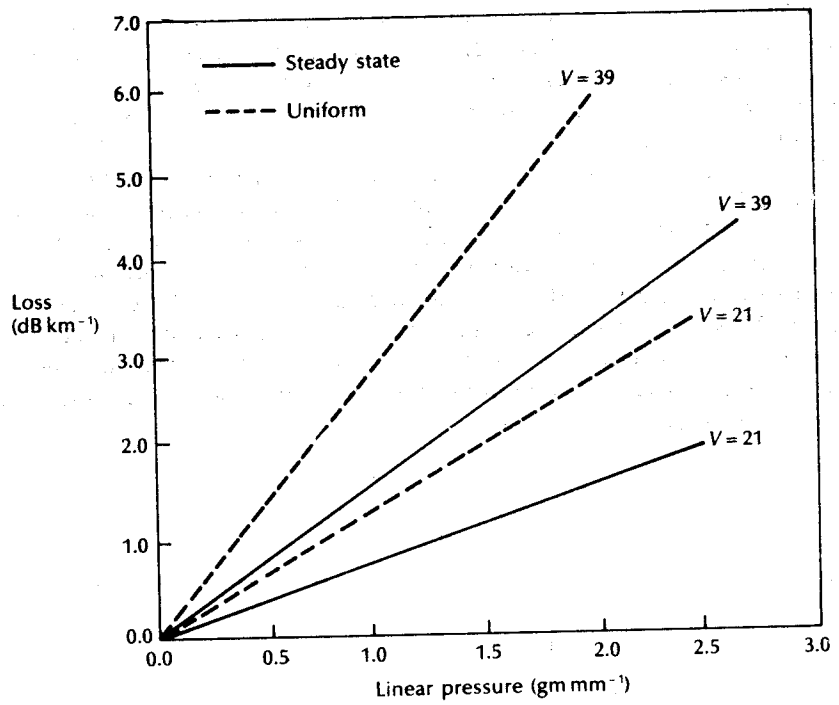

Figure 4.21 Theoretical microbending loss versus linear pressure for graded index multimode fibers ($NA = 0.2$, core diameter of 50 μm. Reproduced with permission from S. Das, C. G. Englefield and P. A. Goud, *Appl. Opt.*, **24**, p. 2323, 1985.

controlled coating and cabling of the fiber is therefore essential in order to minimize the cabled fiber attenuation. Furthermore, the fiber cabling must be capable of maintaining this situation under all the strain and environmental conditions envisaged in its lifetime.

4.8.2 Hydrogen absorption

The diffusion of hydrogen into optical fiber has been shown to affect the spectral attenuation characteristic [Ref. 62]. There are two fundamental mechanisms by which hydrogen absorption causes an increase in optical fiber losses [Ref. 59]. The first is where hydrogen diffuses into interstitial spaces in the glass, thereby altering the spectral loss characteristics through the formation of new absorption peaks. This phenomenon has been found to affect all silica-based glass fibers, both multimode and single-mode. However, the extra losses obtained can be reversed if the hydrogen source is removed. Typically, it causes losses in the range 0.2 to

0.3 dB km^{-1} Atm^{-1} at an optical wavelength of 1.3 μm and a temperature of 25 °C with 500 hours exposure [Ref. 62]. At higher temperatures these additional losses may be substantially increased, as can be observed from Figure 4.22, which displays the change in spectral attenuation obtained for a fiber with 68 hours' hydrogen exposure at a temperature of 150 °C [Ref. 63].

The second mechanism occurs when hydrogen reacts with the fiber deposits to give P–OH, Ge–OH or Si–OH absorption. These losses are permanent and can be greater than 25 dB km^{-1} [Ref. 59]. Studies suggest that hydrogen can be generated by either chemical decomposition of the fiber coating materials or through metal–electrolytic action (that is, moisture affecting the metal sheathing of the fiber cable). These effects can be minimized by careful selection of the cable, the prevention of immersion of the cable in water, or by pressurizing the cable to prevent water ingress. Alternatively, the fiber cable may be periodically purged using an inert gas.

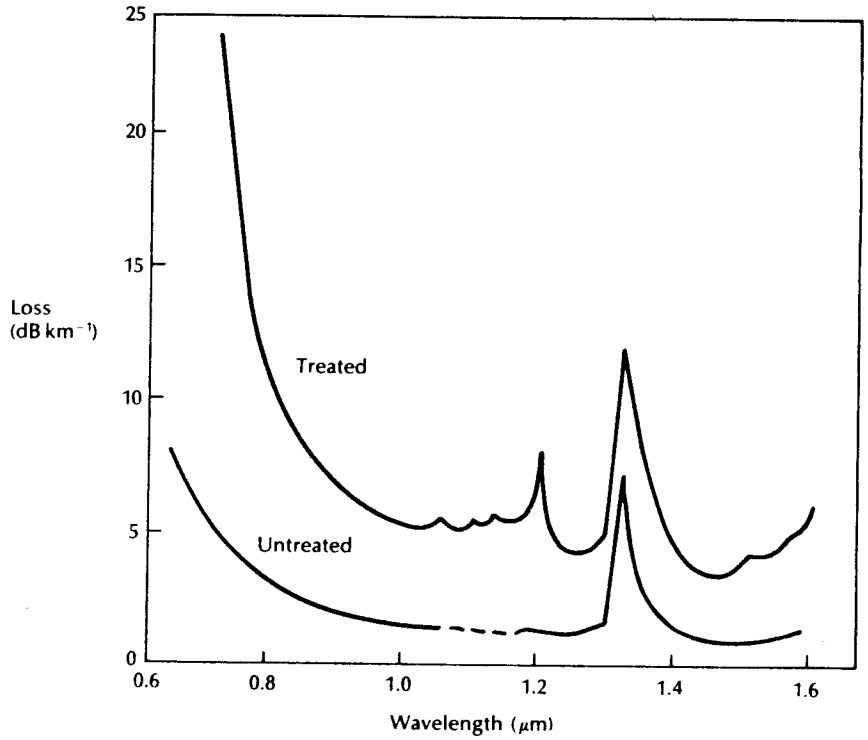

Figure 4.22 Attenuation spectra for multimode fiber before (untreated) and after (treated) hydrogen diffusion [Ref. 63].

4.8.3 Nuclear radiation exposure

The optical transmission characteristics of fiber cables can be seriously degraded by exposure to nuclear radiation. Such radiation forms colour centres in the fiber core which can cause spectral attenuation [Ref. 64]. The precise nature of this attenuation depends upon a number of factors including: fiber parameters such as structure; core and cladding material composition; system parameters such as optical intensity and wavelength as well as temperature; and radiation parameters such as total dose, dose rate and energy levels, together with the length of recovery time allowed. The radiation-induced attenuation comprises a permanent component which is irreversible, and a metastable component which is reversible and contains both a transient (with decay time less than 1 s) and steady state (with decay time less than 10 s) constituents. The nature of both the permanent and decaying components of the attenuation are dependent on the fiber composition.

Typical measured spectral loss characteristics for two single-mode fibers, following exposure to a 10 k rad dose of steady state radiation for 1 hour, are shown in Figure 4.23 [Ref. 64]. The Corning fiber under test had a Ge doped silica core and a pure silica cladding, whereas the Dainichi fiber had a pure silica core and

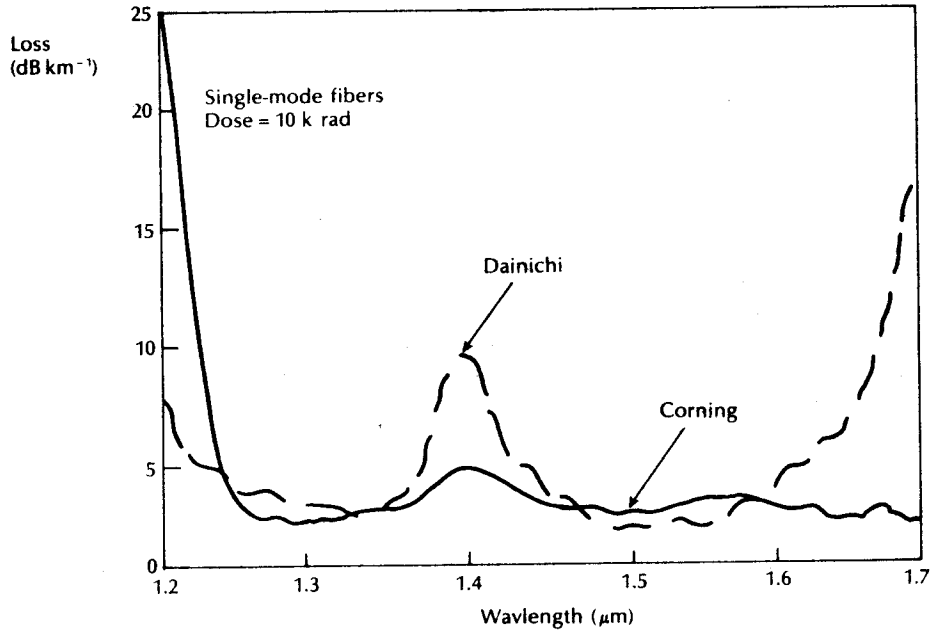

Figure 4.23 Effect of nuclear radiation on the spectral attenuation characteristics of two single-mode fibers. Reproduced with permission from E. J. Friebele, K. J. Long, C. G. Askins, M. E. Gingerich, M. J. Marrone and D. L. Griscom, 'Overview of radiation effects in fiber optics', *Proc. SPIE, Int. Soc. Opt. Eng., Radiation Effects in Optical Materials* **541**, p. 70, 1985.

an F–P doped silica cladding. Figure 4.23 displays the spectral loss characteristics over the wavelength range 1.2 to 1.7 μm, but it should also be noted that pure silica core fibers exhibit considerable radiation-induced losses at wavelengths around 0.85 μm. These losses initially increase linearly with increasing radiation dose and can become hundreds of $dB\,km^{-1}$ [Ref. 64].

Radiation-resistant fibers have been developed which are less sensitive to the effects of nuclear radiation. For example, hydrogen treatment of a pure silica core fiber, or use of boron–fluoride doped silica cladding fiber has been found to reduce gamma-ray-induced attenuation in the visible wavelength region [Ref. 65]. It has also been reported that radiation-induced attenuation can be reduced through photobleaching [Ref. 66]. In general, however, the only fiber structures likely to have an acceptable performance over a wide wavelength range when exposed to ionizing radiation are those having pure undoped silica cores, or those with core dopants of germanium and germanium with small amounts of fluorine–phosphorus [Ref. 67].

Clearly, radiation exposure can induce a considerable amount of attenuation in optical fibers, although the number of possible variable parameters, relating both to fiber structure and the nature of the radiation, make it difficult to generalize on the precise spectral effects. Nevertheless, more specific details relating to these effects can be found in the literature [Refs. 64 to 68].

4.9 Cable design

The design of optical fiber cables must take account of the constraints discussed in Section 4.7. In particular, the cable must be designed so that the strain on the fiber in the cable does not exceed 0.2% [Ref. 49]. Alternatively, it is suggested that the permanent strain on the fiber should be less than 0.1% [Ref. 50]. In practice, these constraints may be overcome in various ways which are, to some extent, dependent upon the cable's application. Nevertheless, cable design may generally be separated into a number of major considerations. These can be summarized into the categories of fiber buffering, cable structural and strength members, and cable sheath and water barrier.

4.9.1 Fiber buffering

It was indicated in Section 4.7 that the fiber is given a primary coating during production in order to prevent abrasion of the glass surface and subsequent flaws in the material. The primary coated fiber is then given a secondary or buffer coating (jacket) to provide protection against external mechanical and environmental influences. This buffer jacket is designed to protect the fiber from microbending losses and may take several different forms. These generally fall into one of three distinct types which are illustrated in Figure 4.24 [Ref. 69]. A tight buffer jacket is shown in Figure 4.24(a) which usually consists of a hard plastic (e.g. nylon,

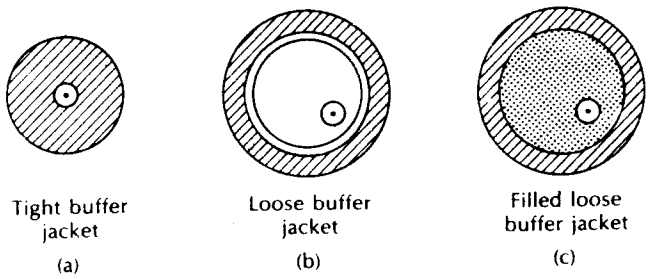

Figure 4.24 Techniques for buffering of optical fibers [Ref. 69]: (a) tight buffer jacket; (b) loose buffer jacket; (c) filled loose buffer jacket.

Hytrel, Tefzel) and is in direct contact with the primary coated fiber. This thick buffer coating (0.25 to 1 mm in diameter) provides stiffening for the fiber against outside microbending influences, but it must be applied in such a manner as not to cause microbending losses itself.

An alternative approach, which is shown in Figure 4.24(b), is the use of a loose buffer jacket. This produces an oversized cavity in which the fiber is placed and which mechanically isolates the fiber from external forces. Loose buffering is generally achieved by using a hard, smooth, flexible material in the form of an extruded tube, or sometimes a folded tape with a diameter between 1 and 2 mm.

Finally, Figure 4.24(c) shows a variation of the loose buffering in which the oversized cavity is filled with a moisture-resistant compound. This technique, which combines the advantages of the two previous methods, also provides a water barrier in the immediate vicinity of the fiber. The filling material must be soft, self-healing and stable over a wide range of temperatures and usually consists of specially blended petroleum or silicon-based compounds.

4.9.2 Cable structural and strength members

One or more structural members are usually included in the optical fiber cable to serve as a core foundation around which the buffered fibers may be wrapped, or into which they may be slotted, as illustrated in Figure 4.25 [Refs. 58 and 69]. The structural member may also be a strength member if it consists of suitable material (i.e. solid or stranded steel wire or Kevlar (DuPont Ltd) yarns). This situation is shown in Figure 4.25(a) where the central steel wire acts as both a structural and strength member. In this case the steel wire is the primary load-bearing element. Figure 4.25(b) shows an extruded plastic structural member around a central steel strength member commonly known as a slotted core. The primary function of the structural member in this case is not load-bearing, but to provide suitable accommodation for the buffered fibers within the cable.

Structural members may be nonmetallic with plastics, fiberglass and Kevlar often being used. However, for strength members the preferred features include a high

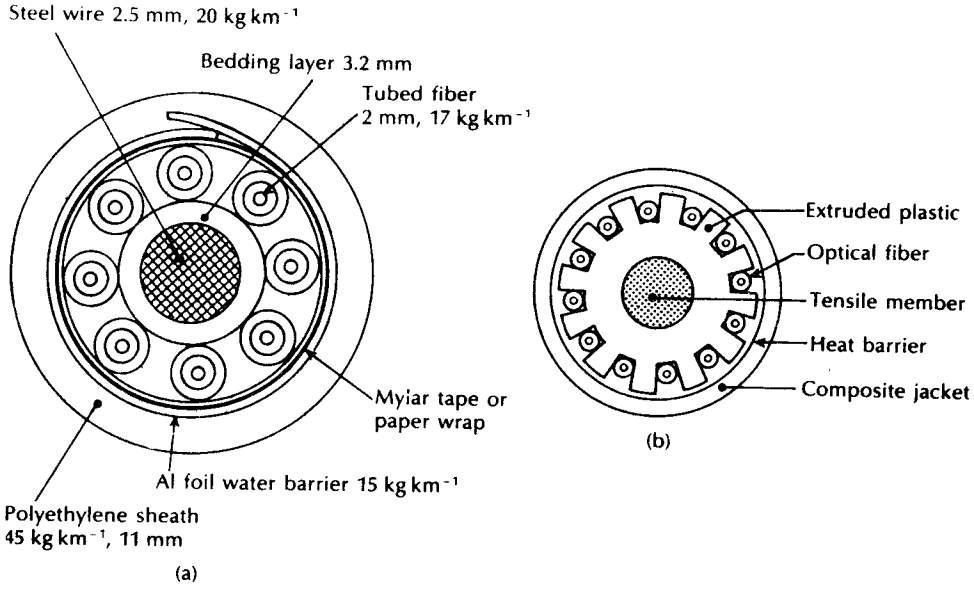

Figure 4.25 Structural and strength members in optical fiber cables: (a) central steel wire structural and strength member [Ref. 58]; (b) Northern Telecom unit core cable with central steel strength member and extruded plastic structural member [Ref. 69].

Young's modulus, high strain capability, flexibility and low weight per unit length. Therefore, although similar materials are frequently utilized for both strength and structural members, the requirement for additional tensile strength of the strength member must be considered within the cable design.

Flexibility in strength members formed of materials with high Young's modulii may be improved by using a stranded or bunched assembly of smaller units, as in the case of steel wire. Similar techniques are also employed with other materials used for strength members which include plastic monofilaments (i.e. specially processed polyester), textile fiber (nylon, Terylene, Dacron and the widely used Kevlar) and carbon and glass fibers. These materials provide a variety of tensile strengths for different cable applications. However, it is worth noting that Kevlar, an aromatic polyester, has a very high Young's modulus (up to $13 \times 10^{10}\,\mathrm{N\,m^{-2}}$) which gives it a strength to weight ratio advantage four times that of steel.

It is usual when utilizing a stranded strength member to cover it with a coating of extruded plastic, or helically applied tape. This is to provide the strength member with a smooth (cushioned) surface which is especially important for the prevention of microbending losses when the member is in contact with the buffered optical fibers.

4.9.3 Cable sheath and water barrier

The cable is normally covered with a substantial outer plastic sheath in order to reduce abrasion and to provide the cable with extra protection against external mechanical effects such as crushing. The cable sheath is said to contain the cable core and may vary in complexity from a single extruded plastic jacket to a multilayer structure comprising two or more jackets with intermediate armouring. However, the plastic sheath material (e.g. polyethylene, polyurethane) tends to give very limited protection against the penetration of water into the cable. Hence, an additional water barrier is usually incorporated. This may take the form of an axially laid aluminium foil/polyethylene laminated film immediately inside the sheath as used by British Telecom [Ref. 70] and illustrated in Figure 4.25(a).

Alternatively, the ingress of water may be prevented by filling the spaces in the cable with moisture-resistant compounds. Specially formulated silicone rubber or petroleum-based compounds are often used which do not cause difficulties in identification and handling of individual optical fibers within the cable form. These filling compounds are also easily removed from the cable and provide protection from corrosion for any metallic strength members within the fiber. Also, the filling compounds must not cause degradation of the other materials within the cable and must remain stable under pressure and temperature variation.

4.9.4 Examples of fiber cables

A number of different cable designs have emerged and been adopted by various organizations throughout the world. Although no definite standards exist, due to the diversity of applications and the approaches chosen to achieve the objectives mentioned in Section 4.7, there is, however, a general consensus on the overall design requirements and on the various materials that can be employed for cable construction [Ref. 71]. In this section we therefore consider some of the more common designs used in optical fiber cable construction to provide the reader with an insight into the developments in this important field.

Leading cable designs in the late 1970s included the use of loose buffer tubes or, alternatively, fiber ribbons [Ref. 72]. In the former design the fibers are enclosed in tubes which are stranded around a central strength (see Figure 4.25(a)) prior to the application of a polymeric sheath, thus providing large fiber strain relief. In the latter case high fiber packing density as well as ease of connectorization can be obtained. More recently, other designs have also found widespread application. In particular the slotted core design, an example of which is shown in Figure 4.25(b), and the loose fiber-bundle design in which the fibers are packaged into bundles before being enclosed in a single, loose fitting tube [Ref. 69]. All of the aforementioned multifiber cable designs are available with both single-mode and multimode fibers.

Figure 4.26 [Ref. 52] shows two examples of cable construction for single fibers. In Figure 4.26(a) a tight buffer jacket of Hytrel is used surrounded by a layer of

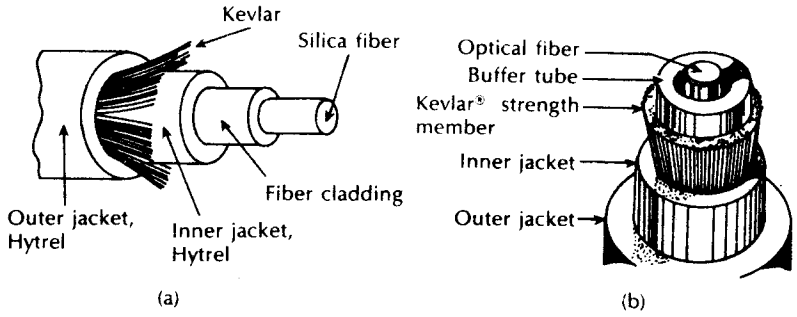

Figure 4.26 Single fiber cables [Ref. 52]: (a) tight buffer jacket design; (b) loose buffer jacket design.

Kevlar for strengthening. In this construction the optical fiber itself acts as a central strength member.

The cable construction illustrated in Figure 4.26(b) uses a loose tube buffer around the central optical fiber. This is surrounded by a Kevlar strength member which is protected by an inner sheath or jacket before the outer sheath layer. The strength members of single optical fiber cables are not usually incorporated at the centre of the cable (unless the fiber is acting as a strength member), but are placed in the surrounding cable form, as illustrated in Figure 4.26(b).

Although the single fiber cables shown in Figure 4.26 can be utilized for indoor applications, alternative simpler designs have been produced for such areas. A dual fiber indoor cable in which steel wire is employed for reinforcement is displayed in Figure 4.27(a) [Ref. 73]. In addition several flat-shaped cable types that can be laid under carpets have been developed [Ref. 74]. An example which is shown in Figure 4.27(b) can withstand pressures of more than 100 $kg\,cm^{-1}$, including that from high heeled shoes.

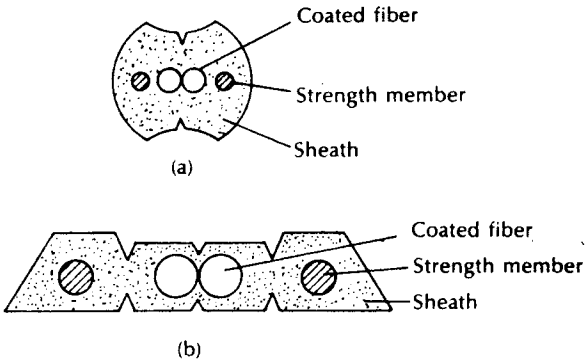

Figure 4.27 Dual fiber cables; (a) indoor cable; (b) flat cable.

Multifiber cables for outside plant applications, as mentioned previously, exhibit several different design methodologies. The use of a central strength member, as illustrated in Figure 4.25(a), is a common technique for the incorporation of either loose-buffer or tight buffer jacketed fibers. Such a structural member is utilized in the loose tube cable structure shown in Figure 4.28(a) in which filled loose tubes are extruded over fiber bundles with up to twelve fibers per tube [Ref. 72]. The tubes are then stranded around a central strength member, forming the cable core which is completed with a polyethylene sheath. A similar technique is used in the tight

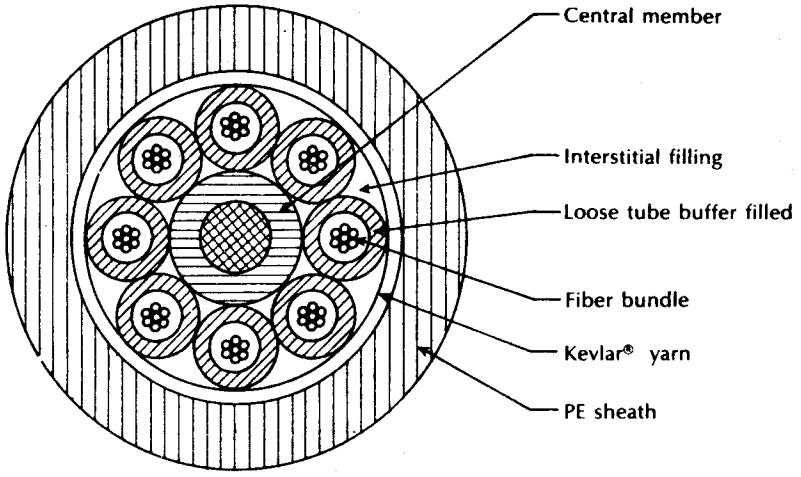

(a)

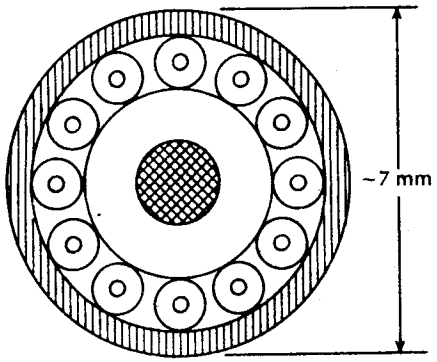

(b)

Figure 4.28 Multifiber cables for outside plant application: (a) loose tube cable; (b) layered cable construction [Ref. 72].

buffer cable design which often results in a layered construction for small cables of twelve fibers or less, as illustrated in Figure 4.28(b) [Ref. 72].

The slotted core structural member design, depicted in Figure 4.25(b) is also popular. A variation on this technique is illustrated in Figure 4.29(a) in which a number of fibers are placed into each of the slots [Ref. 71]. Within this design, radial movement of the fibers is facilitated in a similar manner to the loose tube approach, thus minimizing the possibility of residual fiber strain and the associated microbending losses.

Cable strength members may also be distributed or provided within an armoured cable design. An example of the former technique is shown in Figure 4.29(b) which comprises a multiunit design where each unit incorporates seven loose buffer jacketed fibers [Ref. 69]. In this case each unit contains a central strength member, which has the effect of dispersing the strength member throughout the cable core.

Structural members in the form of an armoured cable design are illustrated in Figure 4.30(a) in which stainless steel wires are provided in the cable sheath together

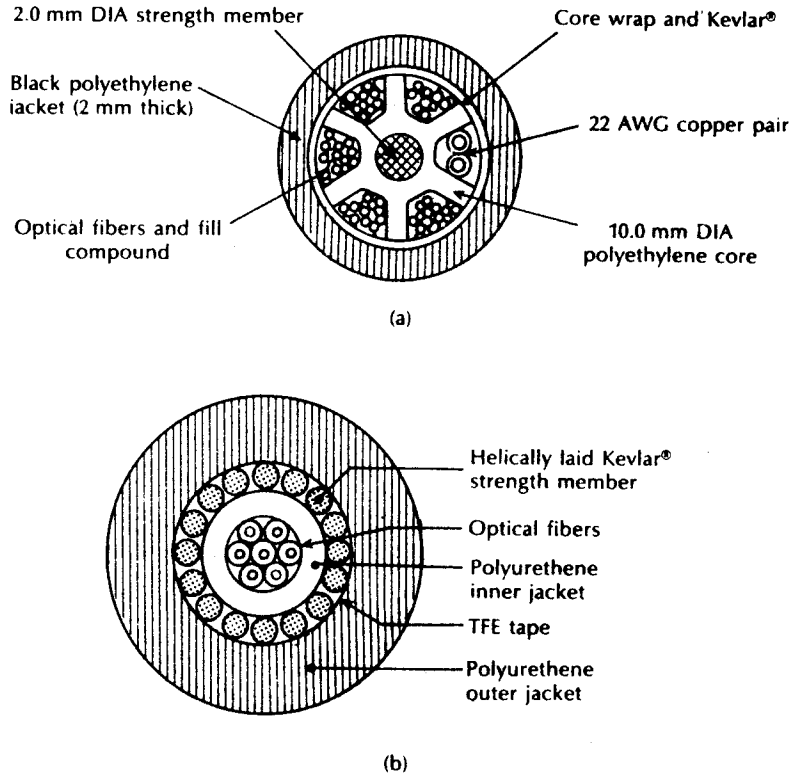

Figure 4.29 Multifiber cables: (a) slotted core cable [Ref. 71]; (b) ITT seven fiber external strength member cable. [Ref. 69].

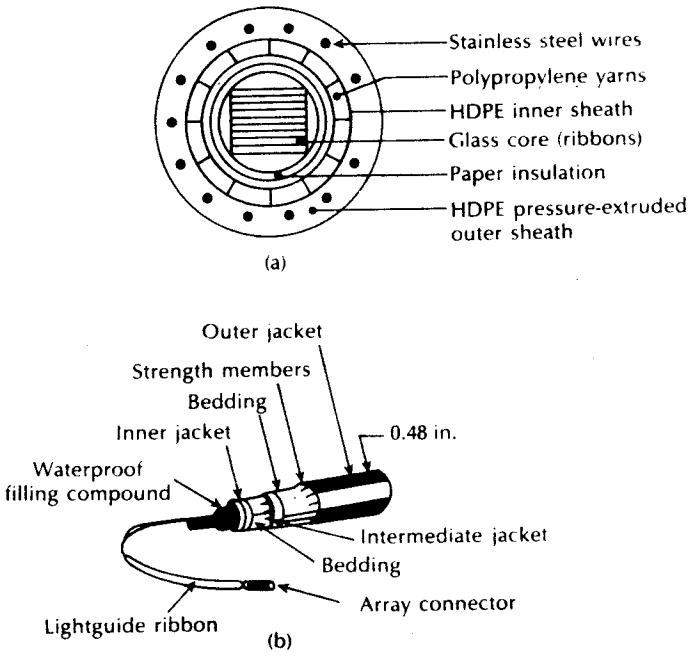

Figure 4.30 Ribbon fiber cables: (a) AT&T ribbon cable [Ref. 69]; (b) slotted core ribbon cable [Ref. 78].

with polypropylene yarns in the inner surrounding cable form. Furthermore, the cable depicted in Figure 4.30(a) is of a type that has found widespread application as it incorporates a ribbon fiber approach which at present provides the most efficient technique for simultaneously handling, splicing and connectorizing a large number of fibers. Between five and twelve fibers per ribbon have been placed into such linear ribbon arrays which may be stacked into twelve ribbon rectangular blocks [Ref. 71] to be placed in the cable core tube (Figure 4.30(a)). The ribbons may be formed with adhesive backed mylar tapes [Ref. 75], with extruded polymer substrates [Ref. 76] or by dipping the fiber array into a UV curable resin bath [Ref. 77]. Alternatively, the fiber ribbons can be placed into the voids of a slotted core structural member or several ribbon subunits may be stranded together to create very large fiber-count cables, as illustrated in Figure 4.30(b) [Ref. 78].

Finally, an approach commercialized by AT & T* is the loose fiber-bundle design shown in Figure 4.31 [Ref. 50]. In this cable up to twelve fibers are assembled into a bundle which is identified with a colour-coded binder. Several of the fiber bundles are then placed inside a core tube. This design does not employ a central strength member but relies upon an armoured design using a reinforced sheath with a

* It is called the Lightpack™ cable.

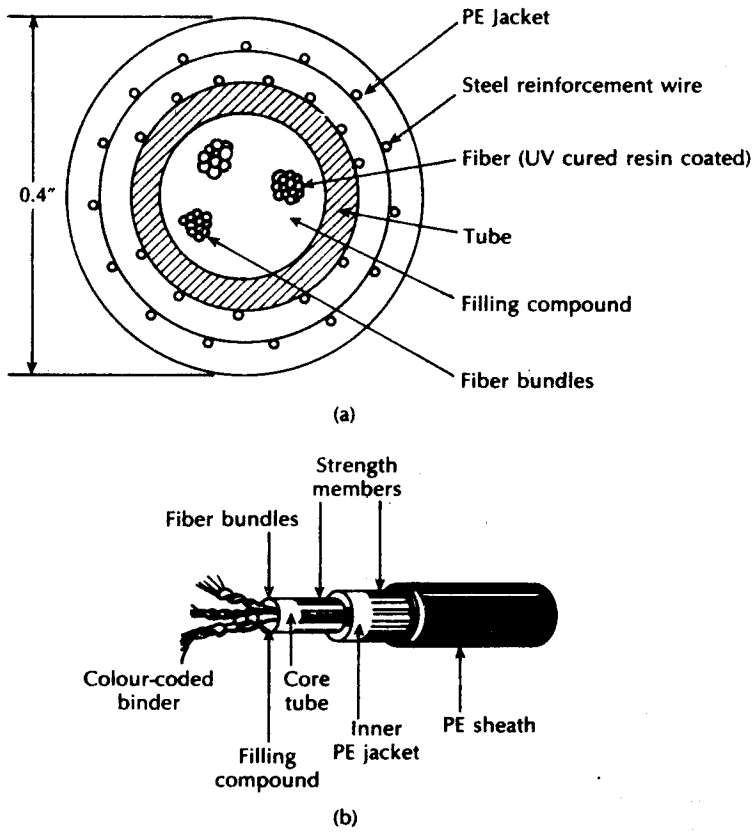

Figure 4.31 The AT & T Lightpack™ cable; (a) cross section showing steel reinforced sheath; (b) section illustrating the cable layers and the colour-coded fiber bundles [Ref. 50].

polyethylene inner jacket. Moreover, the core construction provides for compact, low weight cables with diameters of only 10 mm and 13 mm for fiber counts up to fifty and ninety-six fibers respectively [Ref. 72].

Problems

4.1 Describe in general terms liquid-phase techniques for the preparation of multicomponent glasses for optical fibers. Discuss with the aid of a suitable diagram one melting method for the preparation of multicomponent glass.

4.2 Indicate the major advantages of vapour-phase deposition in the preparation of glasses for optical fibers. Briefly describe the various vapour-phase techniques currently in use.

4.3 (a) Compare and contrast, using suitable diagrams, the outside vapour-phase oxidation (OVPO) process and the modified chemical vapour deposition (MCVD) technique for the preparation of low loss optical fibers.

(b) Briefly describe the salient features of vapour axial deposition (VAD) and the plasma-activated chemical vapour deposition (PCVD) when applied to the preparation of optical fibers.

4.4 Discuss the drawing of optical fibers from prepared glasses with regard to:

(a) multicomponent glass fibers;
(b) silica-rich fibers.

4.5 Indicate the primary advantage associated with the use of fluoride glass fibers and outline the possible methods of preparation for these fibers.

4.6 List the various optical fiber types currently on the market indicating their important features. Hence, briefly describe the general areas of application for each type.

4.7 Briefly describe the major reasons for the cabling of optical fibers which are to be placed in a field environment. Thus state the functions of the optical fiber cable.

4.8 Explain how the Griffith theory is developed in order to predict the fracture stress of an optical fiber with an elliptical crack.

Silica has a Young's modulus of $9 \times 10^{10}\ \mathrm{N\,m^{-2}}$ and a surface energy of 2.29 J. Estimate the fracture stress in psi for a silica optical fiber with a dominant elliptical crack of depth 0.5 μm. Also, determine the strain at the break for the fiber (1 psi $\equiv$ 6894.76 $\mathrm{N\,m^{-2}}$).

4.9 Another length of the optical fiber described in Problem 4.7 is found to break at 1% strain. The failure is due to a single dominant elliptical crack. Estimate the depth of this crack.

4.10 Describe the effects of stress corrosion on optical fiber strength and durability.

It is found that a 20 m length of fused silica optical fiber may be extended to 24 m at liquid nitrogen temperatures (i.e. little stress corrosion) before failure occurs. Estimate the fracture stress in psi for the fiber under these conditions. Young's modulus for silica is $9 \times 10^{10}\ \mathrm{N\,m^{-2}}$ and 1 psi $\equiv$ 6894.76 $\mathrm{N\,m^{-2}}$.

4.11 Outline the phenomena that can affect the stability of the transmission characteristics in optical fiber cables and describe any techniques by which these problems may be avoided.

4.12 Discuss optical fiber cable design with regard to:

(a) fiber buffering;
(b) cable strength and structural members;
(c) cable sheath and water barrier.

Further, compare and contrast possible cable designs for multifiber cables.

Answers to numerical problems

4.8 7.43×10^4 psi, 0.6%
4.9 0.2 μm
4.10 2.61×10^6 psi

References

[1] S. Tanaka, K. Inada, T. Akimoko and M. Kozima, 'Silicone-clad fused-silica-core fiber', *Electron. Lett.*, **11**(7), pp. 153–154, 1975.

[2] K. J. Beales and C. R. Day, 'A review of glass fibers for optical communications', *Phys. and Chem. of Glass*, **21**(1), pp. 5–21, 1980.

[3] T. Yamazuki and M. Yoshiyagawa, 'Fabrication of low-loss, multicomponent glass fibers with graded index and pseudo-step-index Borosilicate compound glass fibers', *Digest of International Conference on Integrated Optics and Optical Fiber Communication*, Osaka (Tokyo, IEEE, Japan), pp. 617–620, 1977.

[4] K. J. Beales, C. R. Day, W. J. Duncan, J. E. Midwinter and G. R. Newns, 'Preparation of sodium borosilicate glass fibers for optical communication', *Proc. IEE (London)*, **123**, pp. 591–595, 1976.

[5] G. R. Newns, P. Pantelis, J. L. Wilson, R. W. J. Uffen and R. Worthington, 'Absorption losses in glasses and glass fiber waveguides', *Opto-Electron*, **5**, pp. 289–296, 1973.

[6] B. Scott and H. Rawson, 'Techniques for producing low loss glasses for optical fibre communication systems', *Glass Technology*, **14**(5), pp. 115–124, 1973.

[7] C. E. E. Stewart, D. Tyldesley, B. Scott, H. Rawson and G. R. Newns, 'High-purity glasses for optical-fibre communication', *Electron. Lett.*, **9**(21), pp. 482–483, 1973.

[8] B. Scott and H. Rawson, 'Preparation of low loss glasses for optical fiber communication', *Opto-Electronics*, **5**(4), pp. 285–288, 1973.

[9] N. S. Kapany, *Fiber Optics*, Academic Press, 1967.

[10] A. M. Reid, W. W. Harper and A. Forbes, British Patent 50543, 1967.

[11] B. P. Pal, 'Optical communication, fiber waveguide fabrication: a review', *Fiber Int. Opt.*, **2**(2), pp. 195–252, 1979.

[12] G. R. Newns, 'Compound glass optical fibres', *2nd European Conference on Optical Fiber Communication* (Paris), pp. 21–26, 1976.

[13] K. J. Beales, C. R. Day, W. J. Duncan, A. G. Dunn, P. L. Dunn, G. R. Newns and J. V. Wright, 'Low loss graded index fiber by the double crucible technique', *5th European Conference on Optical Fiber Communication* (Amsterdam), paper 3.2, 1979.

[14] K. J. Beales, C. R. Day, W. J. Duncan and G. R. Newns, 'Low-loss compound-glass optical fibre', *Electron. Lett.*, **13**(24), pp. 755–756, 1977.

[15] H. Lydtin and F. Mayer, 'Review of techniques applied in optical fibre preparation', *Acta Electron.*, **22**(3), pp. 225–235, 1979.

[16] J. F. Hyde, US Patent 2 272 342, 1942.

[17] F. P. Kapron, D. B. Keck and R. D. Maurer, 'Radiation losses in optical waveguides', *Appl. Phys. Lett.*, **10**, pp. 423–425, 1970.

[18] B. Bendow and S. S. Mitra, *Fiber Optics*, Plenum Press, 1979.

[19] D. B. Keck and R. Bouillie, 'Measurements on high-bandwidth optical waveguides', *Optics Commun.*, **25**, pp. 43–48, 1978.

[20] B. S. Aronson, D. R. Powers and R. Sommer, 'Chloride drying of doped deposited silica preform simultaneous to consolidation', *Technical Digest of Topical Meeting on Optical Fiber Communication*, Washington, DC, p. 42, 1979.

[21] S. R. Nagel, 'Fiber materials and fabrication methods', in S. E. Miller and I. P. Kaminow (Eds.), *Optical Fiber Telecommunications II*, Academic Press, pp. 121–215, 1988.

[22] T. Izawa, T. Miyashita and F. Hanawa, US Patent 4 062 665, 1977.
[23] S. Sudo, M. Kawachi, M. Edahiro, T. Izawa, T. Shoida and H. Gotoh, 'Low-OH-content optical fiber fabricated by vapour-phase axial-deposition method', *Electron. Lett.*, **14**(17), pp. 534–535, 1978.
[24] T. Izawa, S. Sudo and F. Hanawa, 'Continuous fabrication process for high-silica fiber preforms (vapor phase axial deposition)', *Trans. Inst. Electron. Commun. Eng. Jpn. Section E* (Japan), **E62**(11), pp. 779–785, 1979.
[25] D. B. Keck and P. C. Schultz, US Patent 3 711 262, 1973.
[26] W. G. French, J. B. MacChesney, P. B. O'Conner and G. W. Tasker, 'Optical waveguides with very low losses', *Bell Syst. Tech. J.*, **53**, pp. 951–954, 1974.
[27] D. N. Payne and W. A. Gambling, 'New silica-based low-loss optical fibres', *Electron. Lett.*, **10**(15), pp. 289–90, 1974.
[28] T. Miya, Y. Terunuma, T. Mosaka and T. Miyashita, 'Ultimate low-loss single-mode fibre at 1.55 μm', *Electron. Lett.*, **15**(4), pp. 106–108, 1979.
[29] D. Gloge, 'The optical fibre as a transmission medium', *Rep. Prog. Phys.*, **42**, pp. 1778–1824, 1979.
[30] S. R. Nagel, J. B. MacChesney and K. L. Walker, 'An overview of the modified chemical vapour deposition (MCVD) process and performance', *IEEE J. Quantum Electron.*, **QE-18**(4), pp. 459–477, 1982.
[31] C. Lin, P. L. Lin, T. P. Lee, C. A. Burrus, F. T. Stone and A. J. Ritger, 'Measuring high bandwidth fibres in the 1.3 μm region with picosecond InGaAs injection lasers and ultrafast InGaAs detectors', *Electron. Lett.*, **17**(13), pp. 438–440, 1981.
[32] D. Kuppers and J. Koenings, 'Preform fabrication by deposition of thousands of layers with the aid of plasma activated CVD', *2nd European Conference on Optical Fiber Communication* (Paris), p. 49, 1976.
[33] R. E. Jaeger, J. B. MacChesney and T. J. Miller, 'The preparation of optical waveguide preforms by plasma deposition', *Bell. Syst. Tech. J.*, **57**, pp. 205–210, 1978.
[34] J. Irven and A. Robinson, 'Optical fibres prepared by plasma augmented vapour deposition', *Electron. Lett.*, **15**(9), pp. 252–4, 1979.
[35] P. K. Backman, D. Leers, H. Wehr, D. U. Wiechert, J. A. Van Steenwijk, D. L. A. Tjaden and E. R. Wehrhahn, 'Dispersion-flattened single-mode fibers prepared with PCVD: performance, limitations, design and optimization', *J. of Lightwave Technol.*, **LT-4**(7), pp. 858–863, 1986.
[36] H. Lydtin, 'PCVD: a technique suitable for large-scale fabrication of optical fibers', *J. of Lightwave Technol.*, **LT-4**(8), pp. 1034–1038, 1986.
[37] N. Nobukazu, 'Recent progress in glass fibers for optical communication', *Jap. J. Appl. Phys.*, **20**(8), pp. 1347–1360, 1981.
[38] P. W. Black, J. Irven and J. Titchmarsh, 'Fabrication of optical fibre waveguides', in C. P. Sandbank (Ed.), *Optical Fibre Communication Systems*, pp. 42–69, John Wiley, 1980.
[39] J. B. MacChesney, 'Materials and processes for preform fabrication – modified chemical vapour deposition and plasma chemical vapour deposition', *Proc. IEEE*, **68**(10), pp. 1181–1184, 1980.
[40] S. Sakaguchi and S. Takahashi, 'Low-loss fluoride optical fibers for midinfrared optical communication', *J. Lightwave Technol.*, **LT-5**(9), pp. 1219–1228, 1987.
[41] D. E. Quinn, 'Optical fibers', in F. C. Allard (ed.), *Fiber Optics Handbook: For engineers and scientists*, McGraw-Hill, pp. 1.1–1.50, 1990.

[42] T. Nakai, Y. Mimura, H. Tokiwa and O. Shinbori, 'Dehydration of fluoride glasses by NF_3 processing', *J. Lightwave Technol*, **LT-4**, pp. 87–89, 1986.
[43] R. C. Folweiler and D. E. Guenther, 'Chemical vapour purification of fluorides', *Mat. Sci. Forum*, **5**, pp. 43–48, 1985.
[44] J. A. Savage, 'Materials for infrared fibre optics', *Mat. Sci. Reports*, **2**, pp. 99–138. 1987.
[45] H. Iwasaki, 'Development of IR optical fibers in Japan', *Proc. SPIE*, **618**, *Infrared Optical Materials and Fibers IV*, pp. 2–9, 1986.
[46] S. Mitachi, T. Miyashita and T. Kanamori, 'Fluoride glass cladded optical fibers for mid infrared ray transmission', *Electron. Lett.*, **17**, pp. 591–592, 1981.
[47] D G. Tran, C. F. Fischer and G. H. Sigel, 'Fluoride glass preforms prepared by a rotational casting process', *Electron. Lett.*, **18**, pp. 657–658, 1982.
[48] *Fibre Optical Components and Systems*, Belling Lee Limited, Electronic Components Group, UK (now Ray Proof).
[49] H. Murata, *Handbook of Optical Fibers and Cables*, Marcel Dekker, 1988.
[50] P. Kaiser and D. B. Keck, 'Fiber types and their status', in S. E. Miller and I. P. Kaminow (Eds.) *Optical Fiber Telecommunications II*, Academic Press, pp. 29–54, 1988.
[51] C. K. Koa, 'Optical fibres and cables', in M. J. Howes and D. V. Morgan (Eds.), *Optical Fibre Communications, Devices, Circuits and Systems*, pp. 189–249, John Wiley, 1980.
[52] J. McDermott, 'Fiber-optic-cable choices expand to fill design needs', *EDN*, pp. 95–99, May 1981.
[53] G. De Loane, 'Optical fibre cables', *Telecomm. J. (Eng. Ed.) Switzerland*, **48**(11), pp. 649–656, 1981.
[54] G. Galliano and F. Tosco, 'Optical fibre cables', *Optical Fibre Communications*, by Technical Staff of CSELT, pp. 501–540, McGraw-Hill, 1981.
[55] T. Nakahara and N. Uchida, 'Optical cable design and characterization in Japan', *Proc. IEEE*, **68**(10), pp. 1220–1226, 1980.
[56] A. A. Griffith, 'Phenomena of rupture and flow in solids', *Phil. Trans. R. Soc. Lond. Ser. A*, **221**, pp. 163–168, 1920.
[57] W. Weibull, 'A statistical theory of the strength of materials', *Proc. R. Swedish Inst. Res.*, No. 151, publication no. 4, 1939.
[58] M. H. Reeve, 'Optical fibre cables', *Ratio Electron. Eng. (IERE J.)*, **51**(7/8), pp. 327–332, 1981.
[59] B. Wiltshire and M. H. Reeve, 'A review of the environmental factors affecting optical cable design', *J. of Lightwave Technol.*, **LT-6**, pp. 179–185, 1988.
[60] S. Das, G. S. Englefield and P. A. Goud, 'Power loss, modal noise and distortion due to microbending of optical fibres', *Appl. Opt.*, **24**, pp. 2323–2333, 1985.
[61] P. Danielsen, 'Simple power spectrum of microbending in single mode fibers', *Electron. Lett.*, **19**, p. 318, 1983.
[62] R. S. Ashpole and R. J. W. Powell, 'Hydrogen in optical cables', *IEE Proc. Pt. J.*, **132**, pp. 162–168, 1985.
[63] P. J. Lemaire and A. Tomita, 'Hydrogen induced loss in MCVD fibres', *Optical Fiber Communications Conf., OFC '85* (USA) TUII, February 1985.
[64] E. J. Friebele, K. J. Long, C. G. Askins, M. E. Gingerich, M. J. Marrone and D. L. Griscom, 'Overview of radiation effects in fiber optics', *Proc. SPIE, Radiation Effects in Optical Materials*, **541**, pp. 70–88, 1985.

[65] A. Iino and J. Tamura, 'Radiation resistivity in silica optical fibers', *J. of Lightwave Technol.*, **LT-6**, pp. 145–149, 1988.

[66] E. J. Friebele and M. E. Gingerich, 'Photobleaching effects in optical fibre waveguides', *Appl. Opt.*, **20**, pp. 3448–3452, 1981.

[67] R. H. West, 'A local view of radiation effects in fiber optics', *J. of Lightwave Technol.*, **LT-6**, pp. 155–164, 1988.

[68] E. J. Friebele, E. W. Waylor, G. T. De Beauregard, J. A. Wall and C. E. Barnes, 'Interlaboratory comparison of radiation induced attenuation in optical fibers. Part 1: steady state exposure', *J. of Lightwave Technol.*, **LT-6**, pp. 165–178, 1988.

[69] P. R. Bank and D. O. Lawrence, 'Emerging standards in fiber optic telecommunications cable', *Proc. SPIE Int. Soc. Opt. Eng. (USA)*, **224**, pp. 149–158, 1980.

[70] J. C. Harrison, 'The metal foil/polyethylene cable sheath and its use in the Post Office', Institution of Post Office Engineers Paper No. 229, 1968.

[71] P. Kaiser and W. T. Anderson, 'Fiber cables for public communications: state-of-the-art technologies and the future', *J. Lightwave Technol.*, **LT-4**(8), pp. 1157–1165, 1986.

[72] C. H. Gartside III, P. D. Patel and M. R. Santana, 'Optical fiber cables', in S. E. Miller and I. P. Kaminow (Eds.), *Optical Fiber Telecommunications II*, Academic Press, 1988.

[73] F. Nihei, Y. Yamomoter and N. Kojima, 'Optical subscriber cable technologies in Japan', *J. Lightwave Technol.*, **LT-5**(6), pp. 809–821, 1987.

[74] S. Kukita, M. Kawase, H. Kobayashi and O. Ogasawara, 'Design and performance of optical cables and cabinets for local area networks', *ECL Tech. J.*, **34**(5) pp. 905–918, 1985.

[75] M. J. Buckler, M. R. Santana and M. J. Saunders, 'Lightwave cable manufacture and performance', *Bell Syst. Tech. J.*, **57**(6), p. 1745, 1978.

[76] M. Oda, M. Ogai, A. Ohtake, S. Tachigami, K. Ohkubo, F. Nihei and N. Kashima, 'Nylon extruded fiber ribbon and its connection', *Optical Fiber Communications Conf., OFC '82* (USA) paper THAA6, February 1982.

[77] Y. Katsuyama, S. Hatano, K. Hogari, T. Matsumoto and T. Kokubun, 'Single-mode optical-fiber ribbon cable', *Electron. Lett.*, **21**(4), p. 134, 1985.

[78] Y. Katsuyama, K. Hogari, S. Hatano and T. Kobubun, 'Optical loss characteristics of slotted rod cable composed of single-mode fiber ribbons', *Natl. Conv., IECEJ*, **2062**, pp. 9–91, March 1986.

5

Optical fiber connection: joints and couplers

5.1 Introduction

Optical fiber links, in common with any line communication system, have a requirement for both jointing and termination of the transmission medium. The number of intermediate fiber connections or joints is dependent upon the link length (between repeaters), the continuous length of fiber cable that may be produced by the preparation methods outlined in Sections 4.2 to 4.4, and the length of the fiber cable that may be practically or conveniently installed as a continuous section on the link. Although scaling up of the preparation processes now provides the capability to produce very large preforms allowing continuous single-mode fiber lengths of around 200 km, such fiber spans cannot be readily installed [Ref. 1]. However, continuous cable lengths of tens of kilometres have already been deployed, in particular within submarine systems where continuous cable laying presents fewer problems [Ref. 2].

Repeater spacing on optical fiber telecommunication links is a continuously increasing parameter with currently installed digital systems operating over spacings in the range 40 to 60 km at transmission rates of between 400 Mbit s^{-1} and 1.7 Gbit s^{-1} [Refs. 3 to 5]. Moreover, spacings in excess of 100 km are also readily achievable with practical systems at such transmission rates, and unrepeated distances of around 300 km have been obtained in the laboratory [Ref. 4]. For example, a fully operational 2.4 Gbit s^{-1} system operating with a 100 km repeater spacing using dispersion shifted single-mode fiber (see Section 3.12.1) has recently been reported [Ref. 6], together with the experimental transmission at 10 Gbit s^{-1} over a similar unrepeated distance [Ref. 7].

It is therefore apparent that fiber to fiber connection with low loss and minimum distortion (i.e. modal noise) remains an important aspect of optical fiber communication systems (fiber, sources, detectors, etc.) it is clear that, in recent systems. In addition, it also serves to increase the number of terminal connections permissible within the developing optical fiber communication networks (see Chapter 14). Although fiber jointing techniques appeared to lag behind the technologies associated with the other components required in optical fiber communication systems (fiber sources, detectors, etc.) it is clear that, in recent years, significant developments have been made. Therefore, in this and the sections immediately following we review the theoretical and practical aspects of fiber–fiber connection with regard to both multimode and single-mode systems. Fiber termination to sources and detectors is not considered since the important aspects of these topics are discussed in the chapters covering sources and detectors (Chapters 6, 7 and 8). Nevertheless, the discussion on fiber jointing is relevant to both source and detector coupling, as many manufacturers supply these electro-optical devices already terminated to a fiber optic pigtail in order to facilitate direct fiber–fiber connection to an optical fiber link.

Before we consider fiber–fiber connection in further detail it is necessary to indicate the two major categories of fiber joint currently both in use and development. These are as follows:

1. Fiber splices: these are semipermanent or permanent joints which find major use in most optical fiber telecommunication systems (analogous to electrical soldered joints).
2. Demountable fiber connectors or simple connectors: these are removable joints which allow easy, fast, manual coupling and uncoupling of fibers (analogous to electrical plugs and sockets).

The above fiber to fiber joints are designed ideally to couple all the light propagating in one fiber into the adjoining fiber. By contrast fiber couplers are branching devices that split all the light from a main fiber into two or more fibers or, alternatively, couple a proportion of the light propagating in the main fiber into a branch fiber. Moreover, these devices are often bidirectional, providing for the combining of light from one or more branch fibers into a main fiber. The importance and variety of these fiber couplers has increased substantially over

recent years in order to facilitate the widespread deployment of optical fiber within communication networks. Although the requirement for such devices was less in earlier point-to-point fiber links, the growing demand for more sophisticated fiber network configurations (see Chapter 14) has made them essential components within optical fiber communications.

In this chapter we therefore consider the basic techniques and technology associated with both fiber joints and couplers. A crucial aspect of fiber jointing concerns the optical loss associated with the connection. This joint loss is critically dependent upon the alignment of the two fibers. Hence, in Section 5.2 the mechanisms which cause optical losses at fiber joints are outlined, with particular attention being paid to the fiber alignment. This discussion provides a grounding for consideration of the techniques employed for jointing optical fibers. Permanent fiber joints (i.e. splices) are then dealt with in Section 5.3 prior to discussion of the two generic types of demountable connector in Sections 5.4 and 5.5. Finally, in Section 5.6, the basic construction and performance characteristics of the various fiber coupler types are described.

5.2 Fiber alignment and joint loss

A major consideration with all types of fiber–fiber connection is the optical loss encountered at the interface. Even when the two jointed fiber ends are smooth and perpendicular to the fiber axes, and the two fiber axes are perfectly aligned, a small proportion of the light may be reflected back into the transmitting fiber causing attenuation at the joint. This phenomenon, known as Fresnel reflection, is associated with the step changes in refractive index at the jointed interface (i.e. glass–air–glass). The magnitude of this partial reflection of the light transmitted through the interface may be estimated using the classical Fresnel formula for light of normal incidence and is given by [Ref. 8]:

$$r = \left(\frac{n_1 - n}{n_1 + n}\right)^2 \tag{5.1}$$

where r is the fraction of the light reflected at a single interface, n_1 is the refractive index of the fiber core and n is the refractive index of the medium between the two jointed fibers (i.e. for air $n = 1$). However, in order to determine the amount of light reflected at a fiber joint, Fresnel reflection at both fiber interfaces must be taken into account. The loss in decibels due to Fresnel reflection at a single interface is given by:

$$Loss_{Fres} = -10 \log_{10}(1 - r) \tag{5.2}$$

Hence, using the relationships given in Eqs. (5.1) and (5.2) it is possible to determine the optical attenuation due to Fresnel reflection at a fiber–fiber joint.

It is apparent that Fresnel reflection may give a significant loss at a fiber joint even when all other aspects of the connection are ideal. However, the effect of

Fresnel reflection at a fiber–fiber connection can be reduced to a very low level through the use of an index matching fluid in the gap between the jointed fibers. When the index matching fluid has the same refractive index as the fiber core, losses due to Fresnel reflection are in theory eradicated.

Unfortunately, Fresnel reflection is only one possible source of optical loss at a fiber joint. A potentially greater source of loss at a fiber–fiber connection is caused by misalignment of the two jointed fibers. In order to appreciate the development and relative success of various connection techniques it is useful to discuss fiber alignment in greater detail.

Example 5.1

An optical fiber has a core refractive index of 1.5. Two lengths of the fiber with smooth and perpendicular (to the core axes) end faces are butted together. Assuming the fiber axes are perfectly aligned, calculate the optical loss in decibels at the joint (due to Fresnel reflection) when there is a small air gap between the fiber end faces.

Solution: The magnitude of the Fresnel reflection at the fiber–air interface is given by Eq. (5.1) where:

$$r = \left(\frac{n_1 - n}{n_1 + n}\right)^2 = \left(\frac{1.5 - 1.0}{1.5 + 1.0}\right)^2$$

$$= \left(\frac{0.5}{2.5}\right)^2$$

$$= 0.04$$

The value obtained for r corresponds to a reflection of 4% of the transmitted light at the single interface. Further, the optical loss in decibels at the single interface may be obtained using Eq. (5.2) where:

$$Loss_{\text{Fres}} = -10 \log_{10}(1 - r) = -10 \log_{10} 0.96$$
$$= 0.18 \text{ dB}$$

A similar calculation may be performed for the other interface (air–fiber). However, from considerations of symmetry it is clear that the optical loss at the second interface is also 0.18 dB.

Hence the total loss due to Fresnel reflection at the fiber joint is approximately 0.36 dB.

Any deviations in the geometrical and optical parameters of the two optical fibers which are jointed will affect the optical attenuation (insertion loss) through the connection. It is not possible within any particular connection technique to allow

for all these variations. Hence, there are inherent connection problems when jointing fibers with, for instance:

(a) different core and/or cladding diameters;
(b) different numerical apertures and/or relative refractive index differences;
(c) different refractive index profiles;
(d) fiber faults (core ellipticity, core concentricity, etc.).

The losses caused by the above factors together with those of Fresnel reflection are usually referred to as intrinsic joint losses.

The best results are therefore achieved with compatible (same) fibers which are manufactured to the lowest tolerance. In this case there is still the problem of the quality of the fiber alignment provided by the jointing mechanism. Examples of possible misalignment between coupled compatible optical fibers are illustrated in Figure 5.1 [Ref. 9]. It is apparent that misalignment may occur in three dimensions, the separation between the fibers (longitudinal misalignment), the offset perpendicular to the fiber core axes (lateral/radial/axial misalignment) and the angle between the core axes (angular misalignment).

Optical losses resulting from these three types of misalignment depend upon the fiber type, core diameter and the distribution of the optical power between the propagating modes. Examples of the measured optical losses due to the various types of misalignment are shown in Figure 5.2. Figure 5.2(a) [Ref. 9] shows the attenuation characteristic for both longitudinal and lateral misalignment of a 50 μm core diameter graded index fiber. It may be observed that the lateral misalignment gives significantly greater losses per unit displacement than the longitudinal misalignment. For instance in this case a lateral displacement of 10 μm gives about 1 dB insertion loss whereas a similar longitudinal displacement gives an insertion loss of around 0.1 dB. Figure 5.2(b) [Ref. 10] shows the attenuation characteristic for the angular misalignment of two multimode step index fibers with numerical apertures of 0.22 and 0.3. An insertion loss of around 1 dB is obtained with angular

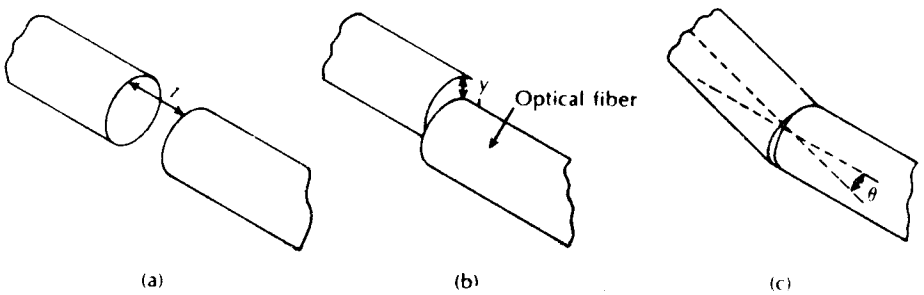

Figure 5.1 The three possible types of misalignment which may occur when jointing compatible optical fibers [Ref. 9]: (a) longitudinal misalignment; (b) lateral misalignment; (c) angular misalignment.

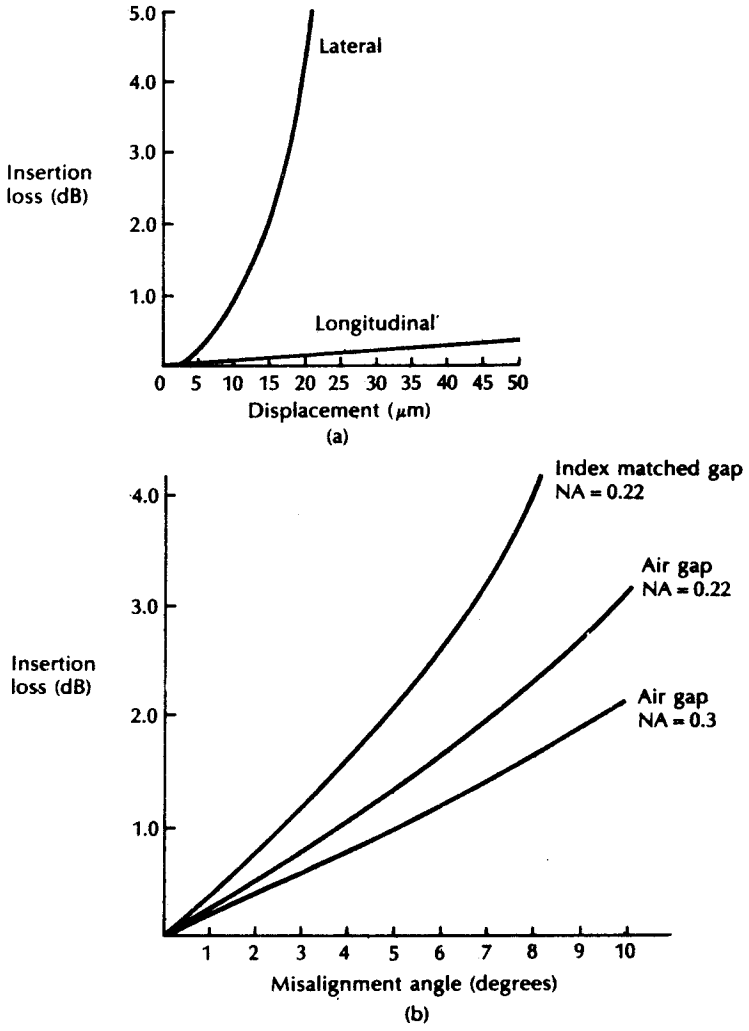

Figure 5.2 Insertion loss characteristics for jointed optical fibers with various types of misalignment: (a) insertion loss due to lateral and longitudinal misalignment for a 50 μm core diameter graded index fiber, reproduced with permission from P. Mossman, *The Radio and Electron. Eng.*, 51, p. 333. 1981; (b) insertion loss due to angular misalignment for joints in two multimode step index fibers with numerical apertures of 0.22 and 0.3, reproduced with permission from C. P. Sandback (Ed.), *Optical Fiber Communication Systems*, John Wiley & Sons, 1980.

misalignment of 4° and 5° for the 0.22 NA and 0.3 NA fibers respectively. It may also be observed in Figure 5.2(b) that the effect of an index matching fluid in the fiber gap causes increased losses with angular misalignment. Therefore, it is clear that relatively small levels of lateral and/or angular misalignment can cause significant attenuation at a fiber joint. This is especially the case for small core diameter (less than 150 μm) fibers which are currently employed for most telecommunication purposes.

5.2.1 Multimode fiber joints

Theoretical and experimental studies of fiber misalignment in optical fiber connections [Refs. 11 to 19] allow approximate determination of the losses encountered with the various misalignments of different fiber types. We consider here some of the expressions used to calculate losses due to lateral and angular misalignment of optical fiber joints. Longitudinal misalignment is not discussed in detail as it tends to be the least important effect and may be largely avoided in fiber connection. Also there is some disagreement over the magnitude of the losses due to longitudinal misalignment when it is calculated theoretically between Miyazaki *et al.* [Ref. 12] and Tsuchiya *et al.* [Ref. 13]. Both groups of workers claim good agreement with experimental results, which is perhaps understandable when considering the number of variables involved in the measurement. However, it is worth noting that the lower losses predicted by Tsuchiya *et al.* agree more closely with a third group of researchers [Ref. 14]. Also, all groups predict higher losses for fibers with larger numerical apertures which is consistent with intuitive considerations (i.e. the larger the numerical aperture, the greater the spread of the output light and the higher the optical loss at a longitudinally misaligned joint).

Theoretical expressions for the determination of lateral and angular misalignment losses are by no means definitive, although in all cases they claim reasonable agreement with experimental results. However, experimental results from different sources tend to vary (especially for angular misalignment losses) due to difficulties of measurement. It is therefore not implied that the expressions given in the text are necessarily the most accurate, as at present the choice appears somewhat arbitrary.

Lateral misalignment reduces the overlap region between the two fiber cores. Assuming uniform excitation of all the optical modes in a multimode step index fiber the overlapped area between both fiber cores approximately gives the lateral coupling efficiency η_{lat}. Hence, the lateral coupling efficiency for two similar step index fibers may be written as [Ref. 13]:

$$\eta_{lat} \simeq \frac{16(n_1/n)^2}{(1+(n_1/n))^4} \frac{1}{\pi} \left\{ 2\cos^{-1}\left(\frac{y}{2a}\right) - \left(\frac{y}{a}\right)\left(1-\left(\frac{y}{2a}\right)^2\right)^{\frac{1}{2}} \right\} \tag{5.3}$$

where n_1 is the core refractive index, n is the refractive index of the medium between the fibers, y is the lateral offset of the fiber core axes, and a is the fiber

core radius. The lateral misalignment loss in decibe's may be determined using:

$$Loss_{lat} = -10 \log_{10} \cdot \eta_{lat} \text{ dB} \tag{5.4}$$

The predicted losses obtained using the formulae given in Eqs. (5.3) and (5.4) are generally slightly higher than the measured values due to the assumption that all modes are equally excited. This assumption is only correct for certain cases of optical fiber transmission. Also, certain authors [Refs. 12 and 18] assume index matching and hence no Fresnel reflection, which makes the first term in Eq. (5.3) equal to unity (as $n_1/n = 1$). This may be valid if the two fiber ends are assumed to be in close contact (i.e. no air gap in between) and gives lower predicted losses. Nevertheless, bearing in mind these possible inconsistencies, useful estimates for the attenuation due to lateral misalignment of multimode step index fibers may be obtained.

Lateral misalignment loss in multimode graded index fibers assuming a uniform distribution of optical power throughout all guided modes was calculated by Gloge [Ref. 16]. He estimated that the lateral misalignment loss was dependent on the refractive index gradient α for small lateral offset and may be obtained from:

$$L_t = \frac{2}{\pi}\left(\frac{y}{a}\right)\left(\frac{\alpha+2}{\alpha+1}\right) \qquad \text{for } 0 \leqslant y \leqslant 0.2a \tag{5.5}$$

where the lateral coupling efficiency was given by:

$$\eta_{lat} = 1 - L_t \tag{5.6}$$

Hence Eq. (5.6) may be utilized to obtain the lateral misalignment loss in decibels. With a parabolic refractive index profile where $\alpha = 2$, Eq. (5.5) gives:

$$L_t = \frac{8}{3\pi}\left(\frac{y}{a}\right) = 0.85\left(\frac{y}{a}\right) \tag{5.7}$$

A further estimate including the leaky modes, gave a revised expression for the lateral misalignment loss given in Eq. (5.6) of $0.75(y/a)$. This analysis was also extended to step index fibers (where $\alpha = \infty$) and gave lateral misalignment losses of $0.64(y/a)$ and $0.5(y/a)$ for the cases of guided modes only and both guided plus leaky modes respectively.

Example 5.2

A step index fiber has a core refractive index of 1.5 and a core diameter of 50 μm. The fiber is jointed with a lateral misalignment between the core axes of 5 μm. Estimate the insertion loss at the joint due to the lateral misalignment assuming a uniform distribution of power between all guided modes when:

(a) there is a small air gap at the joint;
(b) the joint is considered index matched.

Solution: (a) The coupling efficiency for a multimode step index fiber with uniform illumination of all propagating modes is given by Eq. (5.3) as:

$$\eta_{lat} \simeq \frac{16(n_1/n)^2}{(1+(n_1/n))^4}\frac{1}{\pi}\left\{2\cos^{-1}\left(\frac{y}{2a}\right) - \left(\frac{y}{a}\right)\left[1-\left(\frac{y}{2a}\right)^2\right]^{\frac{1}{2}}\right\}$$

$$= \frac{16(1.5)^2}{(1+1.5)^4}\frac{1}{\pi}\left\{2\cos^{-1}\left(\frac{5}{50}\right) - \left(\frac{5}{25}\right)\left[1-\left(\frac{5}{50}\right)^2\right]^{\frac{1}{2}}\right\}$$

$$= 0.293\{2(1.471) - 0.2[0.99]^{\frac{1}{2}}\}$$

$$= 0.804$$

The insertion loss due to lateral misalignment is given by Eq. (5.4) where

$$Loss_{lat} = -10\log_{10}\eta_{lat} = -10\log_{10}0.804$$
$$= 0.95\text{ dB}$$

Hence assuming a small air gap at the joint the insertion loss is approximately 1 dB when the lateral offset is 10% of the fiber diameter.

(b) When the joint is considered index matched (i.e. no air gap) the coupling efficiency may again be obtained from Eq. (5.3) where

$$\eta_{lat} \simeq \frac{1}{\pi}\left\{2\cos^{-1}\left(\frac{5}{50}\right) - \left(\frac{5}{25}\right)\left[1-\left(\frac{5}{50}\right)^2\right]^{\frac{1}{2}}\right\}$$

$$= 0.318\{2(1.471) - 0.2[0.99]^{\frac{1}{2}}\}$$

$$= 0.872$$

Therefore the insertion loss is:

$$Loss_{lat} = -10\log_{10}0.872 = 0.59\text{ dB}$$

With index matching the insertion loss at the joint in Example 5.2 is reduced to approximately 0.36 dB. It may be noted that the difference between the losses obtained in parts (a) and (b) corresponds to the optical loss due to Fresnel reflection at the similar fiber–air–fiber interface determined in Example 5.1.

The result may be checked using the formulae derived by Gloge for a multimode step index fiber where the lateral misalignment loss assuming uniform illumination of all guided modes is obtained using:

$$L_f = 0.64\left(\frac{y}{a}\right) = 0.64\left(\frac{5}{25}\right) = 0.128$$

Hence the lateral coupling efficiency is given by Eq. (5.6) as:

$$\eta_{lat} = 1 - 0.128 = 0.872$$

Again using Eq. (5.4), the insertion loss due to the lateral misalignment assuming

index matching is:

$$Loss_{lat} = -10 \log_{10} 0.872 = 0.59 \text{ dB}$$

Hence using the expression derived by Gloge we obtain the same value of approximately 0.6 dB for the insertion loss with the inherent assumption that there is no change in refractive index at the joint interface. Although this estimate of insertion loss may be shown to agree with certain experimental results [Ref. 12], a value of around 1 dB insertion loss for a 10% lateral displacement with regard to the core diameter (as estimated in Example 5.2(a)) is more usually found to be the case with multimode step index fibers [Refs. 8, 19 and 24]. Further, it is generally accepted that the lateral offset must be kept below 5% of the fiber core diameter in order to reduce insertion loss at a joint to below 0.5 dB [Ref. 19].

Example 5.3

A graded index fiber has a parabolic refractive index profile ($\alpha = 2$) and a core diameter of 50 μm. Estimate the insertion loss due to a 3 μm lateral misalignment at a fiber joint when there is index matching and assuming:

(a) there is uniform illumination of all guided modes only;
(b) there is uniform illumination of all guided and leaky modes.

Solution: (a) Assuming uniform illumination of guided modes only, the misalignment loss may be obtained using Eq. (5.7), where

$$L_t = 0.85\left(\frac{y}{a}\right) = 0.85\left(\frac{3}{25}\right) = 0.102$$

The coupling efficiency is given by Eq. (5.6) as:

$$\eta_{lat} = 1 - L_t = 1 - 0.102 = 0.898$$

Hence the insertion loss due to the lateral misalignment is given by Eq. (5.4), where:

$$Loss_{lat} = -10 \log_{10} 0.898 = 0.47 \text{ dB}$$

(b) When assuming the uniform illumination of both guided and leaky modes Gloge's formula becomes:

$$L_t = 0.75\left(\frac{y}{a}\right) = 0.75\left(\frac{3}{25}\right) = 0.090$$

Therefore the coupling efficiency is

$$\eta_{lat} = 1 - 0.090 = 0.910$$

and the insertion loss due to lateral misalignment is:

$$Loss_{lat} = -10 \log_{10} 0.910 = 0.41 \text{ dB}$$

It may be noted by observing Figure 5.2(a) which shows the measured lateral misalignment loss for a 50 μm diameter graded index fiber that the losses predicted above are very pessimistic (the loss for 3 μm offset shown in Figure 5.2(a) is less than 0.2 dB). A model which is found to predict insertion loss due to lateral misalignment in graded index fibers with greater accuracy was proposed by Miller and Mettler [Ref. 17]. In this model they assumed the power distribution at the fiber output to be of a Gaussian form. Unfortunately, the analysis is too detailed for this text as it involves integration using numerical techniques. We therefore limit estimates of insertion losses due to lateral misalignment in multimode graded index fibers to the use of Gloge's formula.

Angular misalignment losses at joints in multimode step index fibers may be predicted with reasonable accuracy using an expression for the angular coupling efficiency η_{ang} given by [Ref. 13]:

$$\eta_{ang} \simeq \frac{16(n_1/n)^2}{(1+(n_1/n))^4}\left[1-\frac{n\theta}{\pi n_1(2\Delta)^{\frac{1}{2}}}\right] \tag{5.8}$$

where θ is the angular displacement in radians and Δ is the relative refractive index difference for the fiber. The insertion loss due to angular misalignment may be obtained from the angular coupling efficiency in the same manner as the lateral misalignment loss following:

$$Loss_{ang} = -10 \log_{10} \eta_{ang} \tag{5.9}$$

The formulae given in Eqs. (5.8) and (5.9) predict that the smaller the values of Δ the larger the insertion loss due to angular misalignment. This appears intuitively correct as small values of Δ imply small numerical aperture fibers, which will be more affected by angular misalignment. It is confirmed by the measurements shown in Figure 5.2(b) and demonstrated in Example 5.4.

Example 5.4

Two multimode step index fibers have numerical apertures of 0.2 and 0.4, respectively, and both have the same core refractive index which is 1.48. Estimate the insertion loss at a joint in each fiber caused by a 5° angular misalignment of the fiber core axes. It may be assumed that the medium between the fibers is air.

Solution: The angular coupling efficiency is given by Eq. (5.8) as

$$\eta_{ang} \simeq \frac{16(n_1/n)^2}{(1+(n_1/n))^4}\left[1-\frac{n\theta}{\pi n_1(2\Delta)^{\frac{1}{2}}}\right]$$

The numerical aperture is related to the relative refractive index difference following Eq. (2.10) where:

$$NA \simeq n_1(2\Delta)^{\frac{1}{2}}$$

Hence

$$\eta_{ang} \simeq \frac{16(n_1/n)^2}{(1 + (n_1/n))^4}\left[1 - \frac{n\theta}{\pi NA}\right]$$

For the 0.2 NA fiber:

$$n_{ang} \simeq \frac{16(1.48)^2}{(1 + 1.48)^4}\left[1 - \frac{5\pi/180}{\pi 0.2}\right]$$

$$= 0.797$$

The insertion loss due to the angular misalignment may be obtained from Eq. (5.9), where:

$$Loss_{ang} = -10 \log_{10} \eta_{ang} = -10 \log_{10} 0.797$$
$$= 0.98 \text{ dB}$$

For the 0.4 NA fiber:

$$\eta_{ang} \simeq 0.926\left[1 - \frac{5\pi/180}{\pi\ 0.4}\right]$$

$$\simeq 0.862$$

The insertion loss due to the angular misalignment is therefore:

$$Loss_{ang} = -10 \log_{10} 0.862$$
$$= 0{,}64 \text{ dB}$$

Hence it may be noted from Example 5.4 that the insertion loss due to angular misalignment is reduced by using fibers with large numerical apertures. This is the opposite trend to the increasing insertion loss with numerical aperture for fiber longitudinal misalignment at a joint.

Factors causing fiber–fiber intrinsic losses were listed in Section 5.2; the major ones comprising a mismatch in the fiber core diameters, a mismatch in the fiber numerical apertures and differing fiber refractive index profiles are illustrated in Figure 5.3. Connections between multimode fibers with certain of these parameters being different can be quite common, particularly when a pigtailed optical source is used, the fiber pigtail of which has different characteristics from the main transmission fiber. Moreover; as indicated previously, diameter variations can occur with the same fiber type.

Assuming all the modes are equally excited in a multimode step or graded index fiber, and that the numerical apertures and index profiles are the same, then the loss resulting from a mismatch of core diameters (see Figure 5.3(a)) is given by [Refs. 13, 20]:

$$Loss_{CD} \begin{cases} = -10 \log_{10}\left(\dfrac{a_2}{a_1}\right)^2 \text{ (dB)} & a_2 < a_1 \\ = 0 \text{ (dB)} & a_2 \geqslant a_1 \end{cases} \tag{5.10}$$

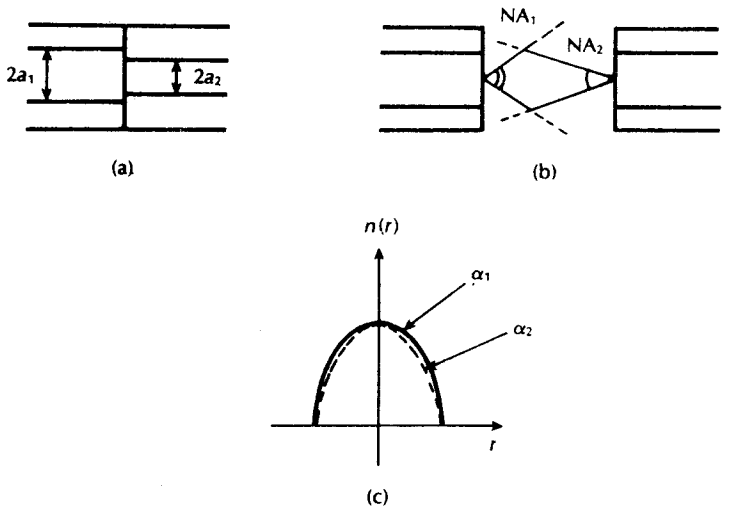

Figure 5.3 Some intrinsic coupling losses at fiber joints: (a) core diameter mismatch; (b) numerical aperture mismatch; (c) refractive index profile difference.

where a_1 and a_2 are the core radii of the transmitting and receiving fibers respectively. It may be observed from Eq. (5.10) that no loss is incurred if the receiving fiber has a larger core diameter than the transmitting one. In addition, only a relatively small loss (0.09 dB) is obtained when the receiving fiber core diameter is 1% smaller than that of the transmitting fiber.

When the transmitting fiber has a higher numerical aperture than the receiving fiber, then some of the emitted light rays will fall outside the acceptance angle of the receiving fiber and they will therefore not be coupled through the joint. Again assuming a uniform modal power distribution, and fibers with equivalent refractive index profiles and core diameters, then the loss caused by a mismatch of numerical apertures (see Figure 5.3(b)) can be obtained from [Refs. 18, 20]:

$$Loss_{NA}\begin{cases} = -10\log_{10}\left(\dfrac{NA_2}{NA_1}\right)^2 \text{ (dB)} & NA_2 < NA_1 \\ = 0 \text{ (dB)} & NA_2 \geqslant NA_1 \end{cases} \tag{5.11}$$

where NA_1 and NA_2 are the numerical apertures for the transmitting and receiving fibers respectively. Equation (5.11) is valid for both step and graded index* fibers and in common with Eq. (5.10) it demonstrates that no losses occur when the receiving parameter (i.e. numerical aperture) is larger than the transmitting one.

* In the case of graded index fibers the numerical aperture on the fiber core axis must be used.

Finally, a mismatch in refractive index profiles (see Figure 5.3(a)) results in a loss which can be shown to be [Ref. 20]

$$Loss_{RI}\begin{cases} = -10\log_{10}\dfrac{\alpha_2(\alpha_1+2)}{\alpha_1(\alpha_2+2)}\ (\text{dB}) & \alpha_2 < \alpha_1 \\ = 0 \qquad\qquad\qquad\qquad\ (\text{dB}) & \alpha_2 \geqslant \alpha_1 \end{cases} \tag{5.12}$$

where α_1 and α_2 are the profile parameters for the transmitting and receiving fibers respectively (see Section 2.4.4). When connecting from a step index fiber with $\alpha_1 = \infty$ to a parabolic profile graded index fiber with $\alpha_2 = 2$, both having the same core diameter and axial numerical aperture, then a loss of 3 dB is produced. The reverse connection, however, does not incur a loss due to refractive index profile mismatch.

The intrinsic losses obtained at multimode fiber–fiber joints provided by Eqs. (5.10) to (5.12) can be combined into a single expression as follows:

$$Loss_{\text{int}}\begin{cases} = -10\log_{10}\dfrac{(a_2NA_2)^2(\alpha_1+2)\alpha_2}{(a_1NA_1)^2(\alpha_2+2)\alpha_1}\ (\text{dB}) & a_2 > a_1,\ NA_2 > NA_1,\ \alpha_2 > \alpha_1 \\ = 0 \qquad\qquad\qquad\qquad\qquad\qquad\ (\text{dB}) & a_2 \leqslant a_1,\ NA_2 \leqslant NA_1,\ \alpha_2 \leqslant \alpha_1 \end{cases} \tag{5.13}$$

It should be noted that Eq. (5.13) assumes that the three mismatches occur together. Distributions of losses which are obtained when with particular distributions of parameters, various random combinations of mismatches occur in a long series of connections, are provided in Ref. 11.

5.2.2 Single-mode fiber joints

Misalignment losses at connections in single-mode fibers have been theoretically considered by Marcuse [Ref. 21] and Gambling *et al.* [Refs. 22 and 23]. The theoretical analysis which was instigated by Marcuse is based upon the Gaussian or near Gaussian shape of the modes propagating in single-mode fibers regardless of the fiber type (i.e. step index or graded index). Further development of this theory by Gambling *et al.* [Ref. 23] gave simplified formulae for both the lateral and angular misalignment losses at joints in single-mode fibers. In the absence of angular misalignment Gambling *et al.* calculated that the loss T_l due to lateral offset y was given by:

$$T_l = 2.17\left(\frac{y}{\omega}\right)^2 \text{ dB} \tag{5.14}$$

where ω is the normalized spot size of the fundamental mode.* However, the normalized spot size for the LP_{01} mode (which corresponds to HE mode) may be

* The spot size for single-mode fibers is discussed in Section 2.5.2. It should be noted, however, that the normalization factor for the spot size causes it to differ in Eq. (5.15) by a factor of $2^{\frac{1}{2}}$ from that provided in Eq. (2.125).

obtained from the empirical formula [Refs. 19 and 22]:

$$\omega = a\,\frac{(0.65 + 1.62V^{-\frac{3}{2}} + 2.88V^{-6})}{2^{\frac{1}{2}}} \tag{5.15}$$

where ω is the spot size in μm, a is the fiber core radius and V is the normalized frequency for the fiber. Alternatively, the insertion loss T_a caused by an angular misalignment θ (in radians) at a joint in a single-mode fiber may be given by:

$$T_a = 2.17\left(\frac{\theta\omega\, n_1 V}{a\, NA}\right)^2 \text{ dB} \tag{5.16}$$

where n_1 is the fiber core refractive index and NA is the numerical aperture of the fiber. It must be noted that the formulae given in Eqs. (5.15) and (5.16) assume that the spot sizes of the modes in the two coupled fibers are the same. Gambling *et al.* [Ref. 23] also derived a somewhat complicated formula which gave a good approximation for the combined losses due to both lateral and angular misalignment at a fiber joint. However, they indicate that for small total losses (less than 0.75 dB) a reasonable approximation is obtained by simply combining Eqs. (5.14) and (5.16).

Example 5.5

A single-mode fiber has the following parameters:

normalized frequency $(V) = 2.40$
core refractive index $(n_1) = 1.46$
core diameter $(2a) = 8\ \mu$m
numerical aperture $(NA) = 0.1$

Estimate the total insertion loss of a fiber joint with a lateral misalignment of 1 μm and an angular misalignment of 1°

Solution: Initially it is necessary to determine the normalized spot size in the fiber. This may be obtained from Eq. (5.15) where:

$$\omega = a\,\frac{(0.65 + 1.62V^{-\frac{3}{2}} + 2.88V^{-6})}{2^{\frac{1}{2}}}$$

$$= 4\,\frac{(0.65 + 1.62(2.4)^{-1.5} + 2.88(2.4)^{-6})}{2^{\frac{1}{2}}}$$

$$= 3.12\ \mu\text{m}$$

The loss due to the lateral offset is given by Eq. (5.14) as:

$$T_l = 2.17\left(\frac{y}{\omega}\right)^2 = 2.17\left(\frac{1}{3.12}\right)^2$$

$$= 0.22 \text{ dB}$$

The loss due to angular misalignment may be obtained from Eq. (5.16) where:

$$T_a = 2.17\left(\frac{\theta\omega\, n_1 V}{a\, NA}\right)^2$$

$$= 2.17\left(\frac{(\pi/180) \times 3.12 \times 1.46 \times 2.4}{4 \times 0.1}\right)$$

$$= 0.49 \text{ dB}$$

Hence, the total insertion loss is

$$T_T = T_i + T_a = 0.22 + 0.49$$
$$= 0.71 \text{ dB}$$

In this example the loss due to angular misalignment is significantly larger than that due to lateral misalignment. However, aside from the actual magnitudes of the respective misalignments, the insertion losses incurred are also strongly dependent upon the normalized frequency of the fiber. This is especially the case with angular misalignment at a single-mode fiber joint where insertion losses of less than 0.3 dB may be obtained when the angular misalignment is 1° with fibers of appropriate V value. Nevertheless, for low loss single-mode fiber joints it is important that angular alignment is better than 1°

The theoretical model developed by Marcuse [Ref. 21] has been utilized by Nemota and Makimoto [Ref. 26] in a derivation of a general equation for determining the coupling loss between single-mode fibers. Their full expression takes account of all the extrinsic factors (lateral, angular and longitudinal misalignments, and Fresnel reflection), as well as the intrinsic factor associated with the connection of fibers with unequal mode-field diameters. Moreover, good agreement with various experimental investigations has been obtained using this generalized equation [Ref. 27]. Although consideration of the full expression is beyond the scope of this text, a reduced equation, to allow calculation of the intrinsic factor which quite commonly occurs in the interconnection of single-mode fibers, may be employed. Hence, assuming that no losses are present due to the extrinsic factors, the intrinsic coupling loss is given by [Ref. 27]:

$$Loss_{int} = -10 \log_{10}\left[4\left(\frac{\omega_{02}}{\omega_{01}} + \frac{\omega_{01}}{\omega_{02}}\right)^{-2}\right] \text{ (dB)} \tag{5.17}$$

where ω_{01} and ω_{02} are the spot sizes of the transmitting and receiving fibers respectively. Equation (5.17) therefore enables the additional coupling loss resulting from mode-field diameter mismatch between two single-mode fibers to be calculated.

Example 5.6

Two single-mode fibers with mode-field diameters of 9.2 μm and 8.4 μm are to be connected together. Assuming no extrinsic losses, determine the loss at the connection due to the mode-field diameter mismatch.

Solution: The intrinsic loss is obtained using Eq. (5.17) where:

$$Loss_{int} = -10 \log_{10}\left[4\left(\frac{\omega_{02}}{\omega_{01}} + \frac{\omega_{01}}{\omega_{02}}\right)^{-2}\right]$$

$$= -10 \log_{10}\left[4\left(\frac{4.2}{5.6} + \frac{5.6}{4.2}\right)^{-2}\right]$$

$$= -10 \log_{10} 0.922$$

$$= 0.35 \text{ dB}$$

It should be noted from Example 5.6 that the same result is obtained irrespective of which fiber is transmitting or receiving through the connection. Hence, by contrast to the situation with multimode fibers (see Section 5.2.1), the intrinsic loss through a single-mode fiber joint is independent of the direction of propagation.

We have considered in some detail the optical attenuation at fiber–fiber connections. However, we have not yet discussed the possible distortion of the transmitted signal at a fiber joint. Although work in this area is in its infancy, increased interest has been generated with the use of highly coherent sources (injection lasers) and very low dispersion fibers. It is apparent that fiber connections strongly affect the signal transmission causing modal noise (see Section 3.10.3) and nonlinear distortion [Ref. 29] when a coherent light source is utilized with a multimode fiber. Also, it has been reported [Ref. 30] that the transmission loss of a connection in a coherent multimode system is extremely wavelength dependent, exhibiting a possible 10% change in the transmitted optical wavelength for a very small change (0.001 nm) in the laser emission wavelength. Although it has been found that these problems may be reduced by the use of single-mode optical fiber [Ref. 29], a theoretical model for the wavelength dependence of joint losses in single-mode fiber has been obtained [Ref. 31]. This model predicts that as the wavelength increases then the width of the fundamental mode field increases and hence for a given lateral offset or angular tilt the joint loss decreases. For example, the lateral offset loss at a wavelength of 1.5 μm was calculated to be only around 80% of the loss at a wavelength of 1.3 μm.

Furthermore, the above modal effects become negligible when an incoherent source (light emitting diode) is used with multimode fiber. However, in this instance there is often some mode conversion at the fiber joint which can make the connection effectively act as a mode mixer or filter [Ref. 32]. Indications are that this phenomenon, which has been investigated [Ref. 33] with regard to fiber splices, is more pronounced with fusion splices than with mechanical splices, both of which are described in Section 5.3.

5.3 Fiber splices

A permanent joint formed between two individual optical fibers in the field or factory is known as a fiber splice. Fiber splicing is frequently used to establish long-haul optical fiber links where smaller fiber lengths need to be joined, and there is no requirement for repeated connection and disconnection. Splices may be divided into two broad categories depending upon the splicing technique utilized. These are fusion splicing or welding and mechanical splicing.

Fusion splicing is accomplished by applying localized heating (e.g. by a flame or an electric arc) at the interface between two butted, prealigned fiber ends causing them to soften and fuse. Mechanical splicing, in which the fibers are held in alignment by some mechanical means, may be achieved by various methods including the use of tubes around the fiber ends (tube splices) or V-grooves into which the butted fibers are placed (groove splices). All these techniques seek to optimize the splice performance (i.e. reduce the insertion loss at the joint) through both fiber end preparation and alignment of the two joint fibers. Typical average splice insertion losses for multimode fibers are in the range 0.1 to 0.2 dB [Ref. 34] which is generally a better performance than that exhibited by demountable connections (see Sections 5.4 and 5.5). It may be noted that the insertion losses of fiber splices are generally much less than the possible Fresnel reflection loss at a butted fiber–fiber joint. This is because there is no large step change in refractive index with the fusion splice as it forms a continuous fiber connection, and some method of index matching (e.g. a fluid) tends to be utilized with mechanical splices. However, fiber splicing (especially fusion splicing) is at present a somewhat difficult process to perform in a field environment and suffers from practical problems in the development of field-usable tools.

A requirement with fibers intended for splicing is that they have smooth and square end faces. In general this end preparation may be achieved using a suitable tool which cleaves the fiber as illustrated in Figure 5.4 [Ref. 35]. This process is

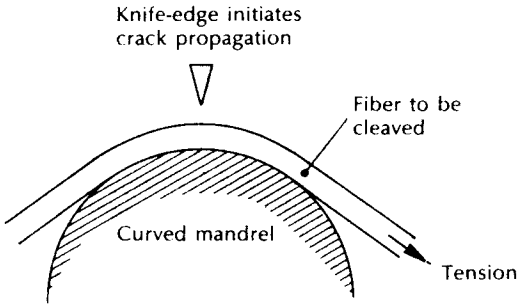

Figure 5.4 Optical fiber end preparation: the principle of scribe and break cutting [Ref. 35].

often referred to as scribe and break or score and break as it involves the scoring of the fiber surface under tension with a cutting tool (e.g. sapphire, diamond, tungsten carbide blade). The surface scoring creates failure as the fiber is tensioned and a clean, reasonably square fiber end can be produced. Figure 5.4 illustrates this process with the fiber tensioned around a curved mandrel. However, straight pull, scribe and break tools are also utilized, which arguably give better results [Ref. 36]. An alternative technique involves circumferential scoring which provides a controlled method of lightly scoring around the fiber circumference [Ref. 31]. In this case the score can be made smooth and uniform and large diameter fibers may be prepared by a simple straight pull with end angles less than 1°

5.3.1 Fusion splices

The fusion splicing of single fibers involves the heating of the two prepared fiber ends to their fusing point with the application of sufficient axial pressure between the two optical fibers. It is therefore essential that the stripped (of cabling and buffer coating) fiber ends are adequately positioned and aligned in order to achieve good continuity of the transmission medium at the junction point. Hence the fibers are usually positioned and clamped with the aid of an inspection microscope.

Flame heating sources such as microplasma torches (argon and hydrogen) and oxhydric microburners (oxygen, hydrogen and alcohol vapour) have been utilized with some success [Ref. 37]. However, the most widely used heating source is an electric arc. This technique offers advantages of consistent, easily controlled heat with adaptability for use under field conditions. A schematic diagram of the basic arc fusion method is given in Figure 5.5(a) [Refs. 34 and 35] illustrating how the two fibers are welded together. Figure 5.5(b) [Ref. 24] shows a development of the basic arc fusion process which involves the rounding of the fiber ends with a low energy discharge before pressing the fibers together and fusing with a stronger arc. This technique, known as prefusion, removes the requirement for fiber end preparation which has a distinct advantage in the field environment. It has been utilized with multimode fibers giving average splice losses of 0.09 dB [Ref. 39].

Fusion splicing of single-mode fibers with typical core diameters between 5 and 10 μm presents problems of more critical fiber alignment (i.e. lateral offsets of less than 1 μm are required for low loss joints). However, splice insertion losses below 0.3 dB may be achieved due to a self alignment phenomenon which partially compensates for any lateral offset.

Self alignment, illustrated in Figure 5.6 [Refs. 38, 40 and 41], is caused by surface tension effects between the two fiber ends during fusing. An early field trial of single-mode fiber fusion splicing over a 31.6 km link gave mean splice insertion losses of 0.18 and 0.12 dB at wavelengths of 1.3 and 1.55 μm respectively [Ref. 42]. Mean splice losses of only 0.06 dB have also been obtained with a fully automatic single-mode fiber fusion splicing machine [Ref. 43].

A possible drawback with fusion splicing is that the heat necessary to fuse the fibers may weaken the fiber in the vicinity of the splice. It has been found that even

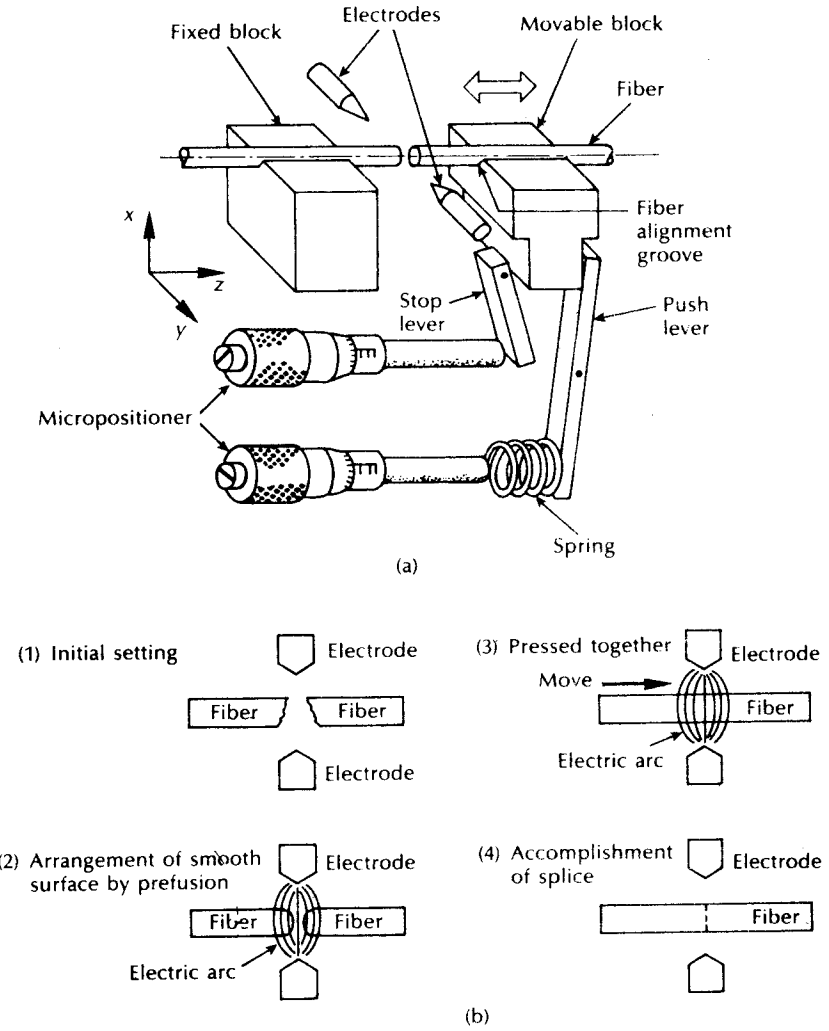

Figure 5.5 Electric arc fusion splicing: (a) an example of fusion splicing apparatus [Refs. 34 and 38]; (b) schematic illustration of the prefusion method for accurately splicing optical fibers [Ref. 24].

with careful handling, the tensile strength of the fused fiber may be as low as 30% of that of the uncoated fiber before fusion [Ref. 45]. The fiber fracture generally occurs in the heat-affected zone adjacent to the fused joint. The reduced tensile strength is attributed [Refs. 45 and 46] to the combined effects of surface damage caused by handling, surface defect growth during heating and induced residential stresses due to changes in chemical composition. It is therefore necessary that the

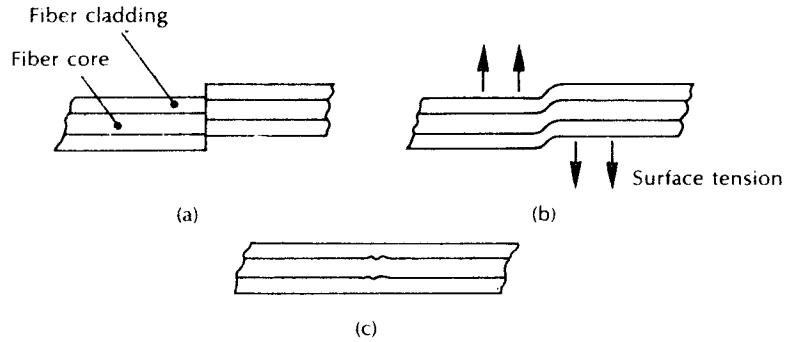

Figure 5.6 Self-alignment phenomenon which takes place during fusion splicing: (a) before fusion; (b) during fusion; (c) after fusion [Refs 38, 40 and 41].

completed splice is packaged so as to reduce tensile loading upon the fiber in the vicinity of the splice.

5.3.2 Mechanical splices

A number of mechanical techniques for splicing individual optical fibers have been developed. A common method involves the use of an accurately produced rigid alignment tube into which the prepared fiber ends are permanently bonded. This snug tube splice is illustrated in Figure 5.7(a) [Ref. 47] and may utilize a glass or ceramic capillary with an inner diameter just large enough to accept the optical fibers. Transparent adhesive (e.g. epoxy resin) is injected through a transverse bore in the capillary to give mechanical sealing and index matching of the splice. Average

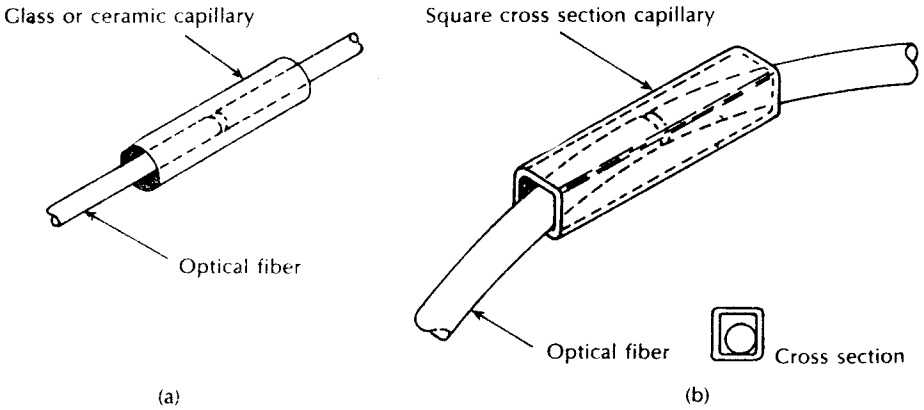

Figure 5.7 Techniques for tube splicing of optical fibers: (a) snug tube splice [Ref. 47]; (b) loose tube splice utilizing square cross section capillary [Ref. 50].

insertion losses as low as 0.1 dB have been obtained [Ref. 48] with multimode graded index and single-mode fibers using ceramic capillaries. However, in general, snug tube splices exhibit problems with capillary tolerance requirements. Hence as a commercial product they may exhibit losses of up to 0.5 dB [Ref. 49].

A mechanical splicing technique which avoids the critical tolerance requirements of the snug tube splice is shown in Figure 5.7(b) [Ref. 50]. This loose tube splice uses an oversized square section metal tube which easily accepts the prepared fiber ends. Transparent adhesive is first inserted into the tube followed by the fibers. The splice is self aligning when the fibers are curved in the same plane, forcing the fiber ends simultaneously into the same corner of the tube, as indicated in Figure 5.7(b). Mean splice insertion losses of 0.073 dB have been achieved [Refs. 41 and 51] using multimode graded index fibers with the loose tube approach.

Other common mechanical splicing techniques involve the use of grooves to secure the fibers to be jointed. A simple method utilizes a V-groove into which the two prepared fiber ends are pressed. The V-groove splice which is illustrated in Figure 5.8(a) [Ref. 52] gives alignment of the prepared fiber ends through insertion in the groove. The splice is made permanent by securing the fibers in the V-groove with epoxy resin. Jigs for producing V-groove splices have proved quite successful, giving joint insertion losses of around 0.1 dB [Ref. 35].

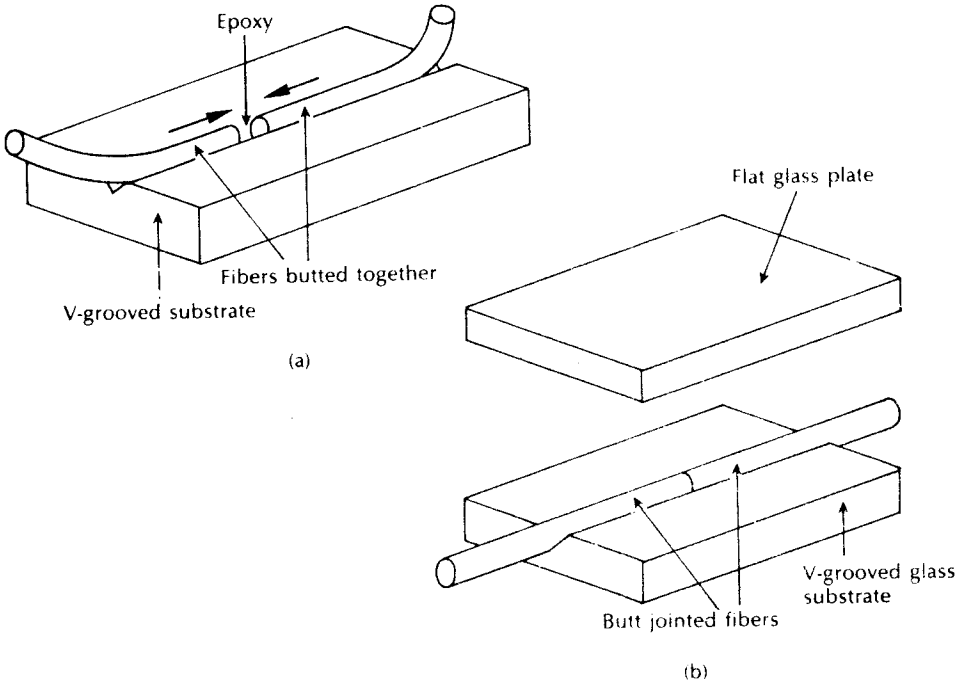

Figure 5.8 V-groove splices [Ref. 52].

V-groove splices formed by sandwiching the butted fiber ends between a V-groove glass substrate and a flat glass retainer plate, as shown in Figure 5.8(b) have also proved very successful in the laboratory. Splice insertion losses of less than 0.01 dB when coupling single-mode fibers have been reported [Ref. 53] using this technique. However, reservations are expressed regarding the field implementation of these splices with respect to manufactured fiber geometry, and housing of the splice in order to avoid additional losses due to local fiber bending.

A further variant on the V-groove technique is the elastic tube or elastomeric splice shown in Figure 5.9 [Ref. 54]. The device comprises two elastomeric internal parts, one of which contains a V-groove. An outer sleeve holds the two elastic parts in compression to ensure alignment of the fibers in the V-groove, and fibers with different diameters tend to be centred and hence may be successfully spliced. Although originally intended for multimode fiber connection, the device has become a widely used commercial product [Ref. 49] which is employed with single-mode fibres, albeit often as a temporary splice for laboratory investigations. The splice loss for the elastic tube device was originally reported as 0.12 dB or less [Ref. 54] but is generally specified as around 0.25 dB for the commercial product [Ref. 49]. In addition, index matching gel is normally employed within the device to improve its performance.

A slightly more complex groove splice known as the Springroove® splice utilizes a bracket containing two cylindrical pins which serve as an alignment guide for the two prepared fiber ends. The cylindrical pin diameter is chosen to allow the fibers to protrude above the cylinders, as shown in Figure 5.10(a) [Ref. 55]. An elastic element (a spring) is used to press the fibers into a groove and maintain the fiber end alignment, as illustrated in Figure 5.10(b). The complete assembly is secured using a drop of epoxy resin. Mean splice insertion losses of 0.05 dB [Ref. 41] have been obtained using multimode graded index fibers with the Springroove® splice. This device has found practical use in Italy.

The aforementioned mechanical splicing methods employ alignment of the bare fibers, whereas more recently alignment of secondary elements around the bare fibers is a technique which has gained favour [Ref. 31]. Secondary alignment generally gives increased ruggedness and provides a structure that can be ground and polished for fiber end preparation. Furthermore, with a good design the fiber coating can be terminated within the secondary element leaving only the fiber end

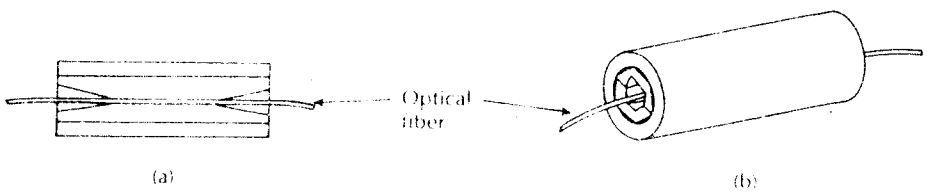

Figure 5.9 The elastomeric splice [Ref. 54]: (a) cross section; (b) assembly.

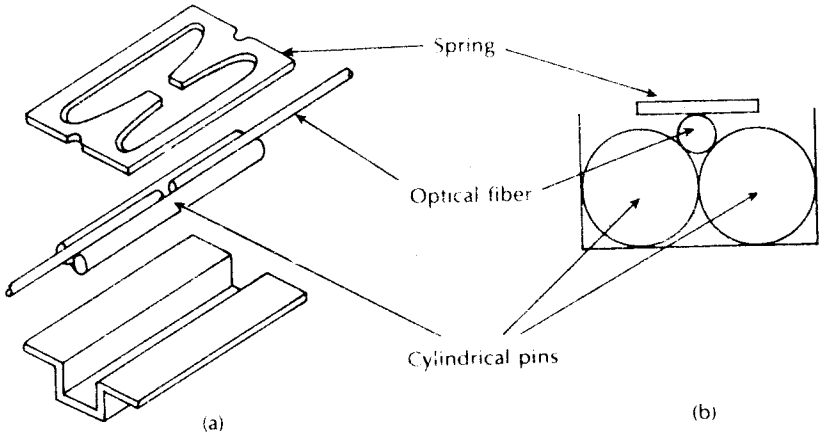

Figure 5.10 The Springroove® splice [Ref. 55]: (a) expanded overview of the splice; (b) schematic cross section of the splice.

face exposed. Hence when the fiber end face is polished flat to the secondary element, a very rugged termination is produced. This technique is particularly advantageous for use in fiber remountable connectors (see Section 5.4). However, possible drawbacks with this method include the time taken to make the termination and the often increased splice losses resulting from the tolerances on the secondary elements which tend to contribute to the fiber misalignment.

An example of a secondary aligned mechanical splice for multimode fiber is shown in Figure 5.11. This device uses precision glass capillary tubes called ferrules as the secondary elements with an alignment sleeve of metal or plastic into which the glass tubed fibers are inserted. Normal assembly of the splice using 50 μm core diameter fiber yields an average loss of around 0.2 dB [Ref. 56].

Finally, the secondary alignment technique has been employed in the realization of a low loss, single-mode fiber mechanical splice which has been used in several large installations in the United States. This device, known as a single-mode rotary splice, is shown in Figure 5.12 [Ref. 57]. The fibers to be spliced are initially terminated in precision glass capillary tubes which are designed to make use of the small eccentricity that is present, as illustrated in Figure 5.12(a). An ultraviolet curable adhesive is used to cement the fibers in the glass tubes and the fiber terminations are prepared with a simple grinding and polishing operation.

Alignment accuracies of the order of 0.05 μm are obtained using the three glass rod alignment sleeve shown in Figure 5.12(b). Such alignment accuracies are necessary to obtain low losses as the mode-field diameter for single-mode fiber is generally in the range 8 to 10 μm. The sleeve has a built-in offset such that when each ferrule is rotated within it, the two circular paths of the centre of each fiber core cross each other. Excellent alignment is obtained utilizing a simple algorithm, and strong metal springs provide positive alignment retention. Using index

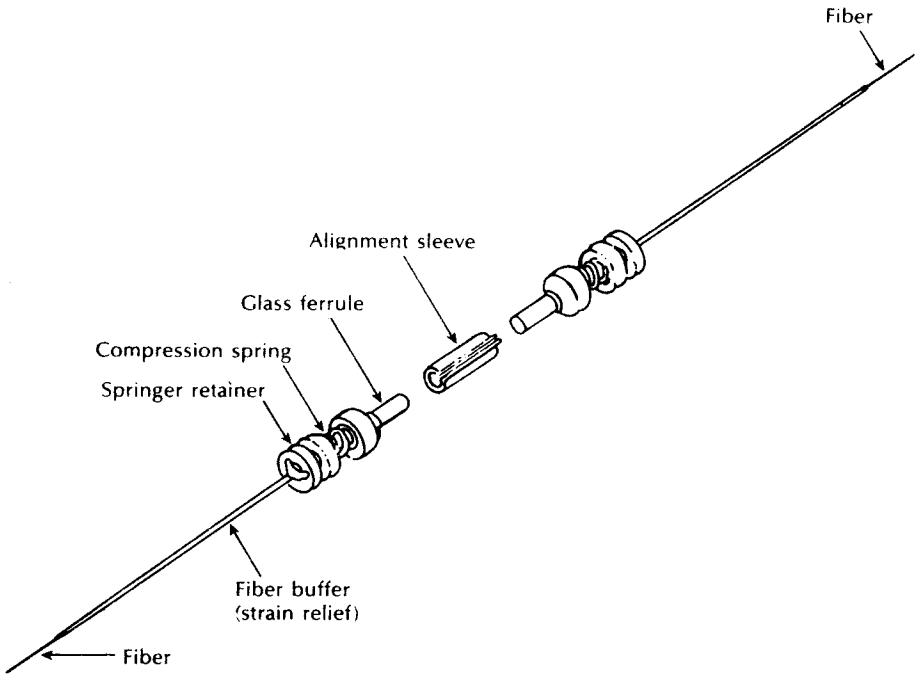

Figure 5.11 Multimode fiber mechanical splice using glass capillary tubes [Ref. 56].

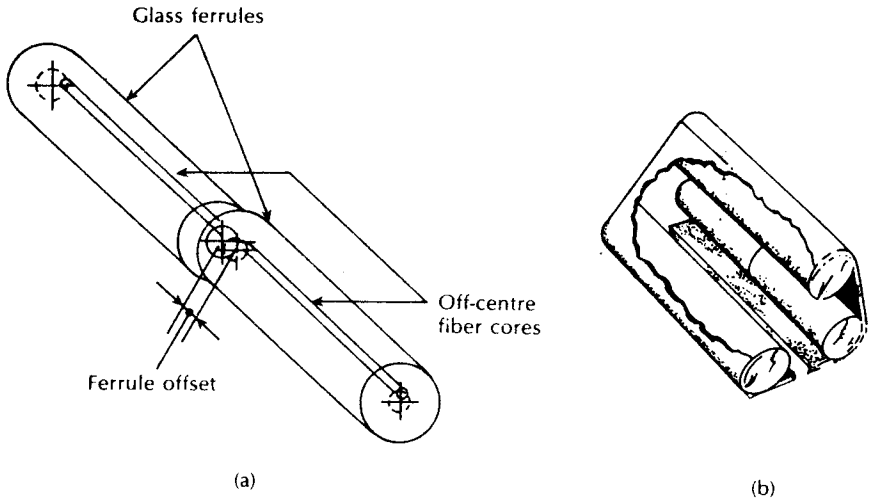

Figure 5.12 Rotary splice for single-mode fibers [Ref. 57]: (a) alignment technique using glass ferrules; (b) glass rod alignment sleeve.

matching gel such splices have demonstrated mean losses of 0.03 dB with a standard deviation of 0.018 dB [Ref. 31]. Moreover, these results were obtained in the field, suggesting that the rotary splicing technique was not affected by the skill level of the splicer in that harsh environment.

5.3.3 Multiple splices

Multiple simultaneous fusion splicing of an array of fibers in a ribbon cable has been demonstrated for both multimode [Ref. 58] and single-mode [Ref. 59] fibers. In both cases a five fiber ribbon was prepared by scoring and breaking prior to pressing the fiber ends on to a contact plate to avoid difficulties with varying gaps between the fibers to be fused. An electric arc fusing device was then employed to provide simultaneous fusion. Such a device is now commercially available to allow the splicing of five fibers simultaneously in a time of around 5 minutes, which compares favourably with the 15 minutes generally required for five single fusion splicings [Ref. 60]. Splice losses using this device with multimode graded index fiber range from an average of 0.04 dB to a maximum of 0.12 dB, whereas for single-mode fiber the average loss is 0.13 dB with a 0.4 dB maximum.

The most common technique employed for multiple simultaneous splicing to date involves mechanical splicing of an array of fibers, usually in a ribbon cable. A

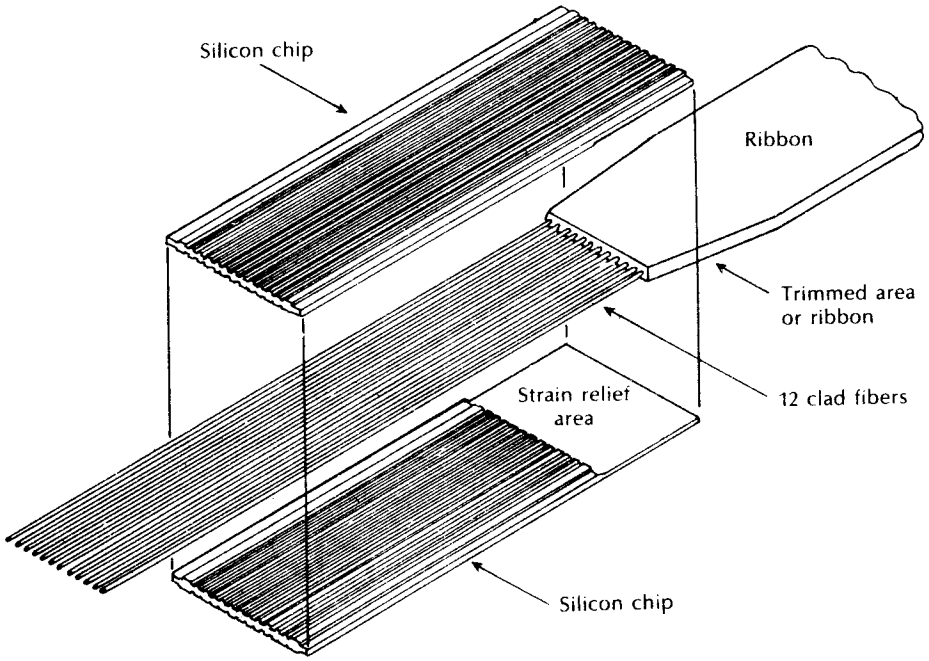

Figure 5.13 Multiple fiber splicing using a silicon chip array.

V-groove multiple splice secondary element comprising etched silicon chips has been used extensively in the United States [Ref. 31] for splicing multimode fibers. In this technique a twelve fiber splice is prepared by stripping the ribbon and coating material from the fibers. Then the twelve fibers are laid into the trapezoidal* grooves of a silicon chip using a comb structure, as shown in Figure 5.13. The top silicon chip is then applied prior to applying epoxy to the chip–ribbon interface. Finally, after curing, the front end face is ground and polished.

The process is normally carried out in the factory and the arrays are clipped together in the field, putting index matching silica gel between the fiber ends. The average splice loss obtained with this technique in the field is 0.12 dB, with the majority of the loss resulting from intrinsic fiber mismatch. Major advantages of this method are the substantial reduction in splicing time (by more than a factor of 10) per fiber and the increased robustness of the final connection. Although early array splicing investigations using silicon chips [Ref. 61] demonstrated the feasibility of connecting 12×12 fiber arrays, in practice only single twelve fiber

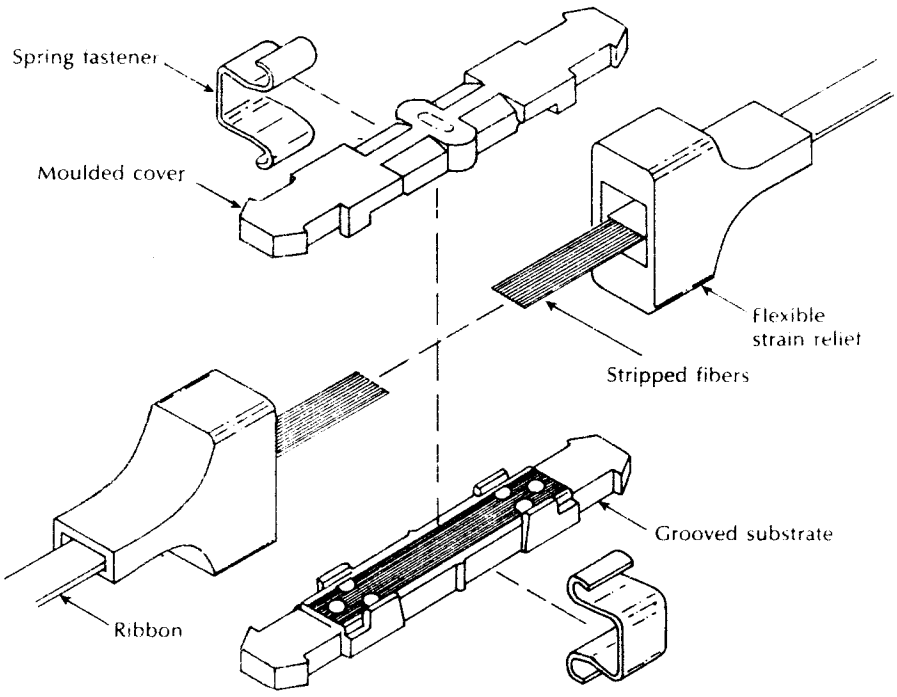

Figure 5.14 V-groove polymer resin ribbon fiber splice [Ref. 63].

* A natural consequence of etching.

ribbons have been spliced at one time due to concerns in relation to splice tolerance and the large number of telecommunication channels which would be present in the two dimensional array [Ref. 31].

An alternative V-groove flat chip moulded from a glass filled polymer resin has been employed in France [Ref. 62], in particular for the Biarritz project (see Section 14:2.3). Moreover, direct mass splicing of twelve fiber ribbons has been accomplished [Ref. 63]. In this technique simultaneous end preparation of all twenty-four fibers is achieved using a ribbon grinding and polishing procedure. The ribbons are then laid in guides and all twelve fibers are positioned in grooves in the glass filled plastic substrate shown in Figure 5.14. A vacuum technique is used to hold the fibers in position whilst the cover plate is applied, and spring clips hold the assembly together. Index matching gel is applied through a hole in the cover plate giving average splice losses of 0.18 dB with multimode fiber

5.4 Fiber connectors

Demountable fiber connectors are more difficult to achieve than optical fiber splices. This is because they must maintain similar tolerance requirements to splices in order to couple light between fibers efficiently, but they must accomplish it in a removable fashion. Also, the connector design must allow for repeated connection and disconnection without problems of fiber alignment, which may lead to degradation in the performance of the transmission line at the joint. Hence to operate satisfactorily the demountable connector must provide reproducible accurate alignment of the optical fibers.

In order to maintain an optimum performance the connection must also protect the fiber ends from damage which may occur due to handling (connection and disconnection), must be insensitive to environmental factors (e.g. moisture and dust) and must cope with tensile load on the cable. Additionally, the connector should ideally be a low cost component which can be fitted with relative ease. Hence optical fiber connectors may be considered in three major areas, which are:

(a) the fiber termination, which protects and locates the fiber ends;
(b) the fiber end alignment to provide optimum optical coupling;
(c) the outer shell, which maintains the connection and the fiber alignment, protects the fiber ends from the environment and provides adequate strength at the joint.

The use of an index matching material in the connector between the two jointed fibers can assist the connector design in two ways. It increases the light transmission through the connection whilst keeping dust and dirt from between the fibers. However, this design aspect is not always practical with demountable connectors, especially where fluids are concerned. Apart from problems of sealing and replacement when the joint is disconnected and reconnected, liquids in this instance may have a detrimental effect, attracting dust and dirt to the connection.

There are a large number of demountable single fiber connectors, both commercially available and under development, which have insertion losses in the range 0.2 to 3 dB. Fiber connectors may be separated into two broad categories: butt jointed connectors and expanded beam connectors. Butt jointed connectors rely upon alignment of the two prepared fiber ends in close proximity (butted) to each other so that the fiber core axes coincide. Expanded beam connectors utilize interposed optics at the joint (i.e. lenses) in order to expand the beam from the transmitting fiber end before reducing it again to a size compatible with the receiving fiber end.

Butt jointed connectors are the most widely used connector type and a substantial number have been reported. In this section we review some of the more common butt jointed connector designs which have been developed for use with both multimode and single-mode fibers. In Section 5.5, following, expanded beam connectors are discussed.

5.4.1 Cylindrical ferrule connectors

The basic ferrule connector (sometimes referred to as a concentric sleeve connector), which is perhaps the simplest optical fiber connector design, is illustrated in Figure 5.15(a) [Ref. 9]. The two fibers to be connected are permanently bonded (with epoxy resin) in metal plugs known as ferrules which have an accurately drilled central hole in their end faces where the stripped (of buffer coating) fiber is located. Within the connector the two ferrules are placed in an alignment sleeve which, using accurately machined components, allows the fiber ends to be butt jointed. The ferrules are held in place via a retaining mechanism which, in the example shown in Figure 5.15(a), is a spring.

It is essential with this type of connector that the fiber end faces are smooth and square (i.e. perpendicular to the fiber axis). This may be achieved with varying success by either:

(a) cleaving the fiber before insertion into the ferrule;
(b) inserting and bonding before cleaving the fiber close to the ferrule end face;
(c) using either (a) or (b) and polishing the fiber end face until it is flush with the end of the ferrule.

Polishing the fiber end face after insertion and bonding provides the best results but it tends to be time consuming and inconvenient, especially in the field.

The fiber alignment accuracy of the basic ferrule connector is largely dependent upon the ferrule hole into which the fiber is inserted. Hence, some ferrule connectors have incorporated a watch jewel in the ferrule end face (jewelled ferrule connector), as illustrated in Figure 5.15(b) [Ref. 10]. In this case the fiber is centred with respect to the ferrule through the watch jewel hole. The use of the watch jewel allows the close diameter and tolerance requirements of the ferrule end face hole to be obtained more easily than simply through drilling of the metallic ferrule end face alone. Nevertheless, typical concentricity errors between the fiber core and the

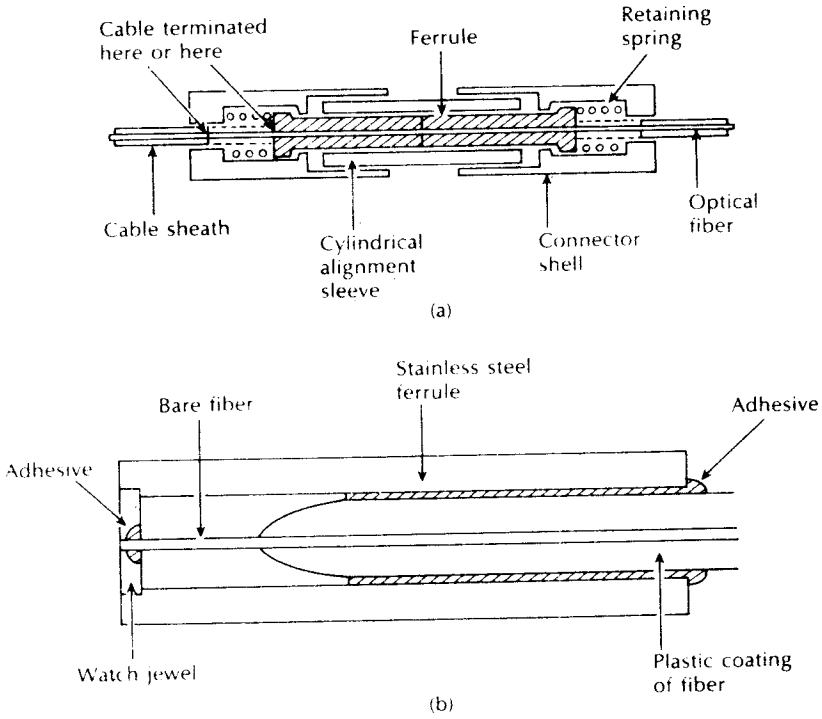

Figure 5.15 Ferrule connectors: (a) structure of a basic ferrule connector [Ref. 9]; (b) structure of a watch jewel connector ferrule [Ref. 10].

outside diameter of the jewelled ferrule are in the range 2 to 6 μm giving insertion losses in the range 1 to 2 dB with multimode step index fibers.

More recently capillary ferrules manufactured from ceramic materials (e.g. alumina porcelain) have found widespread application within precision ferrule connectors. Such capillary ferrules have a precision bore which is accurately centred in the ferrule. Final assembly of the connector includes the fixture of the fiber within the ferrule, using adhesive prior to the grinding and polishing for end preparation. The ceramic materials possess outstanding thermal, mechanical and chemical resistance characteristics in comparison to metals and plastics [Ref. 64]. In addition, unlike metal and plastic components, the ceramic ferrule material is harder than the optical fiber and is therefore unaffected by the grinding and polishing process, a factor which assists in the production of low loss fiber connectors. Typical average losses for multimode graded index fiber (i.e. core/cladding: 50/125 μm) and single-mode fiber (i.e. core/cladding: 9/125 μm) with the precision ceramic ferrule connector are 0.2 and 0.3 dB respectively [Ref. 60].

Numerous cylindrical sleeve ferrule connectors are commercially available for both multimode and single-mode fiber termination. The most common design types

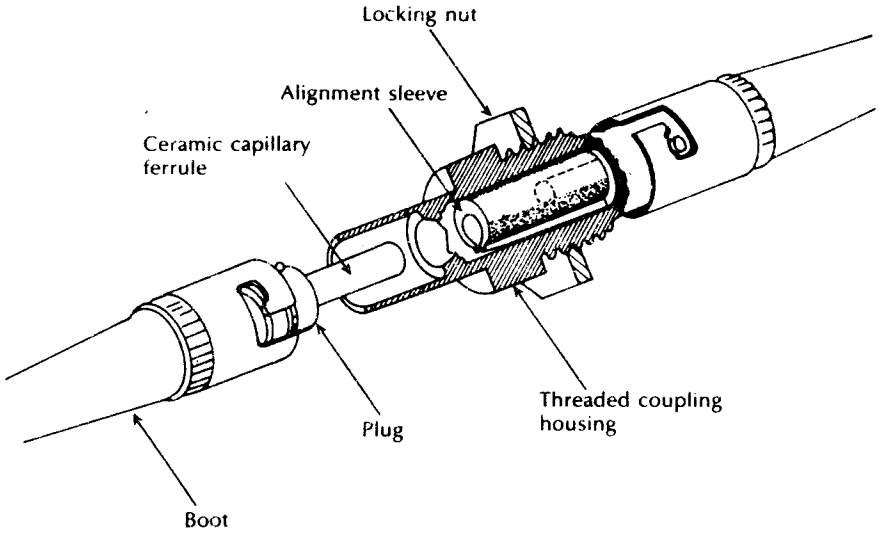

Figure 5.16 ST series multimode fiber connector using ceramic capillary ferrules.

are the straight tip (ST), the subminiature assembly (SMA), the fiber connector (FC), the physical contact (PC)*, the subscriber connector (SC) and the D3/D4 [Refs. 27, 31, 60, 65, 66]. An example of an ST series multimode fiber connector is shown in Figure 5.16, which exhibits an optimized cylindrical sleeve with a cross section designed to expand uniformly when the ferrules are inserted. Hence, the constant circumferential pressure provides accurate alignment, even when the ferrule diameters differ slightly. In addition, the straight ceramic ferrule may be observed in Figure 5.16 which contrasts with the stepped ferrule (i.e. a ferrule with a single step which reduces the diameter midway along its length) provided in the SMA connector design.

The average loss obtained using this connector with multimode graded index fiber (i.e. core/cladding: 62.5/125 μm) was 0.22 dB with less than 0.1 dB change in loss after 1000 reconnections [Ref. 65].

5.4.2 Biconical ferrule connectors

A ferrule type connector which is widely used as part of jumper cable in a variety of applications in the United States is the biconical plug connector† [Refs. 34 and 67]. The plugs are either transfer moulded directly on to the fiber or cast around the fiber using a silica-loaded epoxy resin ensuring concentricity to within 5 μm.

*It should be noted that combinations of the types exist including the ST–PC and the FC–PC designs.
†The device is also referred to as the biconic connector

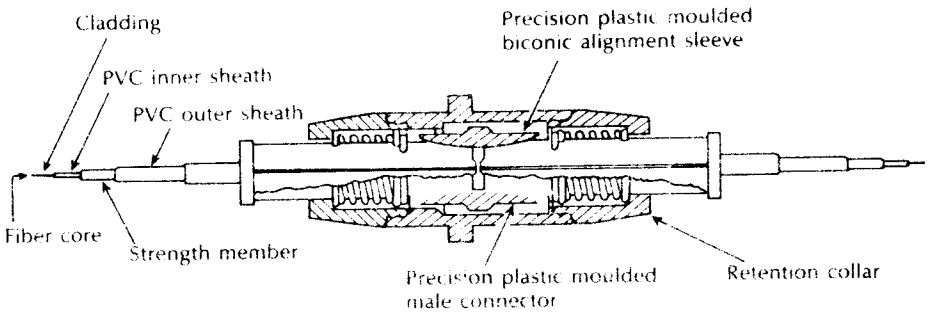

Figure 5.17 Cross section of the biconical connector [Refs. 34 and 67].

After plug attachment, the fiber end faces are polished before the plugs are inserted and aligned in the biconical moulded centre sleeve, as shown in Figure 5.17 [Ref. 34]. The conical ferrule geometry may also be observed in Figure 5.17. Mean insertion losses as low as 0.21 dB have been reported [Ref. 67] when using this connector with 50 μm core diameter graded index fibers. In the original design transparent silicon resin pads were placed over the fiber end faces to provide index matching. However, currently the polished fiber end faces are butted directly, the gap and parallelism of end faces being controlled to a degree that gives insertion losses better than the level normally exhibited by Fresnel reflection. This connector is also used with single-mode fibers by reducing the eccentricity of the tapered cone and also the fiber core eccentricity to 0.33 μm or less, whilst limiting the tilt angle of fibers to 0.35° or less. In this way an average connector loss of 0.28 dB can be obtained using single-mode fibers with a maximum loss of 0.7 dB [Ref. 60].

5.4.3 Double eccentric connector

The double eccentric connector does not rely on a concentric fixed sleeve approach but is an example of an active assembly which is adjustable, allowing close alignment of the fiber axes. The mechanism, which is shown in Figure 5.18 [Refs. 9 and 13], consists of two eccentric cylinders within the outer plug. It may be observed from Figure 5.18 that the optical fiber is mounted eccentrically within the inner cylinder. Therefore, when the two connector halves are mated it is always possible through rotation of the mechanism to make the fiber core axes coincide. This operation is performed on both plugs using either an inspection microscope or a peak optical adjustment. The mechanisms are then locked to give permanent alignment. This connector type has exhibited mean insertion losses of 0.48 dB with multimode graded index fibers: use of index matching fluid within the connector has reduced these losses to 0.2 dB. The double eccentric connector design has also been utilized with single-mode fibers where its adjustable nature has proved advantageous for alignment of the small core diameter fibers giving losses of 0.46 dB without index matching [Ref. 31].

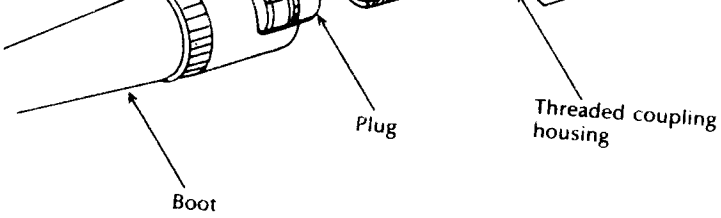

Figure 5.16 ST series multimode fiber connector using ceramic capillary ferrules.

are the straight tip (ST), the subminiature assembly (SMA), the fiber connector (FC), the physical contact (PC)*, the subscriber connector (SC) and the D4/F [Refs. 27, 31, 60, 65, 66]. An example of a ST shown in

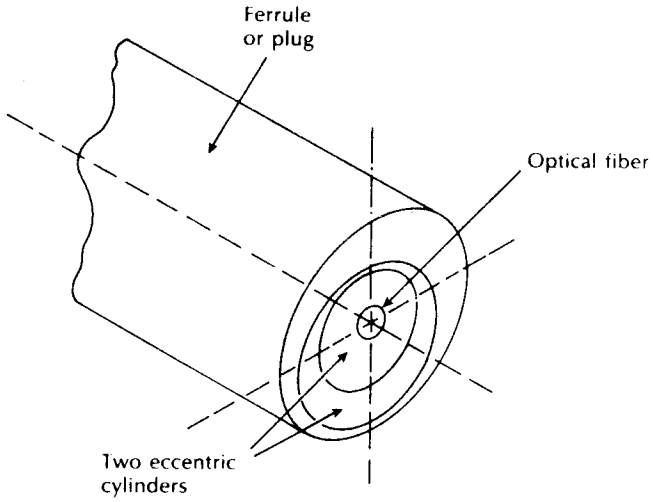

Figure 5.18 Structure of the double eccentric connector plug [Refs. 9 and 13].

5.4.4 Duplex and multiple fiber connectors

A number of duplex fiber connector designs have been developed in order to provide two way communication, but none have found widespread use to date [Ref. 27]. For example, AT & T have a duplex version of the ST single fiber connector (see Section 5.4.1). Moreover, the media interface connector plug shown in Figure 5.19 is part of a duplex fiber connector which has been developed to meet the American National Standards Institute (ANSI) specification for use within

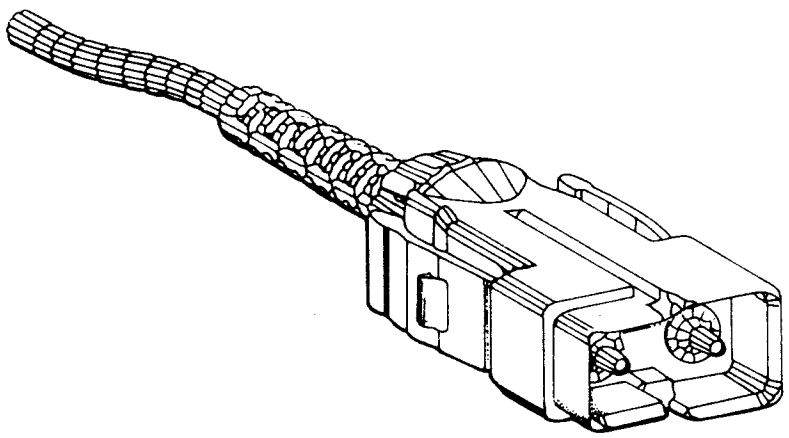

Figure 5.19 An example media interface plug for a duplex fiber connector.